Winter 2016

PASSIVE MICROWAVE SATELLITE SNOW OBSERVATIONS FOR HYDROLOGIC APPLICATIONS

Carrie Micheline Vuyovich
University of New Hampshire, Durham

PASSIVE MICROWAVE SATELLITE SNOW OBSERVATIONS FOR HYDROLOGIC APPLICATIONS

BY

CARRIE M. VUYOVICH

B.E., Civil Engineering, Vanderbilt University, 2002

M.S., Civil Engineering, University of New Hampshire, 2010

DISSERTATION

Submitted to the University of New Hampshire

in Partial Fulfillment of

Requirements for the Degree of

Doctor of Philosophy

in

Civil Engineering

December, 2016

This thesis/dissertation has been examined and approved in partial fulfillment of the requirements for the degree of Doctor of Philosophy in Civil Engineering by:

Dr. Jennifer Jacobs
Professor, Civil and Environmental Engineering, UNH
Thesis/Dissertation Director

Dr. Diane Foster
Professor, Mechanical Engineering, UNH

Dr. Thomas Lippman
Associate Professor, Earth Sciences, UNH

Dr. Michael Palace
Associate Professor, Earth Systems Research Center, UNH

Dr. Robert Davis
Director, US Army Engineer Research Development Center
Cold Regions Research and Engineering Laboratory

On 2 November 2016

Original approval signatures are on file with the University of New Hampshire Graduate School.

ACKNOWLEDGEMENTS

This work was supported by a NASA ESPCoR Grant: NNX11AQ34A, Passive Microwave Detection of Snowmelt and Runoff; a NASA ROSES Grant: NNH13ZDA001N, Satellite Enhanced Snowmelt Flood Predictions in the Red River of the North Basin; and the U.S. Army Terrestrial Environmental Modeling & Intelligence System (ARTEMIS) applied science research program sponsored by the Assistant Secretary of the Army for Acquisition, Logistics, and Technology (ASA-ALT), the University of New Hampshire and the U.S. Army Engineer Research and Development Center's Cold Regions Research and Engineering Laboratory.

TABLE OF CONTENTS

TABLE OF FIGURES

CHAPTER 1

CHAPTER 2

CHAPTER 3

CHAPTER 4

TABLE OF TABLES

CHAPTER 2

CHAPTER 3

CHAPTER 4

ABSTRACT

EVALUATION OF PASSIVE MICROWAVE SATELLITE DATA FOR HYDROLOGIC APPLICATIONS

By

Carrie M. Vuyovich

University of New Hampshire, December 2016

Melting snow provides an essential source of water in many regions of the world and can also contribute to devastating, wide-scale flooding. The objective of this research was to investigate the potential for passive microwave remotely sensed data to characterize snow water equivalent (SWE) and snowmelt across diverse regions and snow regimes to improve snowmelt runoff estimation. The first step was to evaluate the current, empirically-based passive microwave SWE products compared to NOAA's operational SWE estimates from SNODAS across 2100 watersheds over eight years. The best agreement was found within basins in which maximum annual SWE is less than 200 mm, and forest fraction is less than 20%. Next, a sensitivity analysis was conducted to evaluate the microwave signal response to spatially distributed wet snow using a loosely-coupled snow-emission model. The results over an area approximately the size of a microwave pixel found a near-linear relationship between the microwave signal response and the percent area with wet snow present. These results were confirmed by evaluating actual wet snow events over a nine year period, and suggest that the microwave response provides the potential basis for disaggregating melting snow within a microwave pixel. Finally, a similar sensitivity analysis conducted in six watersheds with diverse landscapes and snow conditions confirmed the relationship holds at a basin scale. The magnitude of the microwave response to wet snow was compared to the magnitude of subsequent discharge events to determine if an empirical relation exists. While positive increases in brightness temperature (T_B) correspond to positive increases in discharge, the magnitude of those changes is poorly correlated in most basins. The exception is in basins where snowmelt runoff typically occurs in one event each spring. In similar basins, the microwave response may provide information on the magnitude of spring runoff. Methods to use these findings to improve current snow and snow melt estimation as well as future research direction are discussed.

CHAPTER 1

1.1 INTRODUCTION

The need for accurate, global snow information is long recognized as critical to addressing hydrologic questions (Pope, 2014). Melting snow provides an essential source of water in many regions of the world and can also contribute to devastating, wide-scale flooding. Snow water equivalent (SWE), or the volume of water contained in the snowpack, and snow melt are important hydrologic variables for estimating storage availability and the magnitude and timing of runoff. Water management requires accurate, timely estimates for resource allocation and flood forecasting. Currently, real-time estimates of SWE and snow melt are available from ground observations, numerical modeling and remotely sensed data. While none of these methods individually provides snow data with the necessary accuracy and resolution to meet those requirements globally, a combined, multi-sensor modeling approach may be a viable solution. Remote sensing in particular is well suited to addressing the difficult problem of estimating spatially distributed snow characteristics, but requires extensive investigation and validation. The objective of this research is to investigate the potential for passive microwave remotely sensed data to characterize snow and snow melt and inform snow-emission models, with a specific emphasis on the utility to water resource applications.

All snow estimation methods are subject to uncertainty, and validation of snow distribution and evolution can be challenging given the heterogeneous and dynamic nature of snow, and the varying resolutions of measurements. Ground observations, essential for validation, are accurate at a point scale, but cannot capture the spatial variability of snow processes over a landscape or watershed scale. Ground observations can also be costly and expansion of ground observing networks is unlikely given constrained budgets. Numerical modeling has often been used to

successfully simulate spatial variability in regions with sufficient input data (e.g. Clark et al. 2011; Girotto et al. 2014), but suffers in data sparse regions.

Snow melt evolution is particularly difficult to characterize because most measurement techniques result in the destruction of the snowpack (Mitterer et al 2011). That said, recent research has improved our understanding regarding the spatial distribution of the melt process across a landscape (Egli et al., 2012; Ide and Oguma, 2013; Grunewald et al. 2010). For hydrological purposes, an accurate distribution of melt is essential for estimating the correct runoff response (Lundquist and Dettinger 2005). In addition, a better understanding of the spatial distribution of snowmelt will provide insight into important ecological and biogeochemical processes (Bales et al., 2006).

Remotely sensed passive microwave data offers a potentially viable way of detecting SWE and snow melt processes across a distributed landscape (Schmugge et al. 2002). Global datasets of recorded passive microwave emissions, providing non-destructive, daily information on snow processes, have been available since the late 1970s. Data are available at a high temporal rate (twice daily) and relatively coarse spatial resolution (~ 25 x 25 km pixel size). However, they are not without challenges largely due to significant uncertainty caused by some land surface and snow characteristics (Byun & Choi 2013; Clifford 2010). Considerable research has been done to evaluate these data for accuracy and utility in sensing snow. This work aims to contribute to that body of research by evaluating the passive microwave potential to estimate SWE and snow melt across diverse regions and conditions, focusing on hydrologic validation metrics.

1.2 BACKGROUND

Snow acts as a natural storage of water during the winter months and can have a large impact on the annual water budget, contributing to drought in low snow years and floods during periods of

rapid snowmelt (USACE 1956). Discharge from snowmelt can affect hydrologic patterns in high-latitude regions, resulting in a large percentage of annual runoff occurring during the spring melt period. Before solid snow can to turn to liquid water, energy first goes into warming the snowpack to an isothermal state at the melting point of ice. Liquid water in the snowpack must exceed the maximum storage capacity of snow, estimated between 5-10% (Albert & Krajeski 1998), before it is released to infiltrate the ground or contribute to overland flow. Typically solar radiation initially melts surface snow which percolates downward through the snowpack during the day and refreezes at night, resulting in a diurnal signal in the streamflow. As temperatures warm, continuous daytime and nighttime melt produces the bulk of spring snowmelt runoff, which can last for weeks or months depending on the region and the snow mass. Rain can add energy to a ripe snowpack resulting in widespread melting and additional runoff.

Space-borne microwave sensors have been used to estimate snow depth, SWE and snow wetting due to the sensitivity of the emission signal to snow, primarily at 37 GHz (Schmugge 2002). The measurement unit of the microwave emissions is the brightness temperature (T_B) in Kelvins, which in the microwave spectrum is equal to the surface temperature times the emissivity at a particular frequency. Snow crystals cause upwelling radiation to scatter in dry snow as a function of snow depth and other snow properties such as grain size and density (Chang et al 1982). The microwave signal is also highly responsive to snow wetness due to the sensitivity of the radiance to changes in the dielectric constant (Ulaby et al., 1986). Estimation of SWE from T_B data can be made using empirical relationships or microwave emission models. Empirical methods typically rely on statistical relationships between experimental observations of SWE, snow melt and microwave emissions. In contrast, microwave emission models use a physics-based approach to relate snowpack characteristics to microwave radiation. Emission models

require detailed snowpack information that currently makes them difficult to apply globally, though are useful for evaluating the local, subpixel characteristics.

1.2.1 Empirical Models

SWE retrieval algorithms typically rely on empirical relationships between SWE and the difference between two microwave frequencies (Chang et al., 1987). The 37 GHz frequency is sensitive to the presence of snow, but also impacted by the underlying soil conditions, such as frozen ground and soil moisture (Chang 1982). Therefore a lower frequency that is nominally affected by the snow (approximately 19 GHz) is used to remove the effects of soil state from the 37 GHz signal, such that

$$SWE = c(T_{B,19} - T_{B,37}) \quad (1)$$

where SWE is in mm; T_B is the brightness temperature at different frequencies (K); and c is an empirical conversion coefficient, given as 4.8mm/K. More recently, algorithms have taken into account forest fraction and density variations in their SWE estimations (Kelly et al., 2009; Tedesco & Narvekar 2010). Because naturally emitted microwaves are affected by snowpack properties other than SWE, such as grain size, density, depth, temperature and liquid water content (Chang et al., 1987), the accuracy of satellite SWE algorithms vary regionally (Mote et al., 2003; Derksen et al., 2003). Despite the limitations, empirically-based passive microwave products provide a unique spatially and temporally consistent global SWE product.

1.2.2 Microwave Emission Models

An alternative to the empirically-based satellite SWE products is to assimilate satellite radiance data directly into a coupled snow-microwave emission model. This approach has been investigated to improve simulated snow estimates using meteorological forcing data alone

(Durand et al 2009). A microwave emission model coupled with a physically-based snow model numerically simulates the emission and scattering effects of snow on the microwave emission signatures at various frequencies. These models rely on accurate information about the snowpack including density, temperature, liquid water content and snow grain size, which can be obtained from direct observations or through simulation.

At a point scale, emission models have successfully characterized the scattering of microwave radiance through snow (Weissman & Matzler 1999; Vachon et al 2010), though additional research is needed to reduce uncertainty over a large, heterogeneous region. Several studies indicate the necessity of a multi-layer physically-based model to resolve the snow information from radiance data (Durand et al. 2008; Andreadis and Lettenmaier 2012). However, increased model complexity can also introduce error if validation is not possible. Kang and Barros (2012a, b) investigated the potential use of a coupled model to simulate SWE in data sparse regions and found that SWE estimates improved even with a single layer snow model.

1.2.3 Effect of wet snow on microwave emissions

The presence of water within a snowpack increases the emissivity measured at higher frequencies due to an increase in the dielectric constant (Walker and Goodison 1993, Matzler 1987, Davis et al. 1987). This effect eliminates the difference in T_B used to estimate SWE in empirical methods (Figure 1). The strong signal response to water content has the potential to identify periods of snowmelt (Stiles and Ulaby 1980, Kunzi et al. 1982, Drobot and Anderson 2001). During wet snow periods, the signal response provides a clear indication of increased liquid water content, which overwhelms other snowpack properties impact on the microwave signal (Wang et al. 2001).

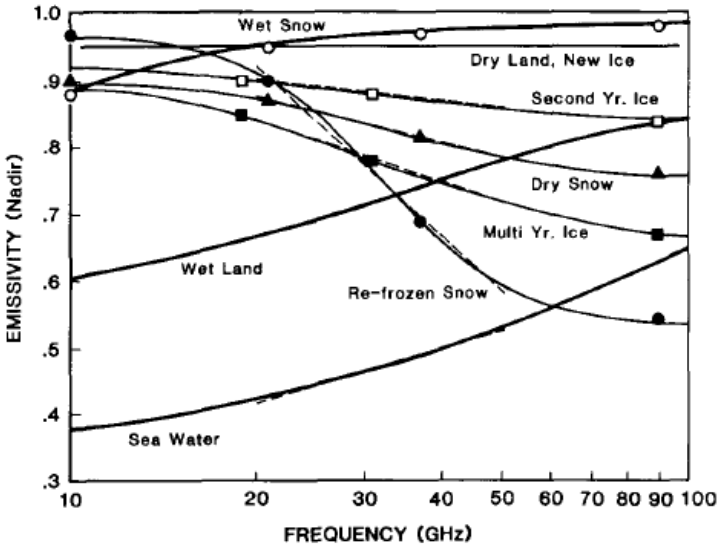

Figure 1. Microwave emissivity for various snow conditions and other surfaces (from Grody, 1988).

Several studies have investigated using this response to determine the melt onset date (Drobot and Anderson 2001; Ramage et al 2006), or identifying rain-on-snow (ROS) events (Grenfell and Putkonen 2009). Others have linked the microwave response at a coarse resolution to basin runoff and shown potential for hydrologic applications (Yan et al 2009; Vuyovich & Jacobs 2011; Ramage & Semmens 2012). A key challenge to using the microwave melt signal is that its spatial resolution is quite coarse and the ability to explicitly characterize subgrid scale variations needed for most water resource applications has not been demonstrated.

1.2.4 LINKING THE PASSIVE MICROWAVE DETECTION OF WET SNOW TO DISCHARGE

While methods have been successful in detecting the onset of snowmelt or melt events caused by rain-on-snow using microwave data, they relate only qualitatively to the hydrologic response. No previous research has investigated the relationship between the spatial extent of snowmelt as observed by passive microwave and discharge. Additionally, it may be possible to resolve the sub-pixel variation in snow state represented in the microwave data. This is important because the spatial distribution of snowmelt influences the hydrologic response of the basin, resulting in different peak flows and timing depending on the contributing area and the characteristics of the

snow. Travel time for water to reach the basin outlet includes time through the snowpack, time for overland or subsurface flow to reach the channel and travel time along the channel itself (Lundquist and Dettinger 2005). Linking the liquid water content (LWC) of the snowpack to discharge requires an understanding of the snowpack characteristics as well as the spatial variability of snow properties on the basin scale (Grayson et al., 2002).

1.3 OBJECTIVE

The objective of this research was to improve snowmelt runoff estimates using passive microwave data. This research was conducted in three parts. The first step, described in Chapter 2, is a broad assessment of the current passive microwave SWE products across diverse regions and conditions in comparison to modeled estimates. The second step, described in Chapter 3, is a sensitivity analysis to determine how heterogeneous distributions of wet snow impact microwave emissions at a pixel scale. Finally, in Chapter 4 the results of the sensitivity analysis are evaluated on a basin scale. The relationship between the microwave response to wet snow and discharge under varied conditions is assessed. Chapter 5 summarizes the main findings of this work and describes future direction.

CHAPTER 2 COMPARISON OF PASSIVE MICROWAVE AND MODELED ESTIMATES OF TOTAL WATERSHED SWE IN THE CONTINENTAL UNITED STATES[1]

2.1 INTRODUCTION

Snow is an important source of water in many temperate regions of the world. In the mountainous, western United States, snowmelt accounts for up to 75% of the annual streamflow [Doesken and Judson 1996, Daly et al., 2001]. Other regions of the US, for example the Great Plains, do not rely as heavily on snow for water supply, but can still experience significant flooding as a result of snowmelt [Todhunter 2001, USACE 2012]. Water management in these regions requires accurate, timely estimates of snow water equivalent (SWE) for resource allocation and flood forecasting. However, validation of SWE estimates can be challenging given the heterogeneous and dynamic nature of snow, and the varying resolutions of measurements.

Satellite-based passive microwave sensors could provide spatially-distributed snowpack information, particularly in remote, data-sparse regions because they have a twice-daily temporal resolution and the ability to see through clouds and at night. However, known sources of error prohibit the operational use of this data set in many regions. In regions where heavy vegetation and significant snowpack depths do not impact the data, studies have shown promising results in the passive microwave estimates of SWE [Dong et al. 2005]. In the Great Plains of the United States and the Canadian Plains where the algorithms were developed, SSM/I SWE compares

[1] Vuyovich, C.M., Jacobs, J.M., & Daly, S.F. (2014). Comparison of passive microwave and modeled estimates of total watershed SWE in the continental United States. Water Resources Research, 50, 9088-9102

well to ground observations [Derksen et al. 2003, Mote et al. 2003, Chang et al. 2005]. Tait [1998] compared passive microwave SWE estimates to ground observations in the United States and Russia, categorized by land-cover, and found good agreement in non-forested, flat regions when wet snow or depth hoar was not affecting the microwave signal. Vuyovich and Jacobs [2011] found that passive microwave data provided reasonable estimates of SWE in the Upper Helmand Watershed in central Afghanistan. Modeled snowmelt runoff estimates from this basin improved when initialized with passive microwave SWE estimates as compared to using available observational and satellite-based meteorological data alone.

Passive microwave SWE retrieval algorithms have typically relied on empirical relationships between either snow depth or SWE and frequency dependent signal scattering through the snowpack at different channels [Chang et al. 1987]. An estimate of the SWE is obtained by taking the difference between the return signals at two different passive microwave frequencies: a low frequency, typically 18-19 GHz, where scattering by snow is less than at a high frequency, typically around 37 GHz, and applying a coefficient derived from radiative transfer theory. Several sources of error in microwave SWE retrievals stem from the dynamic nature of snow and the static assumptions made in the empirical formulations concerning snow properties. Studies have shown emission signatures to be affected by snow depth [Dong et al. 2005, Foster et al. 2005]. It is estimated that the signal "saturates" at 1 m depth (or approximately 250 mm SWE), above which soil emissions through the snowpack at the higher frequency microwave signal are no longer detectable [Clifford 2010]. Liquid water in the snowpack is significantly more absorptive than ice at the microwave frequencies [Mätzler 1987] and eliminates the brightness temperature (T_B) gradient used to estimate SWE [Hallikainen et al. 1986, Walker and Goodison 1993]. Therefore, many studies avoid evaluating passive microwave data during the spring, when

snow melt and rainfall can introduce error in the data. Other snowpack characteristics such as density and crystal size also affect the passive microwave signal by increasing the spectral gradient with increases in grain growth [Foster et al. 1999, Hall et al. 1986, Josberger and Mognard 2002, Durand et al. 2011].

Mätzler and Standley [2000] suggested that topography of the ground has a significant impact on microwave retrievals. However, other studies found little or no evidence of error due to elevation gradients over large regions [Dong et al. 2005, Vuyovich and Jacobs 2011]. It is possible that errors due to terrain are averaged out over large pixel areas or that in high elevation regions more significant error is caused by the saturation of the signal in deep snow. Several studies have shown a significant impact of vegetation on the passive microwave signal because the liquid water in the tree branches and leaves emits microwave radiation [Chang et al. 1996, Foster et al. 2005, Derksen et al., 2005]. Vander Jagt et al. [2013] found that in pixels with significant vegetation, the error in the passive microwave estimate was on the same order of magnitude as the actual snow depth, making the data virtually unusable. Ongoing research, which has attempted to account for these errors and to improve results regionally and seasonally, has had varied success [Farmer et al. 2010, Tedesco and Narvekar 2010, Mizukami and Perica 2012].

The NWS National Operational Hydrologic Remote Sensing Center (NOHRSC) offers a near real-time 1 km^2 spatially distributed estimate of SWE and other snow properties across the continental United States (CONUS) through its SNOw Data Assimilation System (SNODAS). SNODAS integrates a combination of downscaled forcing data, an energy balance snow model and assimilated observations in their daily gridded SWE product to arrive at their best estimate of the snow characteristics over the United States and to minimize error associated with any

individual method [Carroll et al. 2006]. Though these data are also subject to errors, this product provides the only real-time spatially distributed estimate of snowpack conditions throughout the U.S. and is used operationally at several locations [e.g. Lea and Reid 2006, Schneiderman et al. 2013]. The snow model within SNODAS has been evaluated and generally shown to provide good results at a point scale [Rutter et al. 2008, Frankenstein et al. 2008], though over a larger scale, particularly where ground observations are sparse or biased, additional error is introduced [Molotch and Bales, 2005; Meromy et al., 2013]. In the Sierra Nevada, Rittger et al. [2011] and Dozier [2011] showed that SNODAS estimates of SWE are less than reconstructed SWE values and spring runoff volumes, while Guan et al. [2013] found that a blended estimate of reconstruction and ground observations provided the best results. Clow et al. [2012] used field surveys and water balance analysis to evaluate SNODAS SWE in headwater basins in Colorado. They found good agreement in forested areas, but poor agreement in areas impacted by wind redistribution of the snowpack.

A few previous efforts to evaluate the passive microwave estimates of SWE have used the SNODAS product for comparison. Azar et al. [2008] evaluated the SSM/I SWE products in the Great Lakes region using the SNODAS data and found poor results using the original passive microwave algorithm. Tedesco and Narvekar [2010] compared monthly estimates of AMSR-E SWE to SNODAS (resampled at 25km) over the 2004-05 winter season, and found poor correlation when evaluating the entire U.S. They also classified the pixels by forest cover fraction and found better correlations in areas of higher forest fraction and density, which they attributed to shallow snow in the open areas.

This study aims to provide a comprehensive examination of the regional characteristics associated with satellite observations of SWE at a scale useful for water resource applications in

the United States. We hypothesize that existing microwave retrieval algorithms will compare favorably to the SNODAS SWE estimates in basins which have minimal vegetation or topography and where the snow depth does not exceed a saturation threshold. To test this hypothesis, we analyzed the SWE estimates derived from two satellite sensors, AMSR-E and SSM/I, and the SNODAS daily gridded SWE by watersheds across the U.S. to evaluate the value of these snow data in hydrologic processes. Comparison at the basin-scale also provides future opportunity to evaluate the SWE in conjunction with watershed runoff. There are several questions this research aims to answer:

1. In which U.S. basins do passive microwave estimates of SWE compare well to the SNODAS product as evaluated by correlation and rank-order of the peak SWE and seasonal snowpack evolution?
2. Is the level of agreement a function of forest cover, elevation or maximum SWE?
3. In basins where passive microwave SWE does not match the magnitude of SNODAS data, is there a common pattern of snow accumulation and melt, year-to-year variability, or relative magnitude?

2.2 Study Area and Data

For this study, the SWE products were compared by major hydrologic regions of the continental U.S. The USGS fourth level basins, designated by an eight digit Hydrologic Unit Code (HUC), were selected for comparison. There are 2,100 HUC-8 basins, with an average area of 3,700 km^2. The elevation range within each of the HUC-8 basins was determined using the USGS 1 arc-second (approx. 30 m) national elevation dataset (NED) (data available from the USGS). The Vegetation Continuous Field from the University of Maryland [Hansen et al. 2006] was used to estimate the percentage of forest cover by HUC. In addition, regional comparisons were made

using the 18 USGS first level basins, designated by a two digit HUC, which have an average area of 434,000 km^2 (Figure 1).

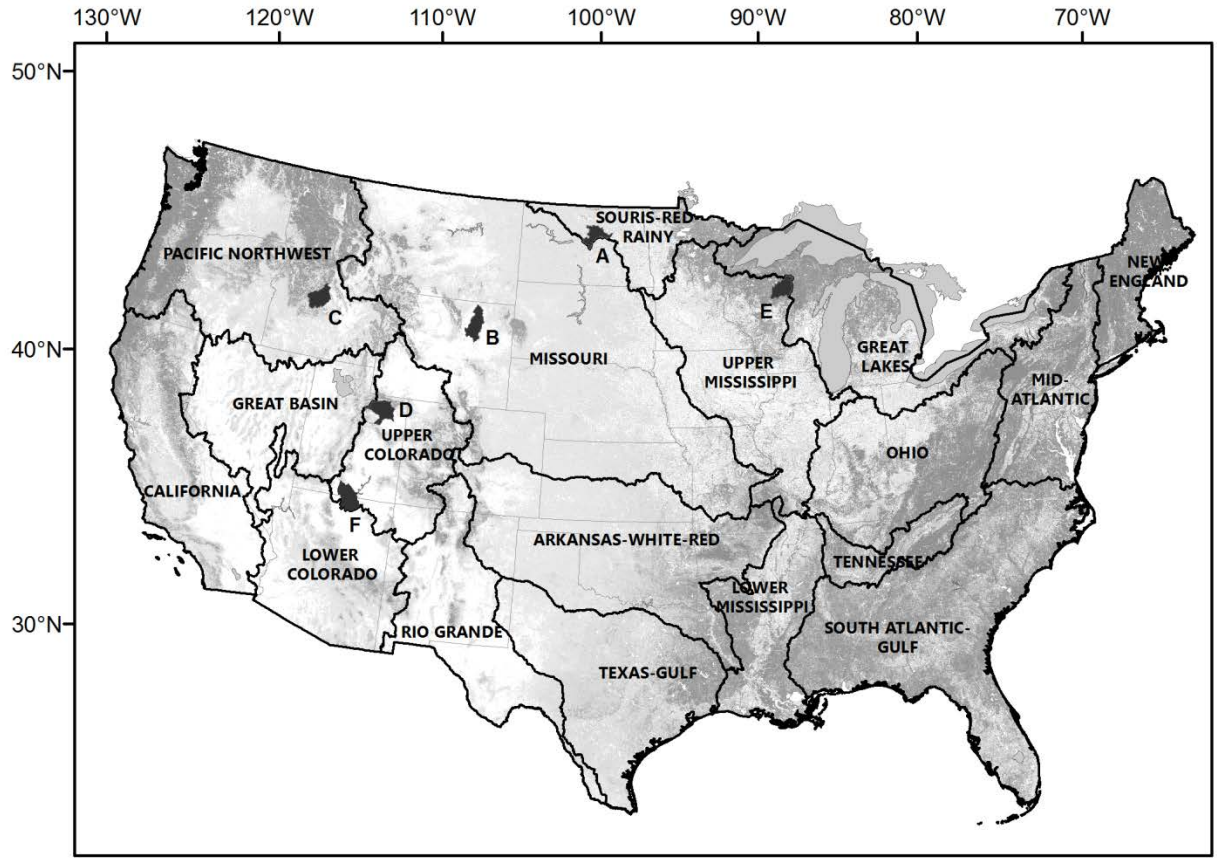

Figure 1. Overview map of the study region with HUC2 watersheds outlined and percentage forest cover shown. Example watersheds are shown in black and labeled.

2.2.1 PASSIVE MICROWAVE

Daily passive microwave SWE data were available from two sources during the period of comparison; the Special Sensor Microwave/Imager (SSM/I) and the Advanced Microwave Scanning Radiometer – Earth Observing System (AMSR-E). The SSM/I sensor was launched in 1987 on board the Defense Meteorological Satellite Program (DMSP) satellites. These data are available near real-time and have the advantage of a long historical record. SWE estimates are derived from the SSM/I brightness temperatures measured at wavelengths 19 and 37 GHz, and

have a spatial resolution of 69x43km (19.4 GHz) and 37x29km [Armstrong et al. 1995]. SSM/I data were processed using the Chang algorithm:

$$SWE = c(T_{B,19} - T_{B,37}) \quad (1)$$

where SWE is in mm; T_B is the temperature brightness at different channels (K); and c is typically given as 4.8mm/K and acquired from the National Snow and Ice Data Center (Mary Jo Brodzik, NSIDC, personal communication, 2012).

AMSR-E was launched on NASA's Aqua satellite in 2002 and calculates SWE based on brightness temperatures measured at wavelengths 19.7 and 36.5 GHz, with a spatial resolution of 28x16km (19.7 GHz) and 14x8km (36.5 GHz) [Kelly 2009]. For this study, AMSR-E data were acquired from NSIDC (http://nsidc.org/data/AE_DySno), which was processed using the Kelly [2009] algorithm. That process uses additional bands at 10 and 89 GHz to aid in the detection of deep and shallow snow, respectively, and the algorithm accounts for the forest fraction of the underlying ground,

$$SD = ff\left[p1\frac{(T_{B,V18} - T_{B,V36})}{(1 - b * fd)}\right] + (1 - ff)\left[p1(T_{B,V10} - T_{B,V36}) + p2(T_{B,V10} - T_{B,V18})\right] \quad (2)$$

where *SD* is snow depth (cm), *ff* is forest fraction, *fd* is forest density, *b* is an optimized coefficient found to be 0.6, and *p1* and *p2* are dynamic coefficients calculated as the difference in polarization at channels 36 and 18, respectively. Snow depths are then converted to SWE using seasonal density estimates for different snow classes based on Sturm et al [1995].

SSM/I and AMSR-E global SWE products are produced using these algorithms and available twice daily; ascending passes which occur in the afternoon and descending passes which occur in the early morning. For this study, only descending SWE data were used to reduce the potential

wet snow impacts in the afternoon. A gap in the satellite swath coverage can occur every 3 to 4 days, depending on the latitude of the region. This study uses the products' EASE-grid projection at a 625 km^2 (25 km x 25 km) resolution.

2.2.2 SNODAS

The NOAA's SNODAS combines data from various sources – ground observations, airborne and satellite estimates – with model results, to arrive at a 1-km^2 spatially distributed estimate of snow cover and SWE [Carroll et al., 2006]. Their procedure follows three main steps; ingest and downscale model weather data, simulate snow cover using a physically based energy balance model, and assimilate snow observations to adjust model results. Forcing data come from the Rapid Update Cycle 2 (RUC2) Numerical Weather Prediction (NWP) model output and is downscaled from 13 km to 1 km resolution using a digital elevation model. The snow model is an energy- and mass-balance, multi-layer model based on SNTHERM.89 [Jordan 1990]. Assimilated observations are acquired from state and federal automated ground observations, snow surveys, and gamma flights as well as satellite-based snow extent information. SNODAS data are available through NSIDC from 01 October 2003 through the present (http://nsidc.org/data/G02158).

2.3 METHODS

Gridded daily SWE data from the two passive microwave sensors and SNODAS were obtained for eight water years, 2004 – 2011, when all three datasets were available. For each of the AMSR-E, SSM/I and the SNODAS SWE datasets, the gridded data were aggregated by HUC-8 to produce a daily time series of average-basin SWE. To avoid large gaps along the watershed boundaries, the passive microwave data were re-sampled to 1 km^2 grid cells using the nearest neighbor method which assigns the same value to the pixel as the data layer in that location

without any interpolation. AMSR-E pixels near large water bodies are flagged within the SWE product and no SWE value is given; therefore only watersheds with no missing data were used in the comparison. Weekly SWE time series were developed for each HUC-8 using the maximum weekly values in order to accommodate the satellite overpass cycle which results in some days without satellite observations. Annual maximum SWE values by HUC were extracted from the weekly time series for each of the eight water years. The results are summarized regionally by aggregating results to the 18 two digit HUCs.

The average, maximum, minimum and standard deviation of the daily SWE was determined for each HUC over the periods of interest. The differences in average annual maximum SWE were calculated between the SNODAS and passive microwave datasets to determine the difference in relative magnitude of the estimates. The correlation coefficients between microwave SWE and SNODAS estimates for the annual and weekly time series were also calculated. Differences between SNODAS and the microwave values of annual maximum SWE values were identified using the Spearman's rank-order test. Spearman's rank-order test determines whether two independent groups are from the same population [Helsel and Hirsch, 2002]. To evaluate spatial variability within the HUC-8s, the SNODAS data were aggregated to the 25 km by 25 km pixel scale using a pixel average. The standard deviation of SNODAS SWE with each HUC-8 was then calculated similarly to the passive microwave data in order to compare the data at the same coarse resolution.

Weekly SWE results were compared using the Nash-Sutcliffe model efficiency index [Nash and Sutcliffe, 1970], which measures the fit between predicted and observed values as

$$Efficiency = 1 - \left(\frac{\sum_{i=1}^{N} (SWE_{obs,i} - SWE_{sat,i})^2}{\sum_{i=1}^{N} (SWE_{obs,i} - \overline{SWE}_{obs,i})^2} \right) \quad (3)$$

where N is the number of weeks during the simulation period, $SWE_{obs,i}$ is the SNODAS i-th weekly SWE, $SWE_{sat,i}$ is the i-th weekly SWE value estimated from the AMSR-E or SSM/I dataset, and $\overline{SWE}_{obs,i}$ is the mean weekly SNODAS SWE value for the simulation period. This metric characterizes the joint evolution of passive microwave and modeled SWE over the entire winter rather than just the peak SWE. While the SNODAS data were used as the observational dataset in this measure, it is important to note that the model itself has errors and is not considered ground truth. The efficiency will approach unity if each SNODAS weekly SWE value matches the remotely sensed weekly SWE value.

The effects of saturation depth, elevation range and forest cover on SWE estimates were evaluated by calculating correlations between SNODAS and passive microwave average maximum SWE for each HUC-8 by category. The saturation depth was assessed by comparing passive microwave to SNODAS at increasing amounts of average maximum annual SWE. The elevation range was evaluated to address the impact of topography on SWE estimates, and was calculated for each HUC-8 as the difference in maximum and minimum elevation in each basin. Correlations between the passive microwave and SNODAS SWE were determined for 8 elevation range categories. Correlations were also determined for SWE estimates by 10% increments in total basin forest fraction.

2.4 Results and Discussion

2.4.1 Overall Performance

The agreement between average annual maximum SWE for the SNODAS product and the AMSR-E and SSM/I passive microwave data varies widely across regions of the United States (Figure 2). As anticipated, the passive microwave data underestimate the SWE for those regions that experience significant annual snowpacks including the Rocky Mountains, the Pacific Mountain Range and Northern New England. The saturation effect appears to be evident when SWE from SNODAS exceeds 150 to 200 mm. For the western ranges, the snowpacks' SWE frequently exceeds 500 mm based on the SNODAS product. AMSR-E is able to identify the location of those ranges as having relatively deeper snow, but greatly underestimates the SWE magnitude. SSM/I entirely misses many of these deep snow features. This result broadens Andreadis and Lettenmaier's [2006] finding that passive microwave data are problematic when snowpacks were deeper than 240 mm for Snake River basin in the western U.S. A new finding is that this disagreement is also broadly evident for those regions in the Northeast in which SWE exceeds 240 mm. In the Northeast region, the AMSR-E data shows better agreement to the SNODAS product than SSM/I which reports little to no snow. This result extends the modest agreement found previously in the Northeast region, which only analyzed a single, historic storm in the Middle Atlantic [Foster et al. 2010].

Interestingly, the passive microwave data are not consistently less than the SNODAS product. In the Plains regions and the southeastern portions of the U.S., microwave SWE products indicated greater maximum annual SWE values than SNODAS (Figure 3). This is a region with relatively few observational data available to correct the SNODAS model. Because both microwave products have deeper snowpacks in the northern Plains region, the actual SWE may be underestimated by SNODAS. This theory is supported by previous work by Josberger et al. [1998] who suggest that the northern Great Plains region is well suited for estimation of SWE

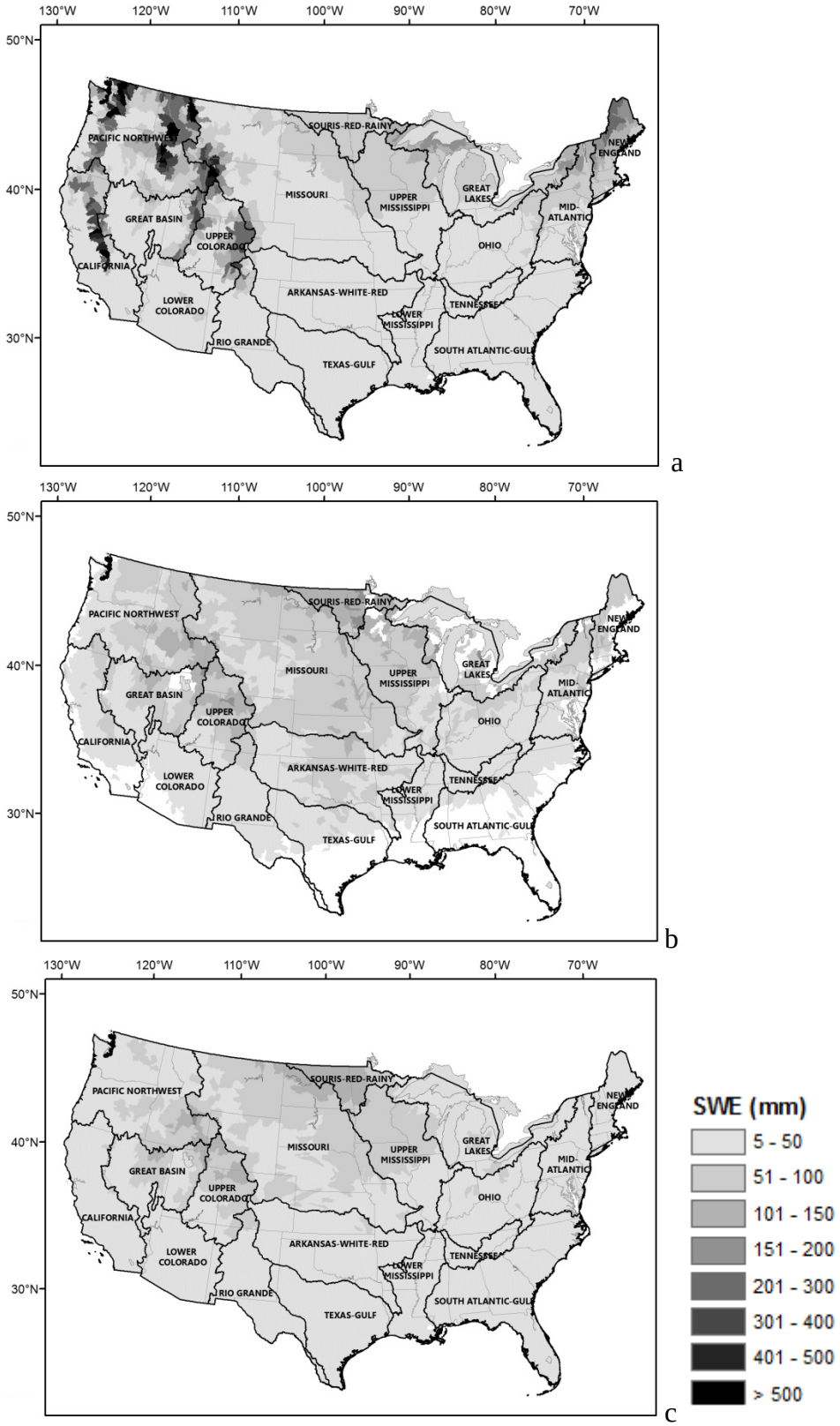

Figure 2. Average maximum annual SWE by HUC8 for (a) SNODAS, (b) AMSR-E and (c) SSM/I.

from microwave observations. In this same region, Chang et al. [2005] showed that the midwinter microwave estimates of snow depth had a calculated error of 88 mm, but also pointed to the strong heterogeneity of snow depth across the region which made validation quite difficult.

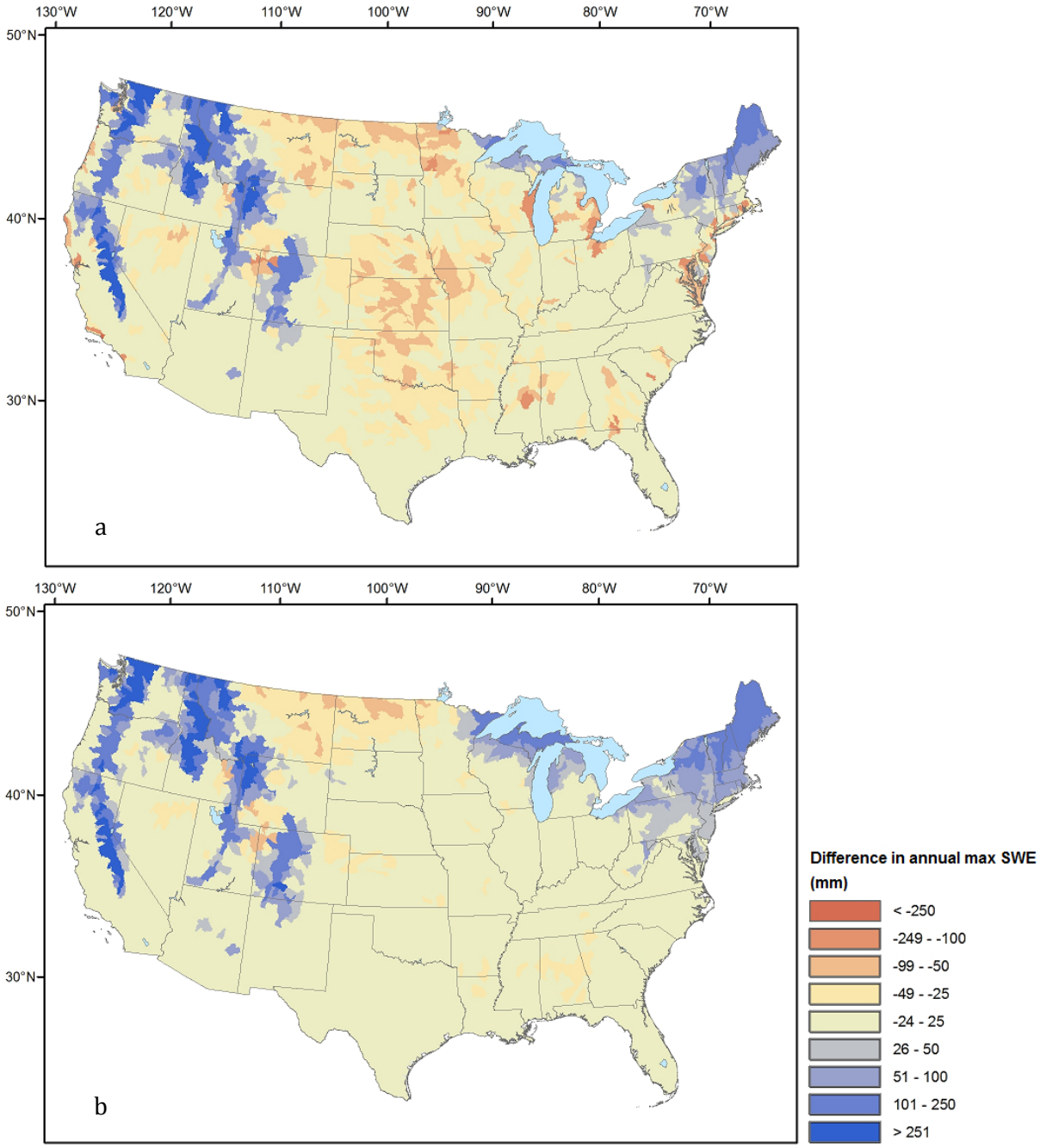

Figure 3. Difference in average maximum annual SWE by HUC8 for (a) SNODAS – AMSR-E, and (b) SNODAS - SSM/I.

In the southern Plains, the SNODAS SWE values are consistent with the SSM/I SWE values but overestimated by the AMSR-E observations. The AMSR-E data appear to be biased high in shallow snow regions, particularly in the southern Plains. A nominal 50 mm snow depth is applied when the AMSR-E algorithm detects shallow snow [Kelly, 2009]. Armstrong and Brodzik [2002] found that inclusion of the shallow snow detection algorithm led to overestimation of SWE in some regions. Daly et al. [2012], similarly found early-season SWE detection by AMSR-E in Afghanistan was not supported by multispectral imagery of snow extent.

In regions with significant SWE biases, the relative SWE magnitude across years may still be robust and able to provide insight for water resource management. Parametric and nonparametric methods were used to characterize the correlation of the annual maximum time series between the SNODAS data and each of the passive microwave datasets (Table 1). The strongest and significant correlations between SNODAS and the AMSR-E and SSM/I products occur in the northern Plains region (Upper Mississippi and Missouri) and in the southern Rocky Mountains (Lower Colorado). SNODAS and the AMSR-E SWE estimates also show good agreement along the Great Lakes region (Ohio), while the SSM/I data are well correlated with SNODAS in the

Table 1. HUC-2 Data and Average annual maximum SWE Statistics (N = 8). Bold indicates statistically significant values where critical values are R^2 equal 0.46 and Spearman's ranked correlation coefficient equal 0.738.

HUC2	Region	Area (x 10^3 km^2)	Forest Fraction	Elev. Range (m)	NOAA Avg Annual Max SWE (mm)	AMSR-E Avg Annual Max SWE (mm)	SSM/I Avg Annual Max SWE (mm)	NOAA and AMSR-E R^2	NOAA and SSM/I R^2	NOAA and AMSR-E Sp. Rho	NOAA and SSM/I Sp. Rho
1	New England Region	158	0.81	1856	118.3	30.1	10.4	0.26	0.15	0.40	0.24
2	Mid Atlantic Region	288	0.73	1511	45.9	23.8	11.9	0.35	**0.79**	**0.86**	**0.95**
3	South Atlantic-Gulf Region	698	0.55	1765	4.3	2.7	5.9	0.08	0.14	0.26	-0.02
4	Great Lakes Region	303	0.42	1200	70.8	32.6	25.4	**0.62**	0.24	**0.83**	0.24
5	Ohio Region	422	0.67	1591	28.2	21.2	13.0	0.37	**0.63**	0.48	0.69
6	Tennessee Region	106	0.90	1849	11.4	10.6	13.8	0.01	0.02	0.67	0.48
7	Upper Mississippi Region	492	0.10	593	46.9	42.0	43.0	**0.63**	0.75	**0.76**	0.83
8	Lower Mississippi Region	262	0.45	822	6.8	8.7	8.4	**0.47**	0.22	0.60	0.38
9	Souris-Red-Rainy Region	154	0.14	521	76.6	95.4	93.1	0.24	**0.53**	0.48	0.52
10	Missouri Region	1324	0.12	4106	39.0	42.6	39.5	**0.66**	**0.65**	0.62	0.57
11	Arkansas-White-Red Region	642	0.25	4233	16.2	21.4	13.4	0.10	**0.67**	0.43	0.76
12	Texas-Gulf Region	464	0.12	1449	4.2	8.2	5.6	0.11	0.13	0.19	0.60
13	Rio Grande Region	344	0.09	4096	16.4	15.1	7.8	0.13	**0.64**	0.17	**0.74**
14	Upper Colorado Region	293	0.27	3204	81.4	62.7	53.1	0.41	0.14	0.57	0.38
15	Lower Colorado Region	363	0.11	3687	14.5	13.3	7.2	**0.65**	**0.97**	**0.76**	**0.90**
16	Great Basin Region	368	0.09	3536	53.0	47.0	36.3	0.09	0.03	0.45	-0.02
17	Pacific Northwest Region	710	0.49	4403	141.4	43.4	30.5	**0.54**	0.30	0.62	0.57
18	California Region	417	0.31	4350	64.7	13.2	7.6	0.09	0.01	0.60	0.26

Pennsylvania region (Mid Atlantic). For many of the regions, there is not a significant correlation suggesting that either passive microwave or SNODAS SWE estimates are not accurate in that region or that the two methods provide different information.

Based on the Spearman's rank-order statistic, AMSR-E and SSM/I are not able to capture the relative magnitude of the annual peak SWE for the Upper Colorado, New England, and the Pacific Northwest; the three HUC-2 regions having SWE values higher than 80 mm. The passive microwave data do not seem to capture the relative magnitude of the annual peak SWE when it underestimates the total SWE. Limited agreement is also evident for the four HUCs, Texas-Gulf, South Atlantic-Gulf, Lower Mississippi and Tennessee, having the lowest peak snow values, which could be due to limited observations available impacting the SNODAS results or SWE values below a threshold level for detection by passive microwave.

The standard deviation of estimated SWE within each HUC-8 watershed was calculated daily over the period of record to assess the spatial variability of estimates within each basin. SNODAS data were aggregated to the microwave EASE-GRID pixel size in order to match the microwave scale. Figure 4 shows an example of the results on 01 February 2011. There is greater variability within the deep snow regions along the Pacific mountains and the Rocky Mountains for SNODAS. The AMSR-E data have greater variability than the SSM/I data, particularly in the New England region where the SSM/I data shows none. In the Plains basins, the three data sources compare favorably in most years with the exception of the southern Plains region (e.g. Texas/Oklahoma). In this region, the relatively high variability of the passive microwave data, particularly AMSR-E, result from positive SWE values in pixels where none is likely to exist.

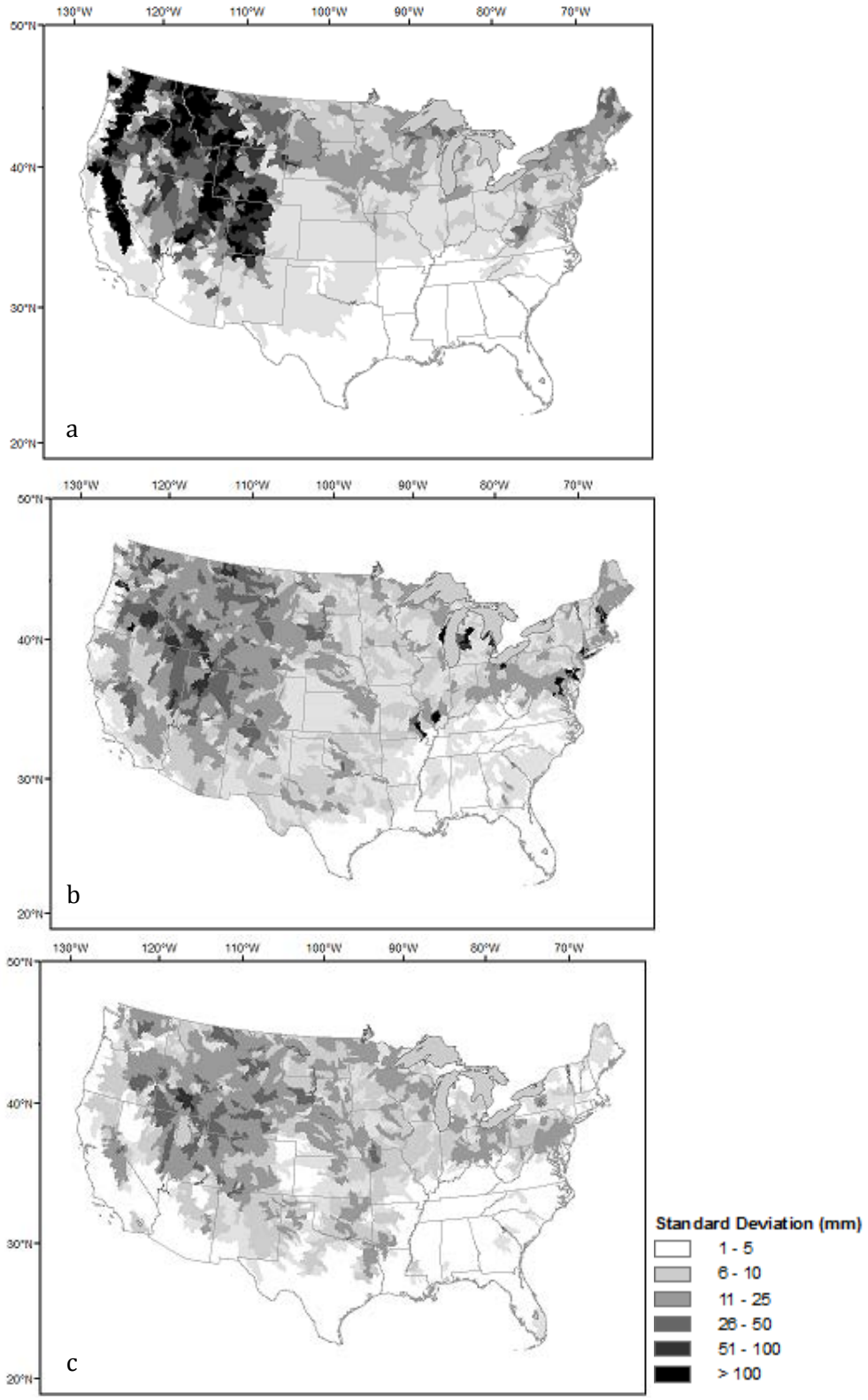

Figure 4. Standard deviation of SWE by HUC8 on 01Feb 2011for (a) SNODAS, (b) AMSR-E, and (c) SSM/I.

The weekly SWE from the microwave products was compared to the SNODAS product using the Nash-Sutcliffe efficiency statistic (Table 2). Strong weekly results are evident for the regions that performed well for interannual variability, e.g. the northern Plains and southern Rockies. Other regions showed promise, such as the Upper Colorado basin, despite having maximum SWE values that might exceed the passive microwave threshold for detection. The passive microwave observations appear to be able to capture the timing of snow accumulation and melt. A region that stands out for the disagreement between SNODAS and passive microwave in the weekly SWE analysis is the central Plains. This region does not have significant vegetation or snow depths that would be expected to impact the microwave signal. It is possible that the SNODAS SWE estimates suffer from lack of observations, though additional work is required to understand the differences seen in this area.

Table 2. HUC-2 Weekly Statistics for winter months: October – April (N = 242)

HUC2	Region	NOAA Avg Weekly SWE (mm)	AMSR-E Avg Weekly SWE (mm)	SSM/I Avg Weekly SWE (mm)	NOAA and AMSR-E Weekly SWE R^2	NOAA and SSM/I Weekly SWE R^2	NOAA and AMSR-E Weekly Nash-Sutcliffe	NOAA and SSM/I Weekly Nash-Sutcliffe
1	New England Region	47.8	11.3	2.4	0.61	0.33	-0.28	-0.85
2	Mid Atlantic Region	13.0	7.0	2.0	0.69	0.43	0.43	-0.30
3	South Atlantic-Gulf Region	0.4	0.3	0.7	0.11	0.00	0.08	-1.44
4	Great Lakes Region	26.8	10.4	5.4	0.71	0.65	0.10	-0.36
5	Ohio Region	5.5	4.0	1.9	0.74	0.50	0.68	0.22
6	Tennessee Region	1.6	1.3	1.0	0.14	0.01	0.01	-0.38
7	Upper Mississippi Region	15.6	14.9	10.9	0.78	0.74	0.77	0.67
8	Lower Mississippi Region	0.6	0.9	0.6	0.04	0.00	-0.34	-0.59
9	Souris-Red-Rainy Region	31.1	32.5	30.7	0.66	0.75	0.62	0.69
10	Missouri Region	17.5	16.9	13.7	0.73	0.76	0.70	0.67
11	Arkansas-White-Red Region	3.2	4.0	2.2	0.48	0.62	0.30	0.58
12	Texas-Gulf Region	0.4	0.7	0.3	0.23	0.07	-0.48	-0.21
13	Rio Grande Region	7.2	4.5	2.2	0.44	0.64	0.27	-0.10
14	Upper Colorado Region	42.4	27.2	20.9	0.67	0.59	0.43	0.14
15	Lower Colorado Region	4.0	3.6	1.2	0.63	0.80	0.62	0.37
16	Great Basin Region	24.3	19.8	12.0	0.60	0.57	0.55	0.20
17	Pacific Northwest Region	73.1	19.6	13.5	0.55	0.55	-0.51	-0.78
18	California Region	27.3	5.3	2.9	0.38	0.45	-0.58	-0.79

Overall, passive microwave derived SWE estimates appear to perform the best when the typical HUC-2 annual maximum SWE values are between 15 and 50 mm. Within this range, there is good correlation for year to year differences and value in the weekly observations. The AMSR-E observations provide SWE estimates that have limited bias as compared to the SNODAS data. At modestly higher SWE values, between 50 and 80 mm, there is a mixture of results with the passive microwave having greater success at matching the snowpack's temporal evolution as compared to the magnitude of the annual maximums.

2.4.2 Effect of Physical Characteristics

The SWE data were analyzed by forest cover, saturation depth and elevation range to determine what impact these factors had on the results. For forest cover, the strongest correlations occur in HUCs with 20% forest coverage or less, with generally poorer correlations occurring with more vegetation (Figure5). The exceptions are along the East coast, where AMSR-E shows good correlations (> 0.5) with SNODAS data in watersheds along the eastern side of the Appalachians, North Carolina up through Virginia, and SSM/I doing well in central Pennsylvania and New York. In the heavily forested regions of New England and around the Great Lakes, both AMSR-E and SSM/I underestimate the maximum SWE values, though AMSR-E performs better than SSM/I. It is expected that these regional differences between the two microwave datasets' results are a function of the retrieval algorithms used. While AMSR-E, unlike SSM/I, accounts for forest fraction in the current algorithm, vegetation type is not included. Azar et al. [2008] were able to improve the SSM/I results in the Great Lakes region by developing an algorithm that uses a Normalized Difference Vegetation Index (NDVI) to classify the mixed use forest in the region.

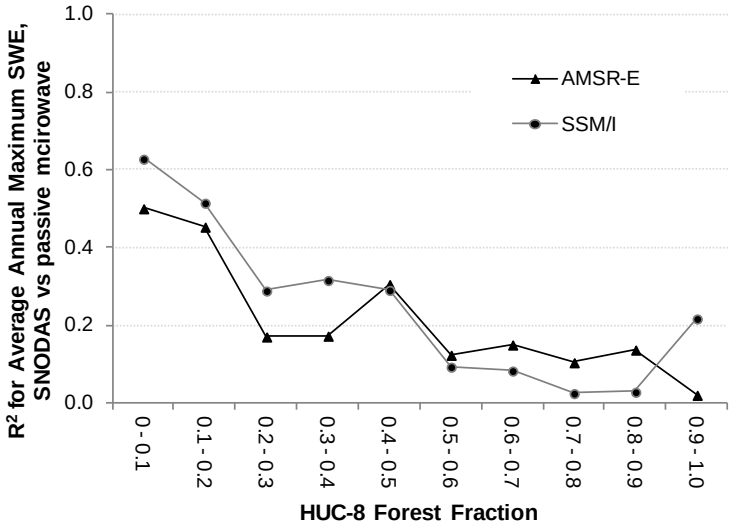

Figure 5. R^2 of average annual maximum SWE in HUC8s by forest fraction

Passive microwave estimates of SWE are best correlated with SNODAS data in regions where the maximum annual SWE values are relatively low and agreement decreases as the SWE increases (Figure 6). In watersheds with an annual maximum SWE less than 100 mm, the SSM/I SWE product is better correlated with SNODAS than AMSR-E. Above 100 mm, AMSR-E has consistently better agreement with SNODAS than SSM/I, though both correlations decrease with increasing snow depth.

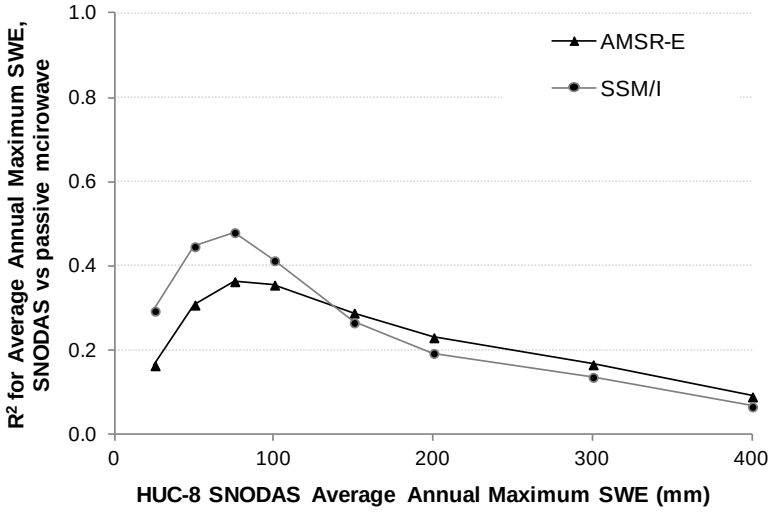

Figure 6. R^2 of average annual maximum SWE in HUC8s for increasing categories of SNODAS SWE

More than half of the eight digit HUCs, or 56% of the total area in the conterminous U.S., have less than 20% forest coverage. For the regions with less than 200 mm annual maximum SNODAS SWE and less than 20% forest cover, the R^2 values between SNODAS and AMSR-E, and SNODAS and SSM/I average annual maximum SWE are 0.48 and 0.66, respectively. Figure 7 shows the R^2 values between SNODAS and the passive microwave weekly SWE for each HUC-8 during the winter months (Oct – Apr). Basins with the best agreement tend to fall outside the areas with greater than 20% forest coverage and greater than 200 mm annual maximum SNODAS SWE, though several basins with weekly correlations greater than 0.5 do reside in those areas.

The analysis of SWE estimates with terrain does not show a consistent relationship between elevation range and correlation of the data. Once basins with greater than 20% forest coverage and a greater than 200 mm average maximum SNODAS SWE were removed, good correlations occur between SNODAS and the passive microwave data despite large changes in topography. Dong et al. [2005] investigated the impacts of topographic roughness on SWE estimates at over 3000 observing stations in Canada, and found no significant impact compared to the effects of deep snow and nearby water bodies. Tong et al. [2010] found that while algorithms performed better in complex terrain when only SWE values less than 250 – 400 mm were considered, the accuracy was still insufficient at a point comparison. At a large watershed scale, the effects of topography are expected to average out, having a minimal effect on error compared to vegetation and snow depth.

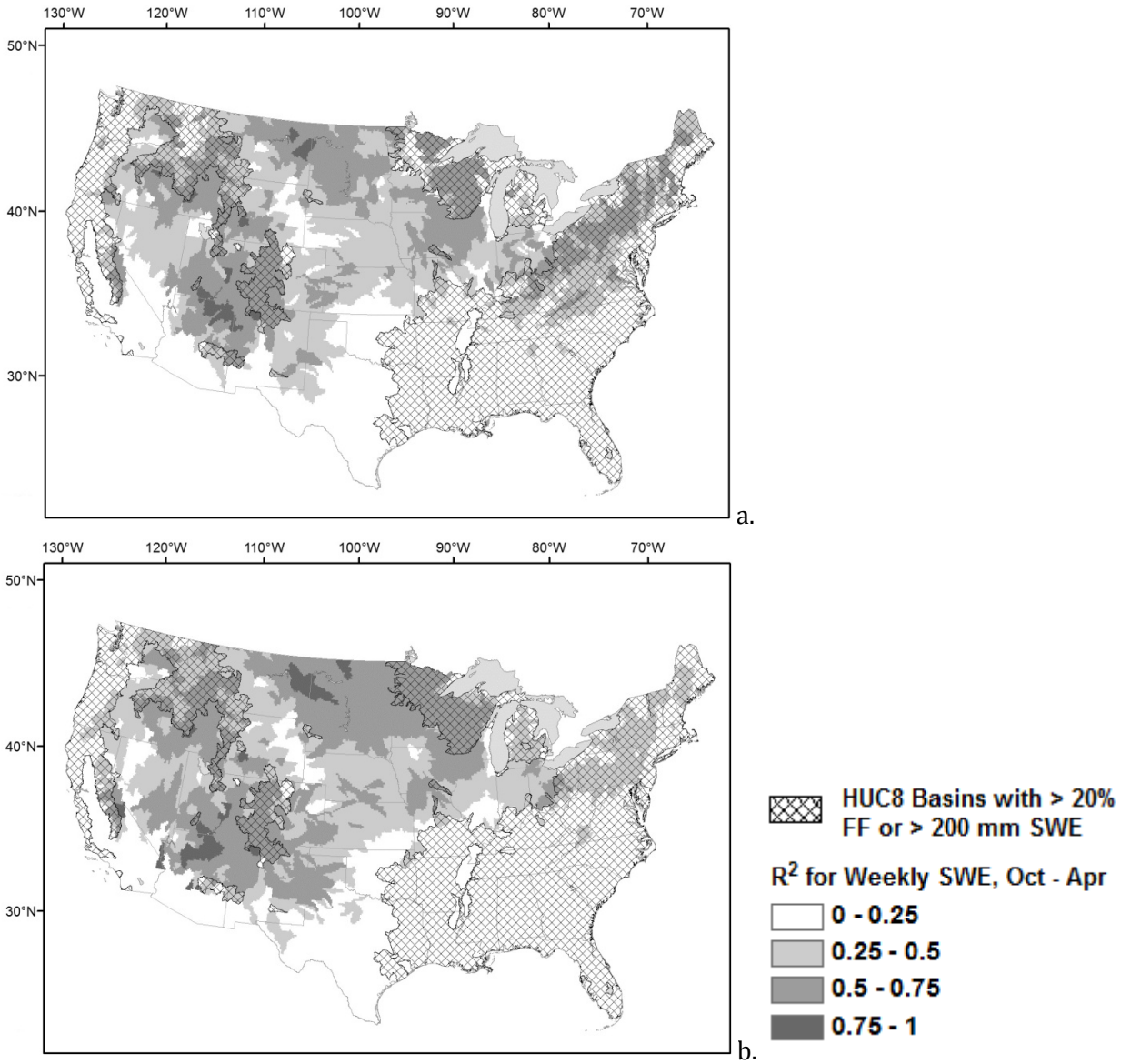

Figure 7. R^2 of weekly winter SWE, Oct – Apr, by HUC8 for (a) SNODAS and AMSR-E (b) SNODAS and SSM/I; hatched area shows HUCs with greater than 20% forest coverage or an average max annual SNODAS SWE greater than 200 mm.

Times series of SWE data in basins from six different regions demonstrate typical regional differences in the weekly comparison (Figure 8). Characteristics of each of the basins and statistical results of the comparison of passive microwave SWE with SNODAS data are given in Table 3. The Sheyenne Basin (A) is in the northern Plains region where all three datasets compare very well. In this region, the evolution and magnitude are typically similar with

correlations between SNODAS and passive microwave of 0.55 and 0.68 for AMSR-E and SSM/I, respectively, and Nash-Sutcliffe efficiencies between SNODAS and passive microwave data of 0.48 and 0.52 for AMSR-E and SSM/I, respectively. The Upper Powder Basin (B) is in the Central Plains region where the agreement is not as strong. The basin has a modest snowpack that is tracked by all datasets, but the strongly negative Nash-Sutcliffe efficiencies show the lack of agreement between the time series. The Upper Salmon Basin (C) in the Pacific Northwest region has considerable vegetation and deep annual snowpacks. The passive microwave follows a similar accumulation and ablation trend, and has a correlation of 0.6 to the SNODAS data. However, the microwave SWE is much lower than the SNODAS SWE, even for relatively shallow snowpacks. The Duschene Basin (D) in the Upper Colorado region also receives deep snowpack but has a forest fraction of less than 20%. In lighter snow years, the passive microwave is similar in magnitude to the SNODAS SWE, but in heavier snow years the microwave data is much less, resulting in an overall negative efficiency measure. The Upper Wisconsin Basin (E) near the Great Lakes region does not experience deep snow, but is significantly forest covered. As compared to the other four watersheds, a difference between AMSR-E and SSM/I SWE estimates is evident with AMSR-E having a Nash-Sutcliffe efficiency of 0.59 in comparison with SNODAS, while SSM/I has an efficiency in -0.04. The Lower Lake Powell Basin (F) is in the Southern Rockies region with a large elevation range, minimal vegetation, and a modest annual snowpack. Strong agreement between SNODAS and the passive microwave SWE are shown by correlations of 0.88 and 0.87 and Nash-Sutcliffe efficiencies of 0.86 and 0.74 for AMSR-E and SSM/I, respectively.

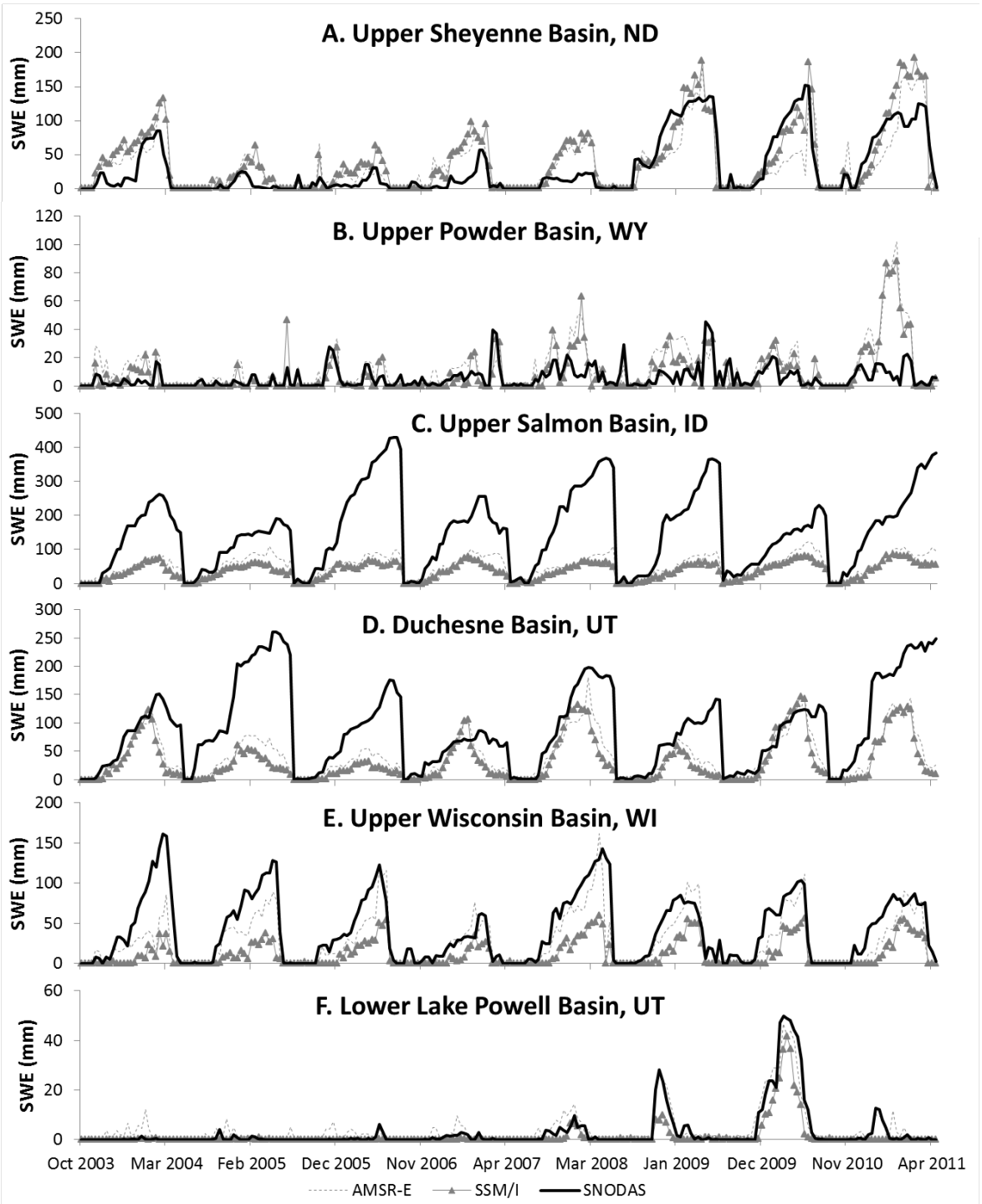

Figure 8. Example time series of average basin SWE in different regions (shown on Figure 1), with high and low forest fractions (ff), elevation ranges (ER), and average maximum annual SWE (based on SNODAS).

Table 3. Weekly Statistics for example HUC8 time series

HUC8	Basin	Forest Cover %	Elev range (m)	Max SWE (mm)	NOAA and AMSR-E R^2	NOAA and SSM/I R^2	NOAA and AMSR-E Nash-Sutcliffe	NOAA and SSM/I Nash-Sutcliffe
9020202	UPPER SHEYENNE, ND (Northern Plains)	8%	208	79.5	0.55	0.68	0.48	0.52
10090202	UPPER POWDER, WY (Central Plains)	0%	770	26.0	0.19	0.21	-3.12	-2.22
17060201	UPPER SALMON, ID (Northern Rockies)	30%	1973	311.5	0.64	0.62	-0.38	-0.71
14060003	DUCHESNE, UT (Central Rockies)	16%	2573	174.8	0.43	0.26	-0.03	-0.33
7070001	UPPER WISCONSIN, WI (Great Lakes)	77%	143	111.4	0.70	0.61	0.59	-0.04
14070006	LOWER LAKE POWELL, AZ, UT (Southern Rockies)	0%	2169	14.3	0.88	0.87	0.86	0.74

Overall, this study supports many of the findings from the earlier studies [Dong et al., 2005; Vander Jagt et al., 2013]. The SNODAS and microwave data agree in relatively flat, non-forested areas where previous studies showed promising microwave results [Derksen et al. 2003, Mote et al. 2003, Chang et al. 2005] and also in mountainous, non-forested regions [Tait, 1998; Vuyovich and Jacobs, 2011]. Unlike Mätzler and Standley [2000], this study did not find that large elevation gradients have significant impact on the passive microwave SWE estimate as compared to SNODAS SWE. Tedesco and Narvakar [2010] reported the highest correlations between SNODAS and AMSR-E SWE occurred in pixels with 0.3-0.4 forest fraction, whereas we found the best agreement in basins with a forest fraction of 0.2 or less. This clearly limits the regions for which microwave observations have value. Thus, inclusion of vegetation information beyond forest fraction in the retrieval algorithm (e.g., NDVI Azar et al. [2008]) may expand the region for which microwave observations provide value. The thresholds are also evident for microwave SWE when snow is too deep – here we found an upper maximum of 200 mm, which is intermediate between Clifford's [2010] 250 mm and Tedesco and Narvakar's [2010] 90 mm.

Furthermore, while there are limited studies on shallow snowpacks, our finding that the algorithm differences between AMSR-E and SSM/I challenge the quantification of watershed scale SWE estimates in southern regions is supported by Daly et al.'s [2012] findings from their work in Afghanistan.

2.5 CONCLUSION

In this study, we compared SWE estimates from AMSR-E and SSM/I passive microwave satellite sensors to the SNODAS gridded SWE product for 2100 watersheds in the U.S. No previous research has evaluated the microwave products over time at this hydrologic scale, and this provided several interesting insights. Regional differences between the AMSR-E and SSM/I point to the need to better understand the algorithms' detection of SWE in both heavily forested basins and basins with shallow annual snow. Current use of forest fraction to characterize the land in the AMSR-E algorithm seems to improve results. A more robust algorithm which includes various vegetation types may improve results further.

A comparison of the standard deviation of SWE within each HUC-8 basin showed that in areas where the passive microwave signal is impacted by deep snow and vegetation, the spatial variation also suffers. This suggests that methods to improve the microwave estimates will likely require ancillary data to determine the spatial distribution of SWE. Further research in this topic will enhance our understanding of how spatial variability within a microwave pixel is established. For instance, additional analysis of the southern plains is needed to determine if the shallow snow algorithm or some other physical process is causing AMSR-E data to overestimate SWE in this region.

Results show large areas where the passive microwave retrievals perform well compared to the SNODAS data, particularly in the northern Great Plains and southern Rocky Mountain regions.

The best correlations are associated with basins in which maximum annual SWE is less than 200 mm, and forest fraction is less than 20%. While this excludes many regions of the country where snow is a significant source of water, it increases confidence in results for characteristically similar regions around the world. In the central Plains region, disagreement between SNODAS and passive microwave SWE will be the focus of future research to better understand the factors impacting the results.

In watersheds with maximum annual SWE values greater than 200 mm, poor correlations between the passive microwave data and SNODAS indicated that the relative magnitude of maximum SWE from year-to-year was not captured. However, the overall temporal pattern of accumulation and ablation did show good agreement in many of these regions, which may provide useful hydrologic information as to the snow season length and melt timing. This analysis provides a foundation for future research assessing the SWE estimates in relation to runoff from these basins.

CHAPTER 3 THE EFFECT OF SPATIAL VARIABILITY OF WET SNOW ON PASSIVE MICROWAVE SATELLITE OBSERVATIONS[2]

3.1 INTRODUCTION

Melting snow provides a reliable water supply in many regions of the world and can also produce wide-scale flooding, particularly when combined with rainfall. Efficient water resource management requires accurate, timely estimates of both snow water equivalent (SWE) and snow melt onset. However, snow characteristics can be highly variable across a landscape, and techniques for accurately characterizing the spatial distribution of snow properties still remain elusive (Elder et al. 1998; Dozier et al. 2016). The presence of liquid water in an existing snowpack, which can be an indicator of snowmelt, is particularly difficult to measure or detect over large areas (Kang et al. 2014). For hydrological purposes, an accurate distribution of melt is essential for estimating the correct runoff response (Lundquist and Dettinger 2005), and will also provide insight into important ecological and biogeochemical processes (Bales et al. 2006).

Increasingly over the past 50 years, satellite remote sensing techniques have been investigated for estimating all components of the land surface water budget (Lettenmaier et al. 2015). Snow measurement in particular has benefited from technology advances due to different responses across the electromagnetic spectrum from other land surface types (Frei et al. 2012). Currently, two methods are available for global monitoring of snow; visible/infrared sensors provide high resolution estimates of snow extent, while passive microwave sensors have been used to derive information on snow mass. Passive microwave observations have been available for over three decades providing non-destructive, daily information on snow depth, snow water equivalent

[2] Vuyovich, C. and J. Jacobs (in press) Snowmelt runoff prediction through spatial characterization of melt-based microwave response, submitted to Remote Sensing of Environment, October 2016.

(SWE) and snowpack state (Schmugge et al. 2002). Passive microwave emissions also offer a potentially viable way to discern snow melt distribution across a landscape.

Microwave emissions are measured in units of brightness temperature (T_B), which in the microwave spectrum is equal to the thermometric temperature of the emitting material times the emissivity. At certain frequencies, snow causes the measured T_B to decrease due to signal extinction through the snowpack; this forms the basis for empirical formulations to estimate snow depth (Chang et al. 1982). The microwave signal is highly responsive to liquid water content (LWC), which is the volume of liquid water per unit volume of snow, due to the sensitivity of the radiance to changes in the dielectric constant (Stiles and Ulaby 1980). The presence of water within a snowpack increases the emissivity resulting in a sharp T_B increase (Davis et al. 1987; Mätzler 1987; Walker and Goodison 1993). T_B increases occur with as little as 1-2% liquid water content in the snowpack (Cagnati et al. 2004; Stiles and Ulaby 1980; Tedesco et al. 2006).

Passive microwave emissions cannot be used to estimate SWE during wet snow periods because of the reduced signal scattering. However, the signal response provides a clear indication of increased liquid water content, which overwhelms the impact of other snowpack properties on the microwave signal (Wang et al. 2001). Several studies have investigated using this response to determine the melt onset date (Drobot and Anderson 2001; Ramage et al. 2006), or to identify rain-on-snow (ROS) events (Grenfell and Putkonen 2008). Others have linked the microwave response at a coarse resolution to basin runoff and shown potential for hydrologic applications (Ramage and Semmens 2012; Vuyovich and Jacobs 2011; Yan et al. 2009).

Two approaches have been developed to detect the timing of snowmelt using microwave signal response to wet snow. The Diurnal Amplitude Variation (DAV) approach identifies the onset of melt using the large differences in T_B between the morning and afternoon overpasses at the 37GHz frequency (Kopczynski et al. 2008; Ramage et al. 2006; Tedesco et al. 2009). A DAV increase indicates the onset of the daytime melt/nighttime refreeze cycle and the beginning of spring snowmelt. The high-DAV period that follows the onset of melt, referred to as the transition period, ends when the snowpack is continuously melting during day and night periods and the brightness temperature difference decreases. Another method uses the gradient and polarization ratios (GR and PR, respectively) to isolate the bulk emissivity of the snowpack and identify significant rain-on-snow events. In the Canadian Arctic, Grenfell and Putkonen (2008) demonstrated that the GR and PR can be used to identify the occurrence as well as the intensity of rain-on-snow events. Using a combination of these two approaches, Semmens et al. (2013) developed an algorithm for detecting early season melt events with AMSR-E passive microwave data, and were able to successfully identify melt events caused by both rain-on-snow and snowmelt alone.

These methods have successfully demonstrated an ability to detect the timing of snowmelt, which has implications for runoff; however, they do not provide information on the volume of runoff. The discharge magnitude during a snowmelt event is a function of the snowpack properties as well as the spatial extent over which snowmelt is occurring. An improved understanding of the T_B retrievals' response to the spatial distribution of snowmelt is needed. Kang et al. (2014) and Pan et al. (2014) conducted the foundation work needed to characterize footprint scale emissions. They used the Microwave Emission Model for Layered Snowpacks (MEMLS) and the Helsinki University of Technology (HUT) snow microwave radiative transfer

models, respectively, to successfully capture the emission signatures in wet snowpacks and compare the results to point observations. Both studies report a sharp increase in the T_B response immediately after wetting (the signal response used in detecting the onset of melt) despite differences in snowpack characteristics and wetness profiles.

The goal of this study is to understand the T_B response to spatially distributed wet snow within a satellite pixel and to begin to evaluate the relationship between the aggregated T_B response and river discharge. In this study, we investigate the sensitivity of T_B to spatially distributed wet snow using loosely coupled, physically-based snow and emission models. A long-term ecological research area in the northeast U.S. was selected as the study location because of its long record of meteorological, hydrological and snow observations (described in Section 2). The methods used to develop a relationship between the change in T_B and the fractional area affected by wet snow are described in Section 3. These include a sensitivity analysis to assess the impacts of artificially distributed LWC on the emission signal, and evaluation of the simulated and observed T_B during wet snow events over an eight year period. Results of the analysis are provided in Section 4 and include a comparison of the T_B response and increases in observed streamflow during wet snow events. In Section 5 we discuss the implications of these results with potential future directions.

3.2 Study Area and Data

The study domain is a 34 km by 34 km area in the White Mountains of New Hampshire, USA which includes the Hubbard Brook Experimental Forest (HBEF), a Long Term Ecological Research (LTER) watershed (Figure 1). The HBEF watershed has an area of 31.6 km^2, which covers approximately 3% of the total study domain and is representative of the larger area. HBEF has more than 50 years of meteorological and hydrological observations, which have

enabled decades of ecologic and hydrologic research. Approximately one-third of the annual precipitation falls as snow, with a mean annual maximum SWE for the period of record at HBEF of approximately 189 mm, and a snow cover that generally persists from mid-December to mid-April (Campbell et al. 2007). The study domain is a mountainous region, characteristic of the northeastern United States Appalachian Mountains with elevations ranging from 120 to 1470 m. Land cover is Eastern Deciduous Forest, with evergreen forest and tundra at the highest elevations. Agricultural and developed areas are primarily limited to the lowest elevations and along rivers. Elevation data for the domain were developed from 30 m resolution National Elevation Data (NED) (USGS 2009). Land cover data were obtained from the National Land Cover Database (NLCD) (Homer et al. 2015). Both the elevation and land cover data were clipped and resampled to a 50 m resolution. Stream channels in this region are generally steep with coarse-grained bed material. Shallow underlying bedrock means minimal loss to deep groundwater and relatively quick runoff response (Campbell et al. 2011). Discharge records demonstrate a seasonal snowmelt signal with the highest runoff volumes occurring in March – May.

Meteorological and snow course data from 1 October 2002 to 30 September 2011 at the Hubbard Brook LTER (Bailey et al. 2003) and National Weather Service stations were used in this study (Table 1). Daily temperature and precipitation observations were available from approximately 10 locations each year. The Hubbard Brook LTER data provided precipitation measurements over a representative elevation range. Relative humidity, wind speed and direction were available at three of the 10 observation stations. Only two stations lacked complete data coverage for the entire period of interest. Snow water equivalent was measured at five Hubbard Brook snow course locations on a weekly basis. HBEF also maintains an NRCS Soil Climate

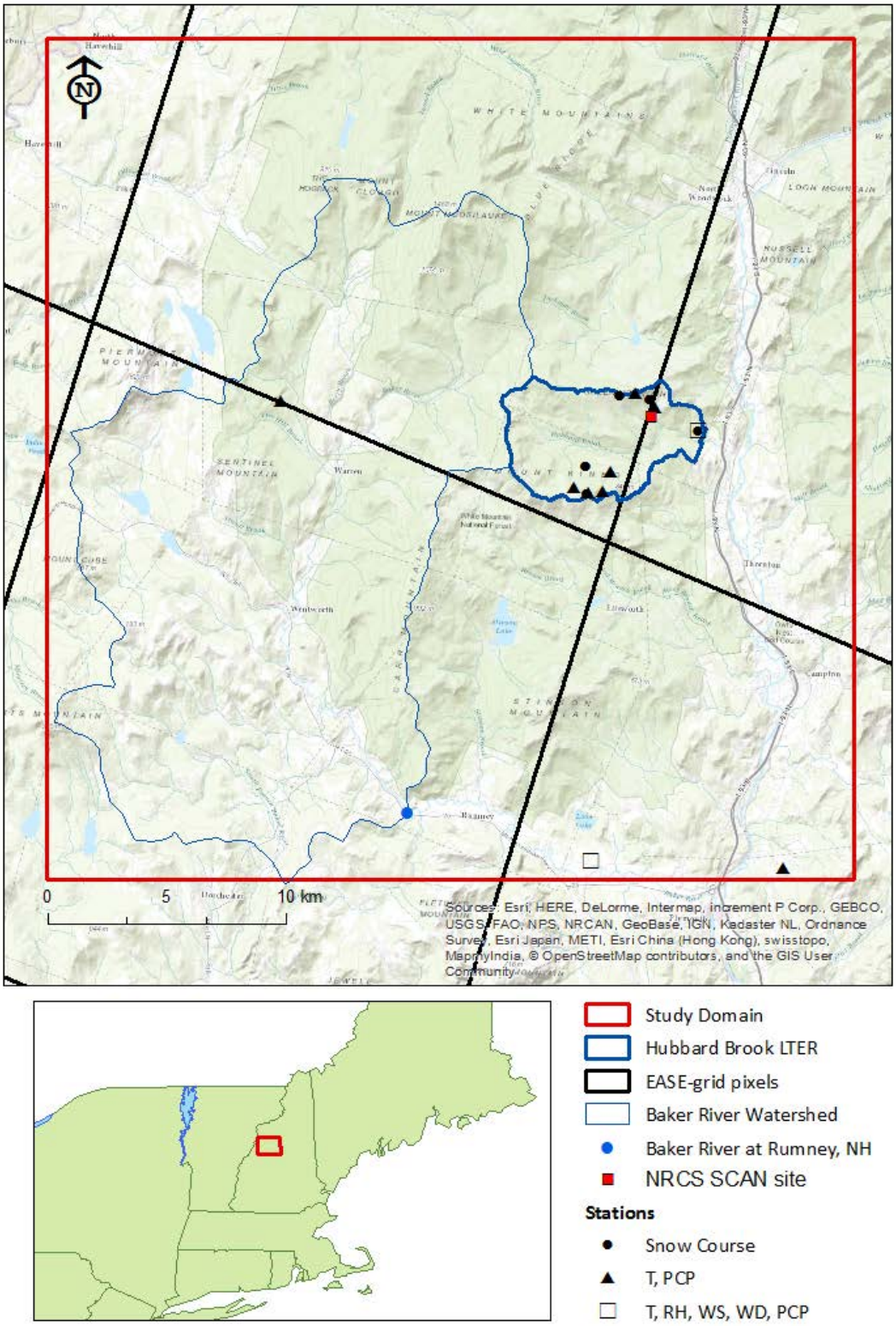

Figure 1. Study region, located in the White Mountains of New Hampshire, US

Analysis Network (SCAN) site; an automated station with a snow pillow to measure SWE, as well as measurements of snow depth, soil moisture and numerous meteorological variables. The station has been collecting hourly data since 2002.

Table 1. List of Meteorological Stations and Snow Survey Sites Used

Station Name (ID)	Lat.	Long.	Elev. (m)	Observations*	Water Years Used
Hubbard Brook HQ (100)	43.94	-71.70	255	T, RH, WS, WD, PCP, SWE	2003-2011
Hubbard Brook 1A (101)	43.95	-71.73	490	T, PCP	2003-2011
Hubbard Brook Station 2 (HB2)	43.95	-71.73	561	SWE	2003-2011
Hubbard Brook Station 6 (106)	43.96	-71.74	740	T, PCP	2003-2011
Hubbard Brook Station 9 (HB9)	43.96	-71.74	762	SWE	2003-2011
Hubbard Brook Station 14 (114)	43.92	-71.77	740	T, PCP	2003-2011
Hubbard Brook Station 17 (117)	43.92	-71.76	740	T, PCP, SWE	2003-2011
Hubbard Brook Station 19 (HB19)	43.92	-71.76	792	SWE	2003-2011
Hubbard Brook Station 23 (123)	43.93	-71.76	669	T, PCP	2003-2011
Hubbard Brook Station 24 (124)	43.92	-71.75	796	T, PCP	2003-2011
NRCS SCAN Site	43.93	-71.72	460	T, PCP, WS, WD, RH, SWE	2003-2011
Plymouth Mun. Airport (200)	43.78	-71.75	157	T, RH, WS, WD, PCP	2006-2011
Plymouth COOP Station (250)	43.78	-71.65	303	T, PCP	2003-2008
Wentworth COOP Station (400)	43.95	-71.92	282	PCP	2003-2011
Mt. Wash Regl. Airprt. (500)**	44.37	-71.54	327	T, RH, WS, WD, PCP	2003-2011

*T = Temperature (°C); RH = Relative Humidity (%); WS = Wind Speed (m/s); WD = Wind Direction (degrees); PCP = Precipitation (mm/day); SWE = Snow Water Equivalent (mm) **Located outside of the domain.

Within the HBEF research area, nine instrumented watersheds have recorded continuous discharge measurements since 1956 (Bailey et al. 2003). Additionally, the Baker River watershed is an unregulated basin, with an area of approximately 370 km^2, which is entirely contained within the study domain but outside of HBEF. Streamflow data were obtained for the Baker River at Rumney, NH from the U.S. Geological Survey (USGS 2001).

Passive microwave brightness temperature data from the Advanced Microwave Scanning Radiometer-Earth Observing System (AMSR-E) were obtained from the National Snow and Ice Data Center (NSIDC) (Cavalieri et al. 2014). AMSR-E was launched on NASA's Aqua satellite in 2002 and data are available through 2011 in Equal-Area Scalable Earth (EASE)-grid projection as 25-km grids. Horizontally and vertically polarized T_B measured at wavelengths 18.7 and 36.5 GHz were used in this analysis. AMSR-E data are available twice daily: ascending

passes that occur in the afternoon and descending passes that occur in the early morning. A gap in the satellite swath coverage over the region of interest occurs every 3 to 4 days.

For each descending overpass during the nine-year period of record, an area-weighted average T_B was computed over the study domain, at both frequencies and polarizations. This study used the descending passes only to limit the occurrence of diurnal melt affecting the signal and instead focus on large-scale, continuous melt events. Values were only computed for images when no data were missing within the study domain. Earlier work by Vuyovich et al. (2014) found that vegetation in this region of the U.S. impacts of accuracy of empirically-based passive microwave SWE estimates. In this study no corrections were made to the satellite observations to adjust for vegetation, instead focusing on the signal response to wet snow.

3.3 METHODS

For this analysis, a physically-based snow model was loosely coupled with a microwave emission model to simulate the snowpack radiance over a 9-year period, 2003 – 2011. A single layer snow model was used to focus the analysis on the impacts of LWC. The models were run at a 50 m resolution over the study domain with a daily time step.

3.3.1 SNOW AND MICROWAVE EMISSION MODELS

SnowModel was used to simulate the snow evolution in the study domain and estimate spatially distributed snow characteristics including snow depth, temperature, density, SWE, albedo and snowmelt. SnowModel combines an energy balance snow model and wind redistribution model and was used to simulate a one-layer spatially distributed snow cover over the study domain (Liston and Elder 2006a). MicroMet, a high-resolution atmospheric model (Liston and Elder 2006b) was used to distribute and downscale the daily meteorological forcing data obtained from observations stations. SnowAssim (Liston and Hiemstra 2008) was used to assimilate SWE field

observations. The HBEF snow course data were assimilated into the model at approximately bi-weekly intervals over the simulation period to better match the snow observations. SWE measurements from the SCAN site were then used to validate model results.

The Microwave Emission Model of Multilayered Snowpack (MEMLS) was used to estimate the microwave emissions over the study domain, with snow characteristics provided from SnowModel output. MEMLS is a semi-empirical radiative transfer model that simulates the scattering effect of snow on microwave emissions at frequencies ranging from 5 – 100 GHz using multiple scattering radiative theory (Matzler and Wiesmann 1999; Wiesmann and Matzler 1999). MEMLS estimates internal scattering based on six-flux theory, which is simplified for upwelling and downwelling radiation. Scattering coefficients are determined based on characteristics of the snow.

MEMLS was used to estimate vertically and horizontally polarized T_B through the snow at 18.7 and 36.5 GHz to match the AMSR-E frequencies used to estimate SWE. The 36.5 GHz frequency is of particular interest and the focus of this paper because of its sensitivity to snow parameters (Tedesco and Kim 2006). Snow characteristics including snow depth, density, temperature, liquid water content (LWC), and the exponential correlation length (p_{ex}) are required as input to MEMLS. Snow temperature, depth and density were used directly from SnowModel output. The p_{ex} is a metric for grain size used in MEMLS to estimate the scattering coefficient. The original approach assumed p_{ex} values ranging from 0.05 – 0.3 mm (Wiesmann and Matzler 1999), which was later extended to handle coarse grains up to 0.6 mm (Matzler and Wiesmann 1999). SnowModel does not simulate grain size. Given that the focus of this investigation is on the effects of LWC, a constant p_{ex} was used for all grid cells.

3.3.2 SENSITIVITY ANALYSIS

The first sensitivity analysis was conducted to develop a relationship between the T_B response and the percent LWC in the snow, uniformly distributed across the study domain. A single date was selected when the study domain was 100% snow covered and no LWC was present in the snow based on SnowModel results. This provided a realistic spatial distribution of snow characteristics with which to test the effects of LWC. In the first series of simulations, LWC was applied across the domain as a constant percentage of the SWE in each grid cell. The LWC was uniformly applied to each grid cell in 0.1% increments increasing from 0 to 5%. In the next series of simulations, the same adjustment to LWC performed in the first test was repeated while individually adjusting the other snow characteristics. The snow depth, density, temperature and exponential correlation length were varied between a selected maximum and minimum average value over the study domain. To adjust the snow depth, density and temperature, the individual grid cell values were scaled by the ratio of the new domain average value to the original average. The exponential correlation length, p_{ex}, was uniformly adjusted across the domain to represent a range of expected grain sizes from fine to coarse.

In the second sensitivity analysis, LWC was applied to increasing areas of the study domain using SnowModel results on the same date as in the previous analysis. The area assigned LWC was increased from 0% to 100% by 10% increments. The goal of this analysis was to develop a relationship between the percent area impacted by wet snow and the change in T_B over the entire domain. Two different spatial distributions were used to assign LWC to the grid cells: random and by elevation. The random distribution assigned LWC to grid cells at random. The elevation distribution assigned LWC to grid cells beginning with the lowest elevations first, and increasing the percent area within the domain as a function of elevation. The elevation distribution was

used to replicate a more realistic melt pattern, which is often strongly correlated with elevation, though it is not the only factor (Lundquist et al. 2004). Table 2 provides a matrix of the tests performed in the sensitivity analysis.

Table 2. Sensitivity analysis test matrix, using SnowModel results on 11 March 2003

LWC Analysis	**Snow Depth (cm)** (average over domain)	**Snow Temperature (K)** (average over domain)	**Snow Density (kg/m^3)** (average over domain)	**Exponential correlation length, p_{ex}**
Tests 1- 5: Uniform application of varying LWC across domain				
Test 1: 51 simulations increasing LWC from 0 – 5% by 0.1% increments	49 cm	266.8 K	301.7 kg/m^3	0.11
Test 2: 51 simulations increasing LWC from 0 – 5% by 0.1% increments, while adjusting snow depth	2 Tests: 25 cm and 80 cm	266.8 K	301.7 kg/m^3	0.11
Test 3: 51 simulations increasing LWC from 0 – 5% by 0.1% increments, while adjusting snow temperature	49 cm	3 Tests: 250, 260 and 270 K	301.7 kg/m^3	0.11
Test 4: 51 simulations increasing LWC from 0 – 5% by 0.1% increments, while adjusting snow density	49 cm	266.8 K	2 Tests: 200 kg/m^3 and 400 kg/m^3	0.11
Test 5: 51 simulations increasing LWC from 0 – 5% by 0.1% increments, while adjusting p_{ex}	49 cm	266.8 K	301.7 kg/m^3	2 Tests: 0.3 and 0.65
Tests 6 - 7: Spatial distribution of constant LWC across domain				
Test 6: 11 simulations, LWC = 1%, assigned randomly to 0 – 10% of the area by 10% increments	49 cm	266.8 K	301.7 kg/m^3	0.11
Test 7: 11 simulations, LWC = 1%, assigned to 0 – 10% of the area by 10% increments based on pixel elevation	49 cm	266.8 K	301.7 kg/m^3	0.11

3.3.3 WET SNOW EVENTS

For the period 2003 – 2011, the snow emission model was run over each winter season and wet snow events were identified using a threshold change in T_B greater than 5K from the previous day. To ensure that the domain was mostly snow covered, the events were limited to the December to March time period when the average SWE over the domain was at least 10 mm. SnowModel output includes snowmelt but not LWC, a snow property required by MEMLS. In grid cells where SnowModel estimated snow melt runoff greater than zero, LWC was assumed to be present in the snowpack. For each event identified, the change in the observed T_B was

compared with the results of the sensitivity analysis. For snow melt events to result in significant runoff the snowpack temperature must be close to the melt temperature. For each wet snow event, the change in T_B from one day, $T_{B,1}$, to the next, $T_{B,2}$, was normalized by the difference between the previous day's brightness temperature and 273.15 K, which represents the largest change in T_B that could occur.

$$T_{B,n} = \frac{(T_{B,2} - T_{B,1})}{(273.15\ K - T_{B,1})} \quad (1)$$

The AMSR-E 36.5 GHz T_B was compared to the modeled T_B over the period, 2003-2011, when the satellite data are available. The normalized change in AMSR-E T_B during the wet snow events was also compared to the results of the sensitivity analysis.

For each wet snow event identified, subsequent discharge changes in the Baker River at Rumney, NH were evaluated. While not all wet snow packs will result in runoff, liquid water detected in the snowpack is a necessary precursor to winter discharge increase. The absolute change in discharge following a wet snow event identified in the microwave signal was compared to the change in T_B estimated from MEMLS and AMSR-E.

3.4 RESULTS

3.4.1 HIGH-RESOLUTION SIMULATION OF SNOW CHARACTERISTICS OVER STUDY DOMAIN

SnowModel results were validated using observed SWE at an NRCS SCAN site located within the Hubbard Brook watershed which was not assimilated into the model. Over the 9 years when both snow pillow observations and SnowModel results were available, the correlation (R^2) between the daily SWE data was 0.82 and the Nash-Sutcliffe efficiency measure was 0.65, indicating a close match between the modeled and observed at that location. The study area is

usually completely snow covered during the winter months, beginning on 10 December and ending on 8 May on average. The average peak SWE date occurs on 10 March, and the estimated average peak SWE over the study domain during the 9-year time period is 172 mm. The maximum peak SWE was 311 mm in 2008 and a minimum peak SWE of 78 mm was estimated in 2006. Simulated snow depths showed variability with topography, which agrees with observed snow measurements. SWE measured at HBEF are consistently deeper at high-elevations than in the valley floors throughout the snow accumulation and ablation season. In addition, melt rates are greater at the lower elevations earlier in the season and at the higher elevations later in the season (Figure 2). This supports the use of elevation as a realistic index for snowmelt patterns.

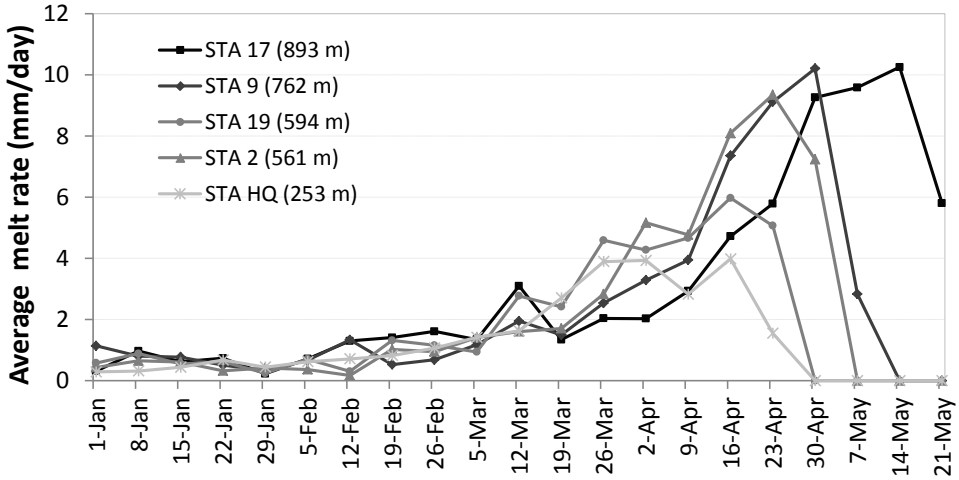

Figure 2. Average daily melt rates at 5 Hubbard Brook snow survey sites (with elevation) during the spring season, based on HBEF data from 1993 – 2015.

3.4.2 SIMULATION OF SNOW MICROWAVE EMISSIONS OVER STUDY DOMAIN

The MEMLS model was run for each 50 x 50 m grid cell over the 9 year study period, using snow characteristics from SnowModel as input. The results were averaged to provide a single T_B for the whole study domain. The vertically polarized 36.5 GHz T_B from the AMSR-E satellite sensor were compared to the model results. No atmospheric or vegetation corrections to the

AMSR-E data were made for this study because we are primarily interested in the relative change in T_B rather than the absolute magnitude. Regardless, both measured and modeled data show a similar decrease in T_B during the winter months when snow is impacting the signal (Figure 3). T_B estimates range from approximately 273 K during the snow-free periods to 220-240 K at the peak snowpack. There is considerable noise in the daily AMSR-E data, which could be due to the vegetation in this region. Dissimilarities between the data could also be due to the differences in the regions being averaged.

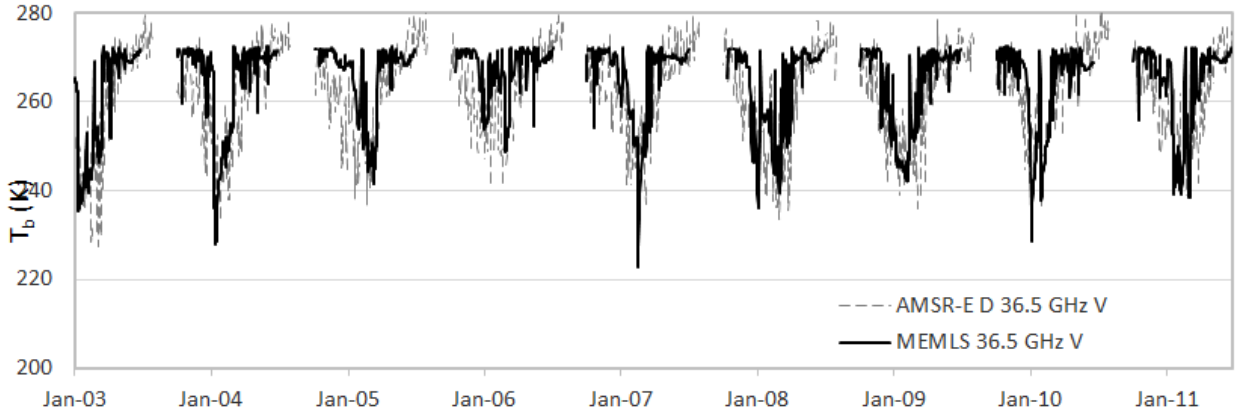

Figure 3. Daily average T_B over study domain for water years 2003 – 2011, from model results and satellite retrievals.

3.4.3 Sensitivity of microwave emissions to LWC in snow

The sensitivity analysis provided the foundation to examine the effect of LWC on microwave emissions over the study domain. On the date selected for the sensitivity analysis, 11 March 2003, SnowModel results estimated 100% snow cover over the domain and no LWC (Figure 4). The average snow depth on this date was 49.1 cm, ranging from a maximum of 145.2 cm to a minimum of 13.7 cm across the study domain. The average snow density and temperature were 301.7 kg/m^3 and -6.32^{o}C (266.8 K), respectively. A constant p_{ex} of 0.11 was used for all grid cells based on observed values for a similar snowpack depth (Proksch et al. 2015; Wiesmann et al. 1998). The 36.5 GHz T_B, estimated by MEMLS on this date, was 248.6 and 237.6 K for the

vertical and horizontal polarizations, respectively. The computed 18.7 GHz T_B on this date was 266.1 K for the vertical polarization and 253.3 K for the horizontal polarizations. For comparison, the AMSR-E T_B observed on this date were 229.7 and 226.4 K for the vertical and horizontal polarizations of the 36.5 GHz frequency, respectively. The T_B observations at 18.7 GHz were 239.1 K in the vertical polarization and 232.0 K horizontal.

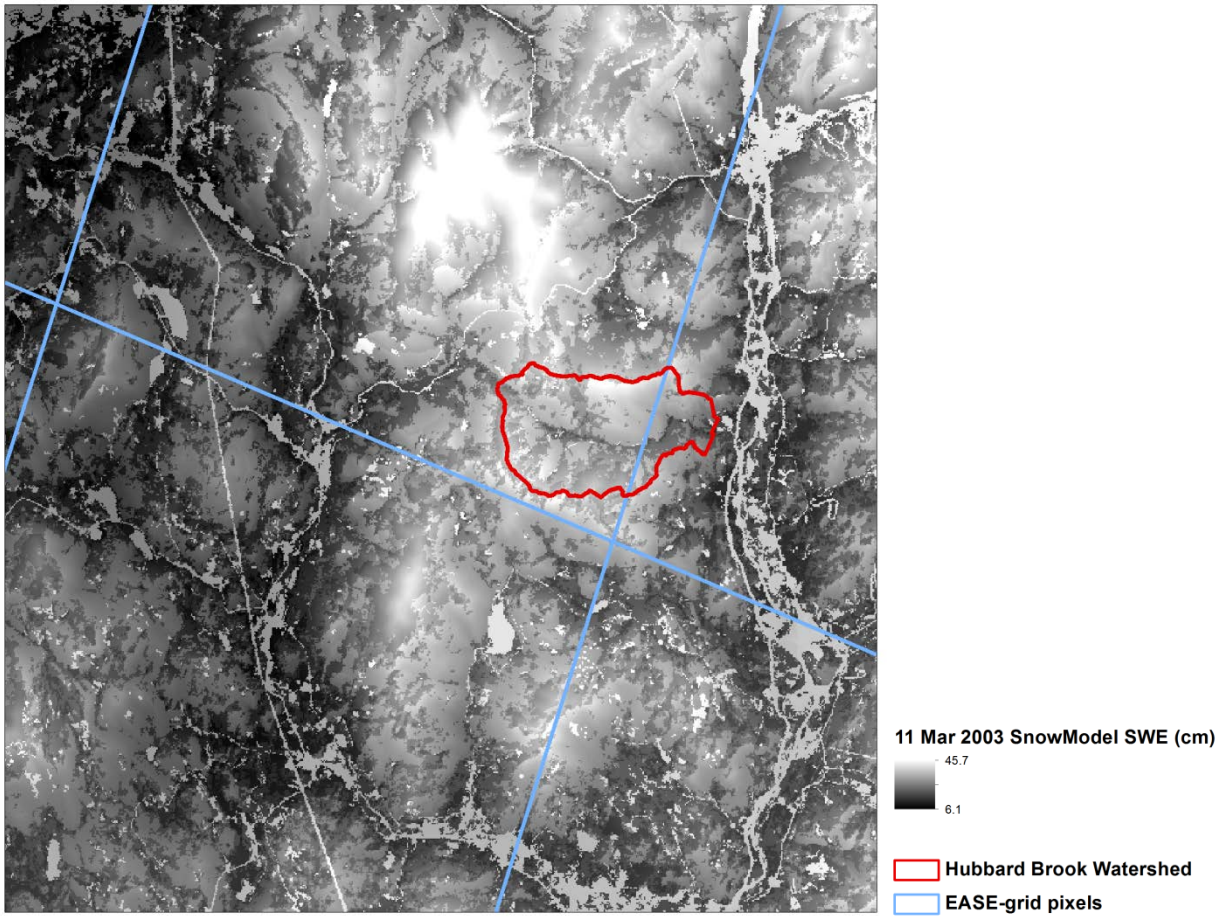

Figure 4. SnowModel SWE on 11 Mar 2003 when domain was 100% snow covered with no LWC.

Homogenous Distribution of LWC percentage

For the first sensitivity analysis, the same LWC was applied to each MEMLS grid cell as a percentage of the SWE in that cell, increasing by 0.1% increments from 0 to 5% LWC. With the initial application of 0.1% LWC, the average T_B across the domain increased by approximately 14.5 and 12.7 K for the vertical and horizontal polarizations, respectively (Figure 5). The

vertically polarized 36.5 GHz brightness temperatures continued to rise with increasing LWC until leveling off around 1% LWC. In contrast, the horizontally polarized 36.5 GHz channel decreased after the initial rise even with increasing amounts of liquid water in the snow. This is caused by further increases in the surface reflectivity (Kang et al. 2014). The vertically polarized 18.7 GHz T_B changed to a smaller degree initially than the 36.5 GHz channel and then closely followed the 36.5 GHz data as additional LWC was introduced to the snow pack. The horizontally polarized 18.7 GHz T_B similarly saw minimal initial changes, but then decreased at a greater rate than the 36.5 GHz horizontally polarized T_B. This suggests that the difference between the 18.7 and 36.5 GHz horizontally polarized T_B may provide some information on the magnitude of LWC, though investigation of this signal is left to future work. The remainder of this study focuses on the vertically polarized 36.5 GHz signal that has a strong response to liquid water and then remains constant.

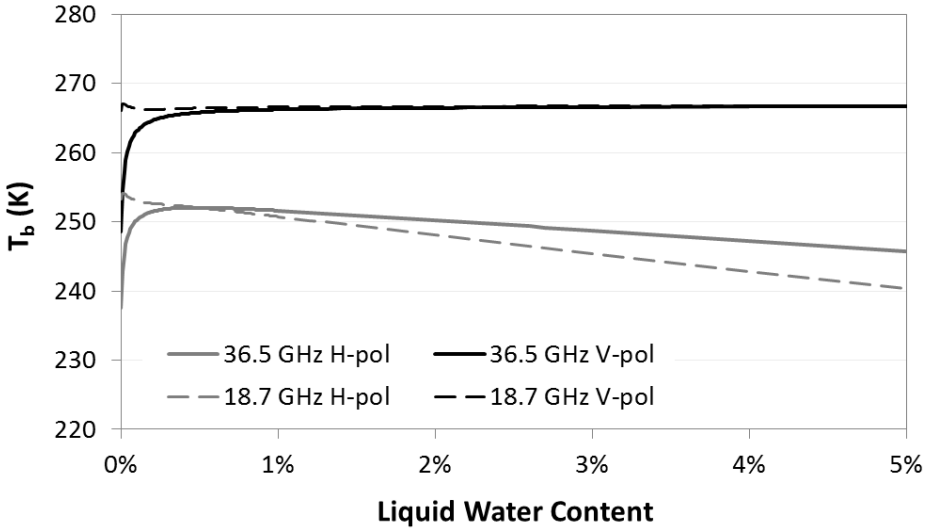

Figure 5. Vertically and horizontally polarized 36.5 GHz T_B for increasing percent LWC, averaged over the study domain

IMPACT OF SNOW PROPERTIES

The LWC sensitivity analysis, using a homogenous LWC percentage across the domain, was repeated while adjusting the other snow characteristics to assess the impact on the 36.5 GHz vertical signal. The average snowpack depth over the domain was scaled from 25 to 80 cm by multiplying each pixel by the ratio of the new depth to the original depth. For dry conditions, the T_B values differ by 15.3 K with the lowest T_B estimated for the 80 cm snowpack (Figure 6a). The initial application of 0.1% liquid water equalizes the T_B to the average snowpack temperature (266.8 K). Next, the domain average snow density was varied between 200 – 400 kg/m^3 by similarly scaling the individual model cells. The initial T_B ranged between 237.4 and 258.4 K for the low- and high-density tests, respectively (Figure 6b). Similar to snow depth, the T_B equalizes to the snowpack temperature with the addition of 0.1% LWC.

Adjusting the correlation lengths had a larger effect on the initial T_B with values for dry snow ranging from 91 to 250 K for p_{ex} values of 0.65 and 0.11 mm, respectively (Figure 6c). These values were selected based on observed correlation lengths of fine and coarse snow grains (Matzler and Wiesmann 1999). With additional amounts of LWC, the T_B values converge on the snowpack temperature, though more LWC is required for T_B to reach the maximum temperature with larger snow grains. Finally, the grid cell snowpack temperatures were scaled to obtain domain-average temperatures of 250 and 270 K. Changing the snow temperature had less of an impact on the initial T_B, which with dry snow ranged from 243 to 251 K, than for some of the other snow characteristics (Figure 6d). However the snow temperature determines the maximum T_B value of the wet snowpack. In almost all cases, with the exception of the largest correlation length, the T_B reached a maximum T_B at approximately 1% LWC.

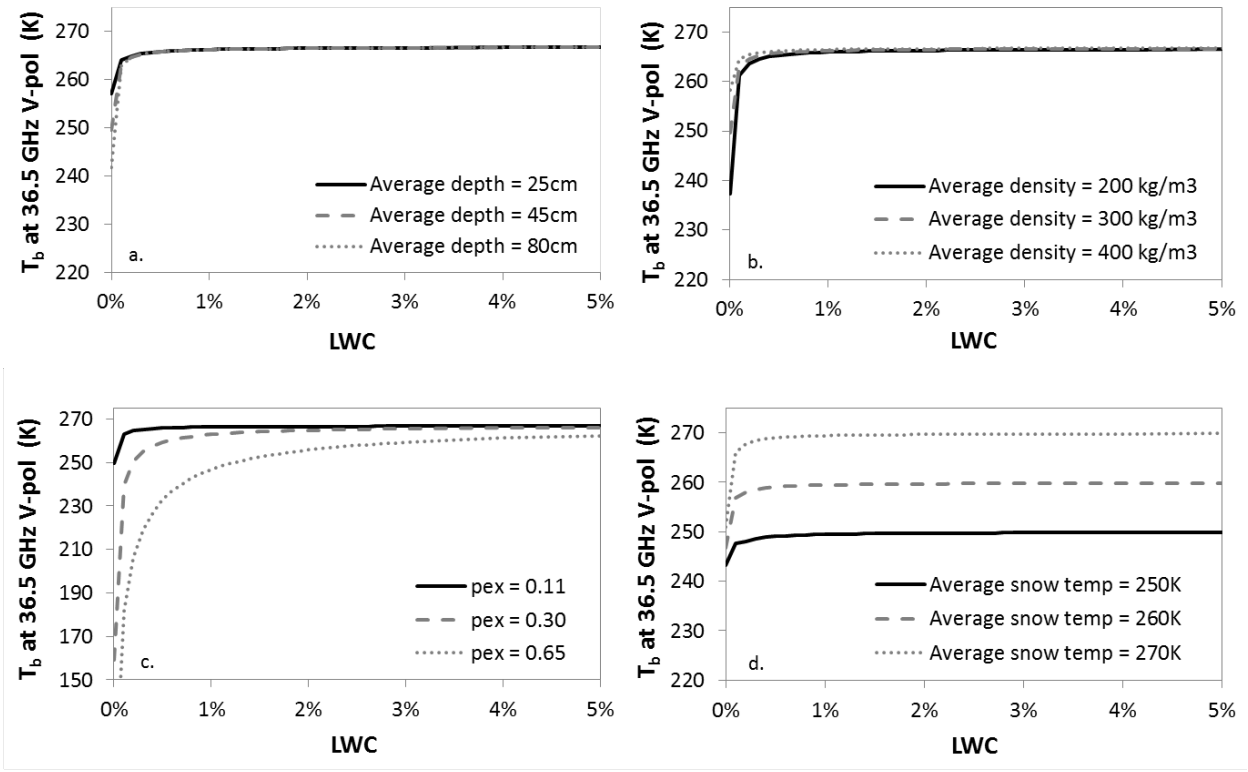

Figure 6. Vertically polarized 36.5 GHz T_B for increasing percent LWC, averaged over the domain as a function of a. snow depth, b. snow density, c. correlation length, and d. snowpack temperature.

Effects of spatially distributed LWC to aggregated T_B signal

The next analysis considered the microwave response for a region in which part of the snowpack was wet and part was dry. A 1% LWC was assigned to a portion of the grid cells in the domain, increasing in area by 10% for each simulation, from 0 – 100%. T_B was modeled using MEMLS for each grid cell, then a single, average T_B value was calculated for the domain. The 1% LWC value was selected based on the results of the previous analysis when the maximum T_B value was typically reached despite variations in snow properties. The 1% LWC was first assigned randomly to grid cells and then by grid cell elevation starting with the lowest elevations. Figure 7 shows examples of the resulting T_B distribution when 1% LWC is assigned randomly (top row) and from low to high elevation (bottom row) over 20, 50 and 80% of the total area. In the randomly distributed examples, the spatial variation in T_B clearly decreases as a greater

percentage of the area is wet, while the low T_B values at higher elevations persist when LWC is distributed by elevation. The relationship between the portion of area with 1% LWC randomly distributed and the average change in T_B over the domain follows a linear trend (Figure 8). When the LWC was distributed by elevation, the results nearly match the linear relationship of the randomly distributed LWC though results are slightly depressed in the middle. The greatest difference in T_B when LWC is distributed randomly and by elevation is 1 K when 50% of the domain is affected. This reduced T_B when approximately half of the area is impacted is likely due to the deeper dry snow remaining at the higher elevations lowering the average microwave emission.

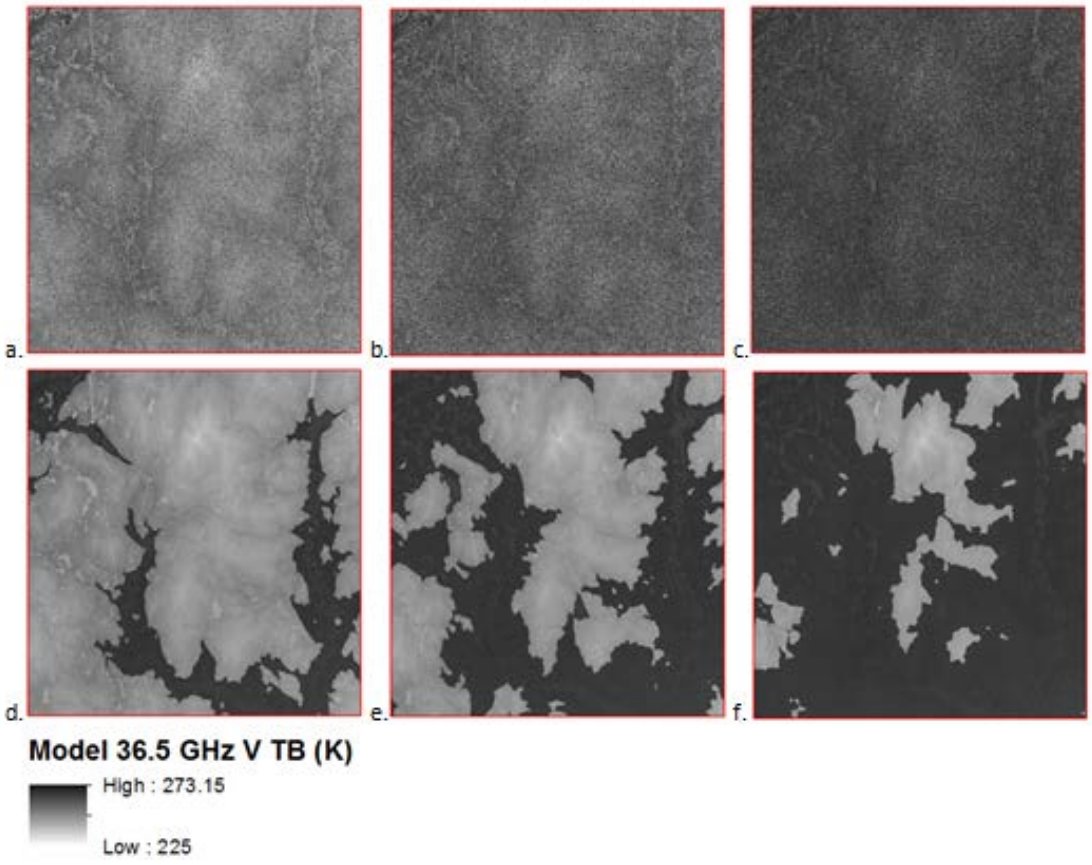

Figure 7. $T_{B,\,36.5\,V}$ resulting from 1% LWC distributed randomly (top row) and by elevation (bottom row) over 20% (a, d), 50% (b, e) and 80% (c, f) of the area.

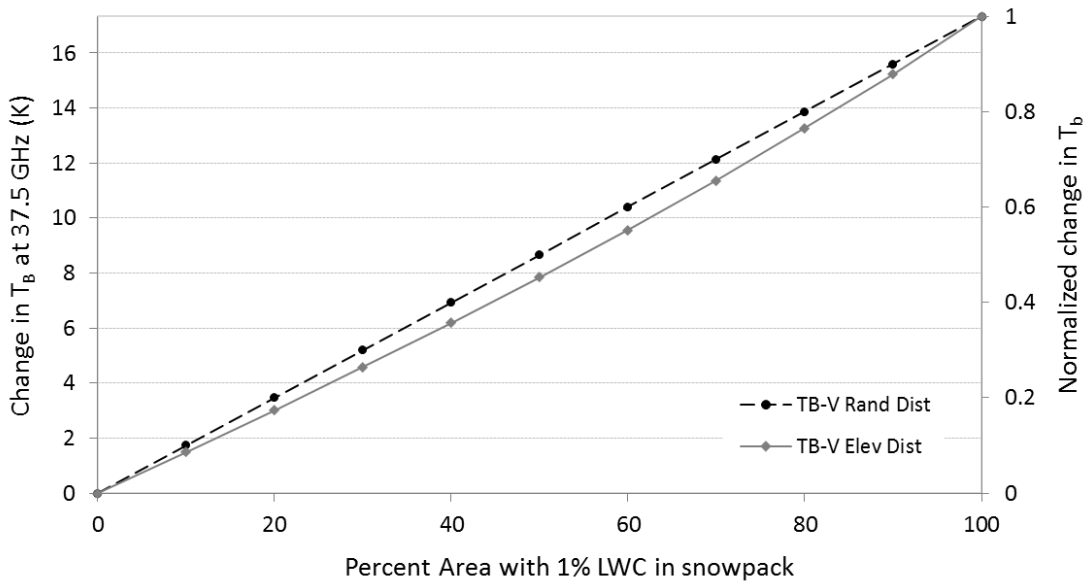

Figure 8. Change in average T_B over domain as a function of percent area with 1% LWC, for a randomly assigned distribution and a distribution based on elevation.

3.4.4 WET SNOW EVENTS

COMPARISON OF MODELED WET SNOW EVENTS TO SENSITIVITY RESULTS

Over the 9-year period, 44 wet snow events were detected using a threshold change in T_B greater than 5K from the previous day and limiting the analysis to the December to March time period when the average SWE over the domain was at least 10 mm. Figure 9 shows the wet snow events plotted along with the sensitivity analysis results when the LWC was distributed by elevation. There is good agreement between the modeled wet snow events and the sensitivity analysis results, indicating that despite variability in snow properties there is a clear response to wet snow events.

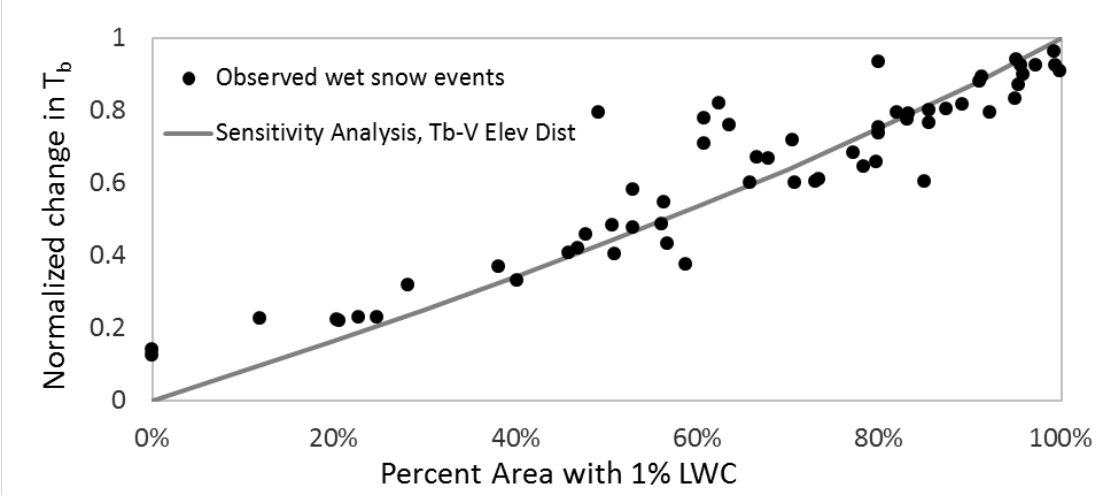

Figure 9. Normalized change in 36.5 GHz T_B (equation 3) for wet snow events and results of the sensitivity analysis when LWC was distributed by elevation

Comparison of modeled emission results to satellite retrievals

For each of the 44 wet snow events identified in the modeled emission results, the AMSR-E vertically polarized 36.5 GHz T_B was obtained for the study domain. For each wet snow event, an increase in the AMSR-E T_B signal was observed. There is a positive linear relationship (R^2 = 0.13) between the satellite observations and model T_B changes during each of the events; there is also considerable scatter (Figure 10). Despite the heavy mixed-forest tree canopy, the magnitude of the AMSR-E T_B changes are as large as those modeled changes.

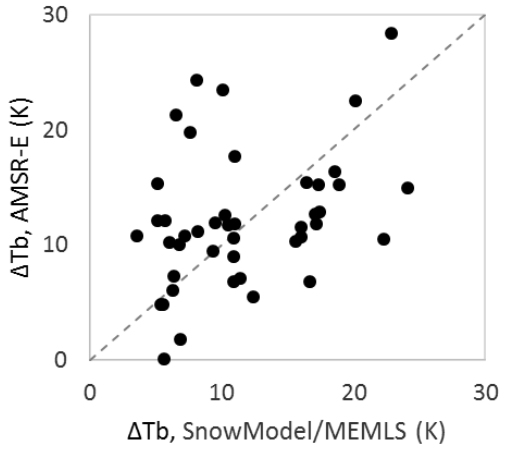

Figure 10. Change in T_B corresponding to wet snow events from MEMLS and AMSR-E, with 1:1 line.

EVALUATION OF DISCHARGE RESPONSE

Wet snow events indicate snowmelt and, in some cases, will be followed by streamflow increases. For the 370 km^2 Baker River watershed, the change in discharge, ΔQ, from the date of the T_B response to the peak flow, up to four days following the wet snow event, was evaluated. Figure 11 shows the relationship between the increasing discharge and the increasing T_B from the model results and AMSR-E observations. While there is not a strong relationship between the magnitude of the T_B increase and discharge (correlation less than 0.1 for MEMLS and 0.22 for AMSR-E), in all cases, an increase in discharge followed the increase in T_B. In approximately 20% of the events the increase in discharge was small (less than 10% of the average peak annual flow, 29 cms), though the change in T_B could be large. Many of these events represent early-season warming periods that did not result in significant increases in discharge. The comparison improves if the events are evaluated by month, though there is still a significant amount of scatter in the microwave response.

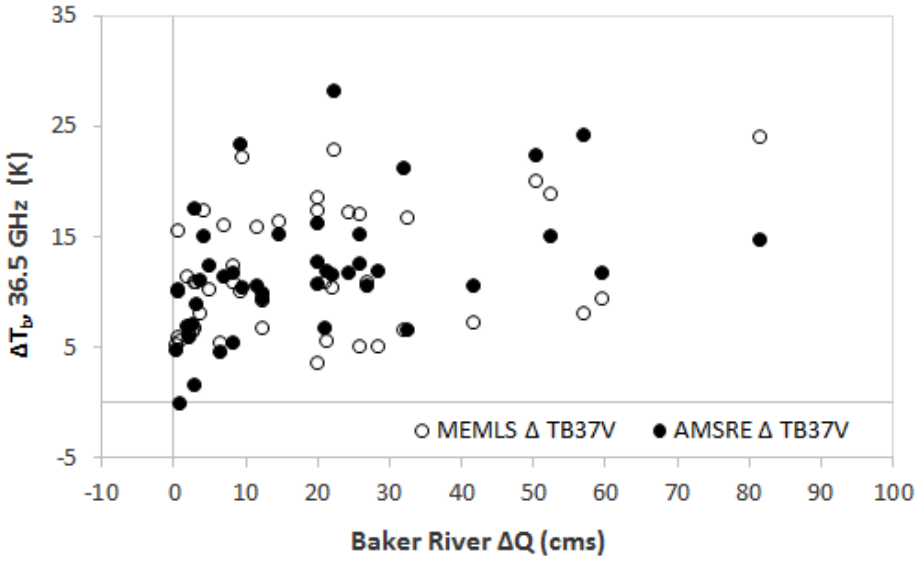

Figure 11. Modeled and observed temperature brightness changes versus discharge increase at the Baker River gage following wet snow events.

3.5 DISCUSSION

The response of T_B to the presence of liquid water in the snow dominates the emission signal. This signal has been identified in previous research as a potential indicator of melt onset. The results of this study agree with earlier research, which showed a sharp increase in the measured 36.5 GHz T_B value with relatively low LWC values. Similarly, we found constant values for the vertically polarized T_B and decreases in horizontally polarized T_B with additional LWC above 1% (Kang et al. 2014). Snow depth, density and grain size have a strong impact on the measured T_B for dry snow, but the change in T_B with wet snow is clearly evident over a range of initial snow characteristics. In contrast to Kang et al. (2014), this study found that different grain sizes can yield a significant difference in the initial T_B response, though the resulting T_B once LWC is present is similar despite differences in snow properties.

Based on the sensitivity analysis performed in this study, there is a near linear relationship between the percent area where wetting has occurred and the change in the aggregated T_B signal over that area. There is only a small difference in the relationship when the LWC is distributed randomly versus by elevation in this region. An accurate distribution is important to correctly estimate the discharge response; therefore additional information can be used to spatially distribute the disaggregated wet snow signal. During the ablation period, snowmelt is driven by energy fluxes that are influenced by topography, vegetation and solar radiation (Melloh et al. 2008). Several studies have observed repeated patterns in spatial distribution of melt using various techniques, such as digital imagery, terrestrial laser scans and remote sensing (Egli et al. 2012; Ide and Oguma 2013), which could be used to describe the melt distribution.

The results of the sensitivity analysis were compared to actual wet snow events as detected by the combined snow-emission model over a 9-year period. There is strong agreement between the

percent area affected by wet snow and the change in T_B across a range of snow conditions and time periods. The comparison of modeled results to the AMSR-E T_B response during wet snow events yielded a moderate positive linear relationship. While all of the detected melt events saw a corresponding positive increase in AMSR-E T_B measured at 36.5 GHz, the correlation between the magnitudes of T_B changes was weak. This may be due to regional effects of vegetation on the satellite signal, timing differences between the satellite observations and model simulations, or the area over which the area-weighted average was computed. Previous research has shown regional differences in the satellite sensor performance in estimating SWE as compared to modeled data (Vuyovich et al. 2014). Thus, it is promising that the satellite observations detect wet snow events in this vegetated region, and the signal response should be investigated in different regions and domains.

The comparison of the wet snow signal response and the discharge at a station within the domain showed a positive relationship between increased T_B and increased discharge. It is encouraging to see agreement at such a small scale, particularly given the daily temporal resolution of the model. Yan et al. (2009) used the melt signal from DAV and a conceptually-based hydrologic model to predict spring snowmelt over a large Alaskan basin. While their hydrograph timing results were accurate in most years, they acknowledge limitations of running at such a coarse resolution (to match EASE-grid pixel size), and the need for better snowpack characterization. This study provides the potential basis for disaggregating melting snow within the microwave pixel based on the T_B response.

3.6 CONCLUSION

Satellite-based, passive microwave data have been investigated over multiple decades for their ability to provide global snow information. More recently, the signal response to liquid water in

the snowpack has been examined for its potential to predict snowmelt onset timing. This study expanded earlier work by Kang et al. (2014) and Pan et al. (2014), investigating the sensitivity of microwave emission at a point, by evaluating the emission response to spatially distributed LWC. A sensitivity analysis was conducted using synthetic distributions of LWC over a realistically distributed snowpack. An increasing, near-linear relationship between the T_B signal response and the percent area with LWC present was found, suggesting that the microwave response provides the potential basis for disaggregating melting snow within a microwave pixel. The results were confirmed by evaluating actual wet snow events over a 9-year period. These results have important implications on the potential use of microwave data to inform not only the melt timing but also the magnitude of runoff. Operational snow hydrology models can assimilate estimates of snowpack characteristics to improve accuracy of melt timing and magnitude, compared to using meteorological forcing data alone. Future work should evaluate the utility of microwave data to initialize model snow state based on the wet snow response.

Wet snow events identified in the microwave signal were compared to discharge data for a basin within the domain. An increase in T_B was followed by a subsequent increase in discharge in all cases; however the magnitude of the change did not correspond. Next steps should include evaluating the spatial distribution of wet snow in larger basins to understand the hydrological impact of large-scale snowmelt events as detected by passive microwave data. The microwave signal should be evaluated across different regions where the satellite-based wet snow signal may perform better. Future work should also investigate whether the relationship holds in other snow regimes, such as a homogenous plains snowpack or deep mountain snowpack with high spatial variability.

CHAPTER 4 MICROWAVE EMISSION AND DISCHARGE RESPONSE TO WATERSHED-SCALE SNOWMELT EVENTS

4.1 INTRODUCTION

Each year snowmelt contributes to water supply and flooding in watersheds across the United States and around the world. Early detection of melt events could have quantifiable benefits to communities by enabling water managers to capture the runoff and mitigate damages due to high flows. Snowmelt evolution is particularly difficult to characterize given the heterogeneous and dynamic nature of snow and because most ground-based measurement techniques result in destruction of the snowpack (Mitterer et al. 2011). Improvements to current global estimation capabilities are limited by our understanding of the physical processes and the need for innovative remote sensing and data assimilation techniques (McCabe et al 2007). The goal of this paper is to evaluate the potential for remotely sensed passive microwave data, which are highly sensitive to liquid water in the snowpack, to provide information on the spatial distribution of melting snow and rain-on-snow phenomena to inform hydrological applications.

In the United States, operational agencies (e.g. NWS, USACE) use hydrologic forecast models to predict the volume of water flowing through rivers. These models estimate the amount of runoff a precipitation or snowmelt event generates, compute how the water will move downstream, and predict the flow of water at a given location throughout the forecast period. To forecast the results of precipitation or snowmelt events, these models require both observed and forecast meteorological data and often assimilate state variables (e.g., SWE, snow covered area, soil moisture, etc.) to improve model results. Lack of data to initialize the model state can result in poor model performance and in some instances expensive consequences (Parrett & Hunrichs 2006; NOAA 2012). Ground-based snow observations are accurate at a point, but can be both

temporally and spatially scarce and therefore miss the spatial variability of snow processes over a landscape.

Currently, available sources of real-time, spatially distributed snow data in the United States include operational models and remote sensing. The NWS National Operational Hydrologic Remote Sensing Center (NOHRSC) produces a near real-time 1 km^2 gridded estimate of snow water equivalent (SWE) and other snow properties through its SNOw Data Assimilation System (SNODAS). SNODAS integrates a combination of downscaled forcing data, an energy balance snow model and assimilated observations in their daily gridded SWE product to arrive at their estimate of the snow characteristics over the United States (Carroll et al. 2006).

Satellite-based passive microwave sensors are another source of spatially-distributed snowpack information, with a coarse spatial resolution but relatively high temporal resolution (twice-daily overpasses) and the ability to sense through clouds and at night. Microwave emissions, measured in brightness temperature (T_B), at 37 GHz frequency are sensitive to the presence of snow on the Earth's surface because of the extinction of the signal from the ground by snow. These data have the potential to be a viable source of snow information, particularly in remote, data-sparse regions where no ground observations or operational models exist. Unfortunately, the passive microwave SWE estimation capability suffers under certain conditions, including heavy vegetation (Derksen et al., 2003; 2005), deep snow (Clifford, 2010), coarse snow texture (Foster et al., 1999; Hall et al., 1986; Josberger and Mognard, 2002), and wetness (Hallikainen et al., 1986; Walker and Goodison, 1993). Vuyovich et al. (2014) compared passive microwave SWE products to SNODAS SWE in 2100 watersheds across the U.S. and found the best comparison occurred in basin with an average forest cover less than 20% and average maximum annual SWE less than 200 mm.

During the winter months snow acts as a natural storage of water and can have a large impact on the annual water budget, contributing to drought in low snow years and floods during periods of rapid snowmelt. Discharge from snowmelt can affect hydrologic regimes in high-latitude regions, resulting in a large percentage of annual runoff occurring during the spring melt period. Before solid snow can to turn to liquid water, energy first goes into warming the snowpack to an isothermal state at the melting point. Liquid water in the snowpack must exceed the maximum storage capacity of snow, estimated between 5-10% (Albert & Krajeski 1998), before it is released to infiltrate the ground or contribute to overland flow. Typically solar radiation initially melts surface snow which then percolates downward through the snowpack during the day and refreezes or cools at night, resulting in a diurnal signal in the streamflow. As temperatures warm, continuous daytime and nighttime melt produces the bulk of spring snowmelt runoff, which can last for weeks or months depending on the region and the snow mass. Rain can add energy to a ripe snowpack resulting in widespread melting and additional runoff.

The spatial distribution of snowmelt influences the hydrologic response of the basin, resulting in different peak flows and timing depending on the contributing area and the characteristics of the snowpack (Lundquist and Dettinger 2005). Previous research has demonstrated the use of remote sensing techniques to relate the aerial extent of snowpack warming to runoff magnitude. In the Taylor Valley of Antarctica, Dana et al (2002) used an index of surface temperature data derived from AVHRR at a basin scale to successfully predict the magnitude of seasonal runoff across different landscapes. While snowmelt due to solar radiation is the dominant runoff signal in Polar Regions, numerous additional contributing factors challenge the ability to forecast spring runoff magnitude in mid-latitude watersheds, including liquid precipitation, evapotranspiration and antecedent soil moisture.

Recent work by Vuyovich et al. (in press) found a near-linear relationship between the spatial distribution of wet snow and the microwave signal response. This paper investigated the hypothesis that the magnitude of the melt response as detected by microwave sensors on a watershed scale was predictive of the watershed runoff response. An additional goal of this research was to determine if satellite-based passive microwave data have the potential to inform operational snow models of melt events in diverse regions and snow conditions. The accuracy of satellite-based SWE estimates has been shown to vary regionally with vegetation and snow depth (Vuyovich et al. 2014), however the wet snow signal response may still provide predictive information even in regions where the SWE products perform poorly. In particular, this paper seeks to address the following questions:

1. Does the relationship between spatial extent of wet snow and 36.5 GHz T_B response found in Vuyovich et al. (in press) hold at the basin scale, across diverse regions and snow regimes?
2. Does the 36.5 GHz T_B response to wet snow correspond to the magnitude of the discharge response during individual and seasonal runoff events?
3. Does the satellite 36.5 GHz T_B response show potential skill for forecasting snowmelt volume to inform hydrological applications?

For this study, several diverse watersheds across the U.S. were selected to evaluate the microwave signal. This study focused on the 36.5 GHz vertically polarized emission signal (denoted as T_{B37} throughout the rest of this paper) based on previous research demonstrating the sensitivity of this frequency to snow parameters (Tedesco and Kim 2006) and the constancy of the vertically polarized signal once affected by wet snow (Kang et al 2014; Vuyovich et al, in press). A sensitivity analysis was conducted to evaluate the basin-average T_{B37} signal to

increasing areas with LWC. T_{B37} was modeled using a loosely-coupled snow emission model at a 1 km^2 resolution using a one-layer snow model to evaluate the effects of wet snow. The model was then used to simulate T_B over eight winter seasons on a daily time step and compared to satellite observed T_{B37}. The modeled and observed T_{B37} values were then evaluated during snowmelt runoff events to assess skill in predicting both individual event discharge and seasonal discharge.

4.2 STUDY AREA AND DATA

Six basins across the United States were selected for this analysis (Figure 1). The basins range in size, vegetation cover, elevation gradient, and mean annual snow depth (Table 1). Five of the basins were selected from the Geospatial Attributes of Gages for Evaluating Streamflow, version II (GAGES II) dataset, which identifies reference basins with near-natural flow conditions (Falcone 2011): the White River Basin in Vermont; the Sheyenne River Basin in North Dakota; the White River Basin in South Dakota, the Clearwater River Basin in Idaho; and the Tuolumne River Basin in California. The Uncompahgre Basin in Colorado is not classified as a reference basin due to regulation at the Ridgeway Reservoir and possibly irrigation withdrawals. It was selected to represent the Southern Rockies region of the U.S. where few reference basins of adequate size exist. The discharge gage upstream of the Ridgeway Reservoir was used in the analysis. Basin boundaries were obtained from the GAGES II dataset for five of the basins. The Uncompahgre basin boundary came from the Watershed Boundary Dataset (WBD) 8-digit hydrologic unit code (huc) delineation (USGS & NRCS 2013).

Percent tree cover information was obtained from the University of Maryland Vegetation Continuous Fields (VCF) product (DiMiceli et al. 2011). The product uses NASA MODIS satellite imagery to estimate percent tree cover at 250 m resolution. For this study the VCF

product was used to calculate the percent tree cover of each of the basins. The elevation range within each of the basins was determined using the USGS 1 arc sec (approximately 30 m) national elevation data set (NED) (data available from the USGS).

Table 1. Characteristics of watersheds used in study

Map ID	State	Basin	Area (km^2)	Elevation Range (m)	VCF Forest Fraction	Average Max Annual SNODAS SWE (mm)
A	ID	Clearwater	14,270	317 – 2640	0.49	320.3
B	CA	Tuolumne	776	1348 – 3817	0.16	452.2
C	CO	Uncompahgre	2,900	1507 – 3964	0.13	107.1
D	SD	White River	25,790	425 – 1491	0.03	34.2
E	ND	Sheyenne	7,582	392 – 639	0.05	80.8
F	VT	White	1,790	144 – 1113	0.59	172.3

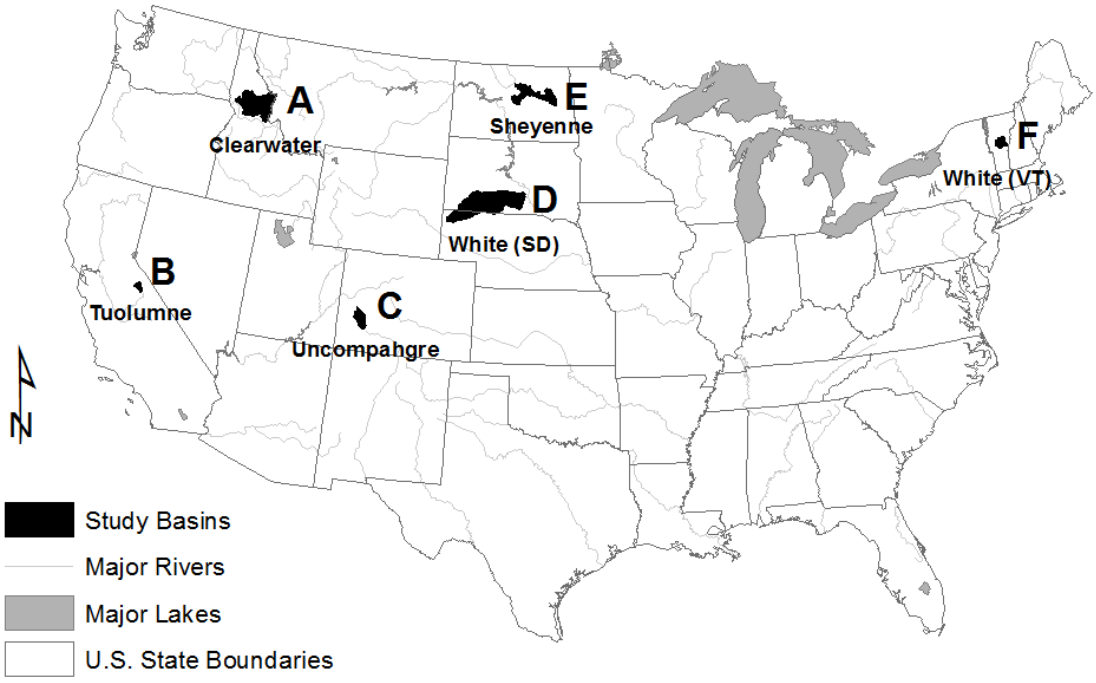

Figure 1. Map of CONUS, showing basins used in study: A. Clearwater River, ID, B. Tuolumne River, CA, C. Uncompahgre River, CO, D. White River, SD, E. Sheyenne River, ND, F. White River, VT

4.2.1 DISCHARGE DATA

Streamflow data were obtained for the USGS gage located at the basins' outlets, with the exception of the Uncompahgre River, which uses a gage upstream of the reservoir (Table 2). Time series of discharge data during the spring runoff period were extracted for each basin.

Individual events were identified and peak annual flow and seasonal volume discharge was calculated. Data were collected for the analysis period (2003 – 2011) in all basins except for the Tuolumne. Tuolumne observations at the USGS gage began in 2006. A time series of unimpaired inflow to the Hetch Hetchy Reservoir, just downstream of the Tuolumne gage, that calculated based on a mass balance of the reservoir inflows and outflows (personal communication, B. McGurk, Hydrologist) were used only in the seasonal analyses. All of the basins show a clear seasonal spring runoff signal (Figure 2) with the largest outflow occurring during the snowmelt period and a relatively low flow for the remainder of the year.

Table 2. USGS stream gages used in study

State	Basin	USGS Gage Number	USGS Stream Gage Name	Spring Runoff Period	Average Annual Peak Discharge (cms)
ID	Clearwater	13340000	Clearwater River at Orofino ID	Mar – Jul	1,456.1
CA	Tuolumne	11274790	Tuolumne R at Grand Canyon of Tuolumne above Hetch Hetchy	Mar – Aug	65.6
CO	Uncompahgre	9146200	Uncompahgre River at Ridgeway, CO	Mar – Aug	26.1
SD	White River	6452000	White River near Oacoma SD	Feb – Jun	280.2
ND	Sheyenne	5057000	Sheyenne River near Cooperstown, ND	Mar - May	51.0
VT	White	1144000	White River at West Hartford	Mar – May	393.4

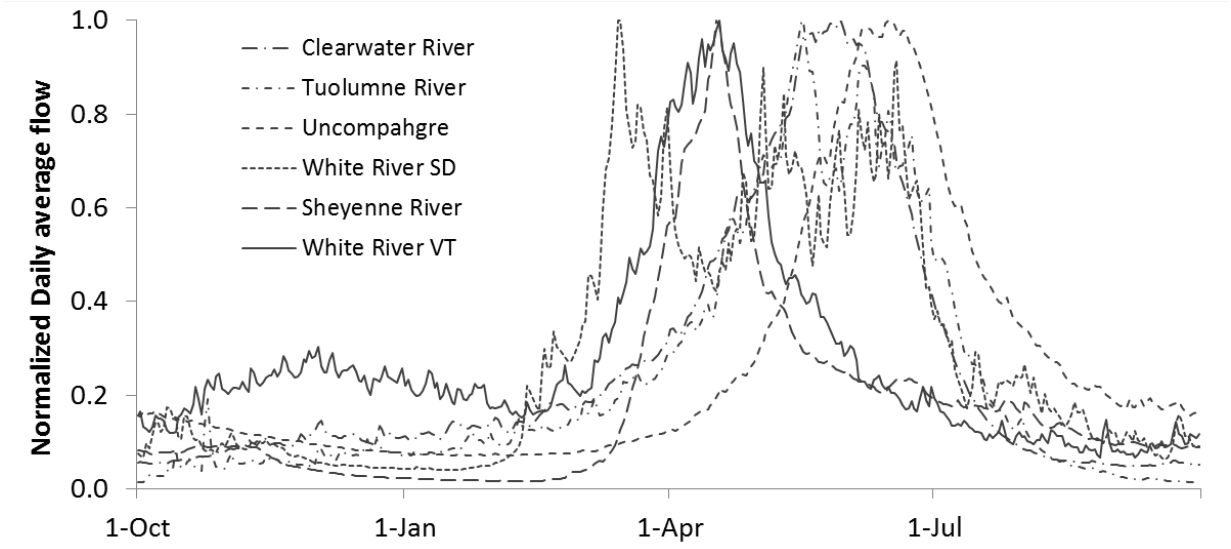

Figure 2. Average daily flow for each basin based on period of record, normalized by maximum daily average flow

4.2.2 *SNOW DATA*

SNODAS combines data from various sources—ground, airborne and satellite observations—with model results, to arrive at a 1 km^2 spatially distributed estimate of snow cover and SWE [Carroll et al., 2006]. Their procedure follows three main steps; ingest and downscale model weather data, simulate snow cover using a physically based energy balance model, and assimilate snow observations to adjust model results. Forcing data come from the Rapid Update Cycle 2 (RUC2) Numerical Weather Prediction (NWP) model output and is downscaled from 13 to 1 km resolution using a digital elevation model. The snow model is an energy and mass-balance, multilayer model based on SNTHERM.89 [Jordan, 1990]. Assimilated observations are acquired from state and federal automated ground observations, snow surveys, and gamma flights as well as satellite-based snow extent information. Daily SNODAS data are available through NSIDC from 1 October 2003 to the present (http://nsidc.org/data/G02158).

4.2.3 *PASSIVE MICROWAVE DATA*

Daily passive microwave brightness temperatures data from the Advanced Microwave Scanning Radiometer-Earth Observing System (AMSR-E) were obtained from the National Snow and Ice Data Center (NSIDC) (Knowles et al 2006). AMSR-E was launched on NASA's Aqua satellite in June 2002 and is available through September 2011. Brightness temperatures measured at wavelengths 6.9, 10.7, 18.7, 23.8 and 36.5 GHz are provided in EASE-Grid projection at 25 km resolution. AMSR-E global T_{B37} data are available twice daily; ascending passes which occur in the afternoon and descending passes which occur in the early morning. The focus of this study was on large-scale melt events resulting in a significant discharge response, therefore only descending passes were used to reduce the potential detection of diurnal surface melt observed in the ascending overpasses. A gap in the satellite swath coverage can occur every three to four

days, depending on the latitude of the basin. A basin average T_{B37} was only computed on days when data for at least 75% of the basin was available.

The effects of vegetation, snow depth and atmosphere can impact the microwave signal. Algorithms to account for these effects have been developed to reduce the error in snow depth and SWE estimation (Kelly et al., 2009; Tedesco & Narvekar 2010). In this analysis, since the relative change in T_{B37} due to wet snow was of interest rather than SWE, no corrections to the signal were made.

4.3 METHODS

4.3.1 SNOW AND MICROWAVE EMISSION MODEL

For this study, the Microwave Emission Model of Multilayered Snowpack (MEMLS) was used to estimate the microwave emissions over the study basins. The model was run on a daily time step over eight years, 2004-2011, at a 1 km^2 resolution. MEMLS is a semi-empirical radiative transfer model that simulates the scattering effect of snow on microwave emissions at frequencies ranging from 5 – 100 GHz using multiple scattering radiative theory (Matzler and Wiesmann 1999; Wiesmann and Matzler 1999). MEMLS estimates internal scattering based on six-flux theory, which is simplified for upwelling and downwelling radiation. Scattering coefficients are determined based on characteristics of the snow.

MEMLS requires snow information, including snow depth, density, temperature, liquid water content (LWC), and the exponential correlation length (p_{ex}). Most of these data were obtained from NOAA's SNODAS operational snow model output (described in Section 4.2.2). Snow depth and temperature were used directly from SNODAS output. Density was calculated from SNODAS SWE and snow depth. The snow depth and SWE estimates from SNODAS have been

evaluated and generally shown to provide good results at a point scale (Rutter et al., 2008; Frankenstein et al., 2008), though over a larger scale, particularly where ground observations are sparse or biased, additional error is introduced (Molotch and Bales, 2005; Meromy et al., 2013). The snow temperature and melt estimated by SNODAS have not been evaluated to date.

The p_{ex} is a metric for grain size used in MEMLS to estimate the scattering coefficient. SNODAS does not provide any estimation of snow grain size, therefore for this study a constant value of 0.11 was assumed to focus the analysis on the change in T_{B37} caused by LWC. SNODAS output includes snowmelt, but not LWC, therefore it was assumed that when melt occurred there was liquid water present in the snow. The LWC was set to 1% when model-estimated melt was greater than zero, based on previous research showing the T_{B37} response reaches a near maximum value at 1% LWC (Cagnati et al. 2004; Stiles and Ulaby 1980; Tedesco et al. 2006).

4.3.2 Sensitivity Analysis

A sensitivity analysis was conducted in each basin to test whether the increasing, near-linear relationship between the change in T_{B37} and the percent area with wet snow found by Vuyovich et al. (in press) holds true for larger basins with diverse landscape characteristics and snow regimes. For each basin, a date was selected when the snow model data estimated complete or near-complete snow coverage and zero melt. This provided realistically distributed baseline snow conditions. Snow model output on that date was used in MEMLS to estimate T_{B37}. A sensitivity analysis was then conducted by systematically increasing the percentage of the total basin area containing wet snow (non-zero LWC) from 0% to 100% in 10% increments. Two different spatial distributions were used to assign LWC to the grid cells: random and by elevation. The random distribution assigned either zero or a constant percentage LWC to grid

cells at random. The elevation distribution assigned LWC to grid cells beginning with the lowest elevations first, and increasing the percent area within the domain as a function of elevation. The elevation distribution was used to replicate a more realistic melt pattern, which is often strongly correlated with elevation, though it is not the only factor (Lundquist et al. 2004), and which in relatively flat areas may not be a significant factor. A LWC value of 1% was used to represent wet snow based on previous research showing the T_{B37} response reaches a near maximum value at 1% LWC (Vuyovich et al. in press, Cagnati et al. 2004; Stiles and Ulaby 1980; Tedesco et al. 2006).

4.3.3 BASIN-AVERAGE T_{B37} COMPARISON

Daily T_{B37}, estimated over the period of analysis, 2003 – 2011 using the snow-emission model, were compared to satellite observed T_{B37} using several statistical metrics. Aggregated basin-average T_{B37} values were used to represent the contributing area to the discharge signal and to avoid introducing error associated with rescaling. To compute the basin-average T_{B37} from both the model results and satellite data, an area-weighted average of the pixel values within the basin boundary was computed. These data were qualitatively compared and not evaluated to assess the absolute accuracy of either estimate. Differences in magnitude and scattering could be due to vegetation or deep snow impacts affecting the satellite signal that were not accounted for; they could also be due to errors in the model data and assumptions affecting the simulated T_{B37}. Following Wilmott (1982), two difference measures were computed to evaluate the average difference: root mean square error (RMSE), and mean absolute error (MAE), calculated as,

$$RMSE = \left[\frac{1}{N}\sum_{i=1}^{N}(M_i - O_i)^2\right]^{\frac{1}{2}} \quad (1)$$

$$MAE = \frac{1}{N}\sum_{i=1}^{N}|M_i - O_i| \quad (2)$$

where *N* is the number of data points being compared; *M* is the snow-emission model predicted value, and *O* is the satellite observation. Differences in measured and simulated T_{B37} relate to the magnitude of SWE potentially estimated by either data. Bias was evaluated using the mean bias error (MBE) measure to evaluate systematic differences in the estimated and observed T_{B37},

$$MBE = \frac{1}{N}\sum_{i=1}^{N}(M_i - O_i) \quad (3)$$

Time series of the data were also visually inspected to evaluate how the data tracked over each season. The data were compared during the winter period only when snow was likely to be on the ground.

4.3.4 Basin-average T_{B37} Difference Index

A brightness temperature difference index (T_BDI) was derived from the T_{B37} data for comparison to discharge data in each of the basins. T_BDI represents the total area within the basin affected by wet snow, assuming a linear relationship with the change in T_{B37}, based on Vuyovich et al. (in press). T_BDI was computed over each basin as,

$$T_B\text{DI} = \begin{cases} \frac{\sum_{j=1}^{n}(T_{B37(j,i)} - T_{B37(j,i-1)}) * A_j}{n}, & T_{B37(j,i)} \geq T_R \\ 0, & T_{B37(j,i)} < T_R \end{cases} \quad (4)$$

where *i* is the current date, *n* is the number of pixels in the basin, and *A* is the fraction of the pixel, *j*, within the basin. A threshold minimum T_{B37} value, T_R, was used to filter out increases that occurred while the T_{B37} was still well below the melting point, when the snow melt was not

likely to contribute to runoff. A separate minimum T_BDI threshold of 5 K was used to filter out small scatter in the signal that occurs throughout the year.

During the snow period, the peak flow and maximum change in flow during individual runoff events was compared to the maximum daily T_BDI that occurred in the week prior to the event. This 7-day window allows for melt water travel time which is likely to result in a lag between the snow melt observed in the T_{B37} signal and that melt water driven discharge response at the basin outlet. Seasonal discharge signals were also evaluated in comparison to the maximum annual T_BDI. The total discharge volume, computed over the spring runoff period for each basin, and the peak discharge that occurred during that same period were compared to the peak winter T_BDI value.

Discharge metrics for individual runoff events and seasonal discharge signals were compared to the observed and modeled T_BDI using regression analyses. An error matrix analysis (Congalton, 1991) was performed to determine the accuracy of T_BDI in predicting changes in discharge. Again, a 5 K minimum T_BDI threshold was used to identify large T_{B37} changes. Large runoff events were considered discharge increases greater than 10% of the average annual peak flow. Events where both the T_{B37} change and the discharge change were above (below) the threshold were considered correctly predicted (rejected). Events where the T_BDI threshold was exceeded but the discharge threshold was not are considered "false alarms". Events where the T_BDI was not exceeded but the discharge threshold was exceeded are considered "misses". The overall accuracy, *A*, is the percentage of pixels that were correctly classified by the model as,

$$A = (CP + CR)/N \tag{5}$$

where *CP* is the number of correctly predicted events; *CR* is the number of correctly rejected events; and *N* is the total number of events. Figure 3 illustrates the concept.

	$\Delta Q > 0.1 * Q_p$	$\Delta Q < 0.1 * Q_p$
$\Delta T_B > 5K$	Correct Prediction (CP)	Miss
$\Delta T_B < 5K$	False Alarm	Correct Rejection (CR)

Figure 3. Error matrix used to evaluate T_BDI performance

4.4 RESULTS

4.4.1 BASIN AVERAGE T_{B37} COMPARISON

The T_{B37} observed by AMSR-E and estimated by SNODAS-MEMLS were compared for each of the basins over nine snow seasons (Table 3, Figure 4). Both datasets showed a decrease in magnitude of the T_{B37} in all basins during winter months when snow was expected to impact the signal. The difference between T_{B37} during the winter periods and snow-free periods was related to the snow depth. Large, rapid T_{B37} signal increases during the winter period, most likely indicated a snow melt event was occurring. The SNODAS/MEMLS and AMSR-E signals often showed large increases at the same time. In all basins except the White River (VT), the model T_{B37} was biased higher than AMSR-E. This was particularly evident in the Sheyenne Basin (ND) where cold winter temperatures and frozen soil could be affecting snow texture and other properties controlling dynamics of the satellite signal. Additional information about snow grain size would help understand what factors were influencing the signal differences in this region. In the Tuolumne and Clearwater basins, where the snow is deepest, the model T_{B37} consistently decreased sharply at the start of the season and then generally increased throughout the rest of the season. These effects seem to be related to the SNODAS simulated snow temperature based

on an evaluation of the model output. The modeled snow temperature data in these two basins followed a similar pattern of sharp decreases early in the season, likely due to thin snow and cold temperatures, while deeper snow likely had an insulating effect from cold air temperature later in the season. Using multiple layers in the snow model rather than one average snow temperature may reduce the impact this seems to have on the T_{B37} results. Interestingly, the T_{B37} results show the poorest comparison in the Sheyenne Basin, a region of the country where a comparison of SNODAS SWE and the AMSR-E SWE product had the best results (Vuyovich et al. 2014).

Table 3. Statistical measures of modelled and observed T_{B37} comparison during analysis period, 2003-2011

Basin	Snow Period	N	AMSR-E $\bar{O}$ (K)	SNODAS/ MEMLS $\bar{M}$ (K)	σ_O (K)	σ_M (K)	R^2	RMSE (K)	MAE (K)	MBE (K)
Clearwater	Dec - May	926	259.0	260.6	7.6	10.8	0.47	8.0	6.3	1.6
Tuolumne	Dec - May	1010	242.5	250.6	8.6	15.7	0.01	19.0	16.1	8.1
Uncompahgre	Dec - May	1014	247.2	257.3	9.0	9.1	0.48	12.3	10.7	10.1
White SD	Jan - Mar	247	251.6	262.8	8.7	8.9	0.41	13.4	11.9	11.2
Sheyenne	Jan - Mar	531	234.6	251.9	14.9	13.7	0.06	24.6	21.0	17.3
White VT	Jan - Mar	539	251.9	249.3	8.5	14.8	0.13	14.4	11.5	-2.5

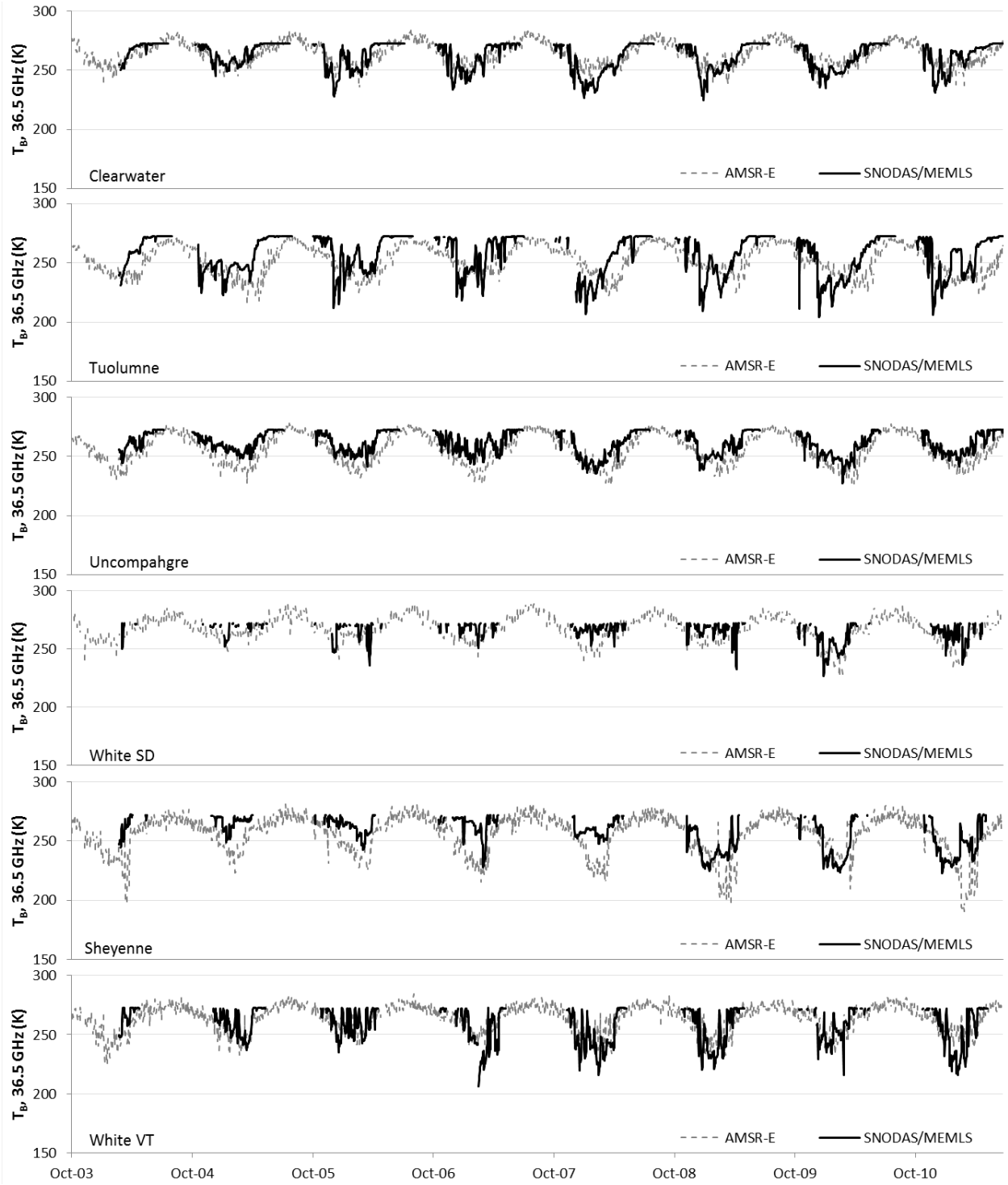

Figure 4. T_B 36.5 observed by AMSR-E and estimated from SNODAS-MEMLS at each basin

4.4.2 *SENSITIVITY ANALYSIS*

A sensitivity analysis was conducted to evaluate how the spatial distribution of snowmelt influences the microwave response in the basin. The relationship between the change in T_{B37} and the percent of the basin area with liquid water in the snow showed an increasing response in all the basins (Figure 5). The response demonstrates that change in T_{B37} is a function of the percent of the basin area that is affected by wet snow. When the LWC was distributed randomly, there was a linear relationship in all basins. When the LWC was distributed by elevation, the relationship was near linear in most basins. In reality, numerous factors affect melt distribution and further analysis of the important factors in each basin should provide insight to the actual relationship. In this study, random and elevation distributions were used for demonstration purposes and to be consistent with previous work (Vuyovich et al., in press).

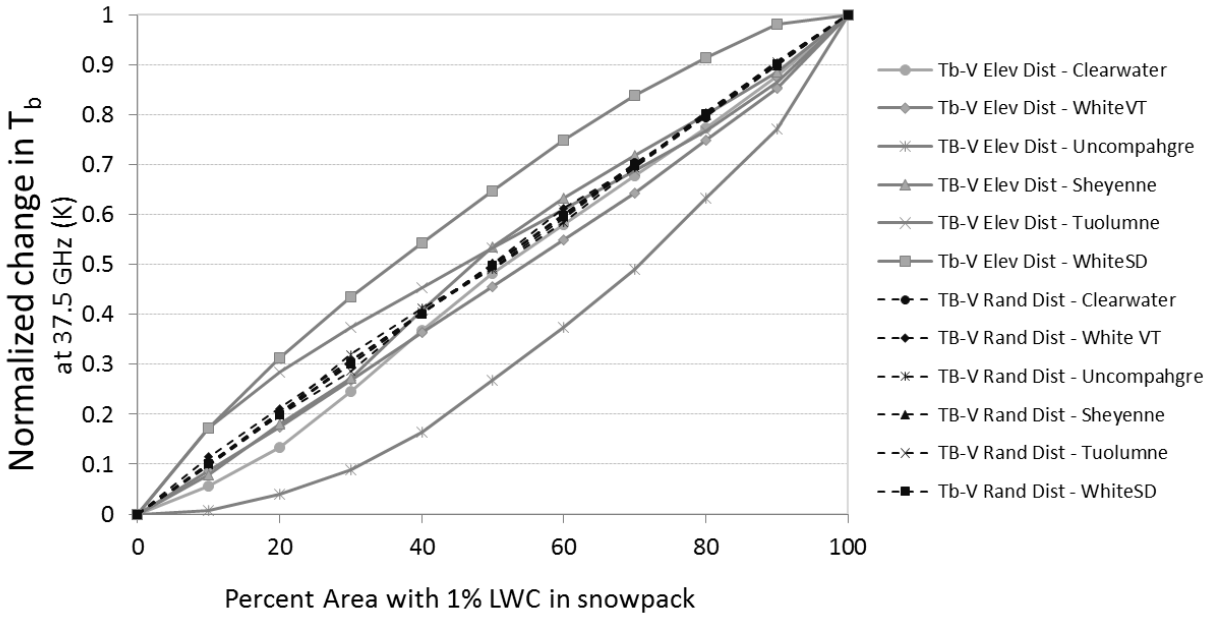

Figure 5. Sensitivity analysis of change in basin average 36.5 GHz T_B when 1% LWC is assigned randomly and by elevation to SNODAS-MEMLS computation

In two basins, the spatial distribution of snow had a noticeable impact on the relationship between aerial extent of distributed LWC and change in T_{B37}. In the Uncompahgre, deep snow

was limited to the highest elevations while approximately 50% of the basin at lower elevations had a shallow snowpack (Figure 6a). This caused the change in T_{B37} to be modest when only the lower elevations were affected and increase sharply as the deeper snow got wet. The White Basin (SD) is relatively flat and most likely melts homogenously or as a function of latitude rather than elevation (Figure 6b). The deepest snow in the White Basin, based on SNODAS estimates, occurs in the northeast of the basin near the basin outlet. At the highest elevations, in the southwest of the basin, the snow is typically not as deep. This causes the change in T_{B37} to appear to increase more quickly at the smaller percent areas when LWC is assigned by elevation. The T_{B37} difference between a LWC that is distributed randomly versus that distributed based on elevation can be quite large. For example, when 40% of the Uncompahgre had LWC, a random distribution had a 40% increase in T_{B37} while the elevation based distribution had only a 15% change. Thus, detection of wetting would be delayed in the Uncompahgre and accelerated in the White (SD) if a linear model were used to relate T_{B37} changes to percent wet area. While basin differences in snowpack and melt distributions were organized by elevation in this study, any basin with a correlation (positive or negative) between melt patterns and snowpack distribution (e.g., latitude) would likely result in a nonlinear T_{B37} response.

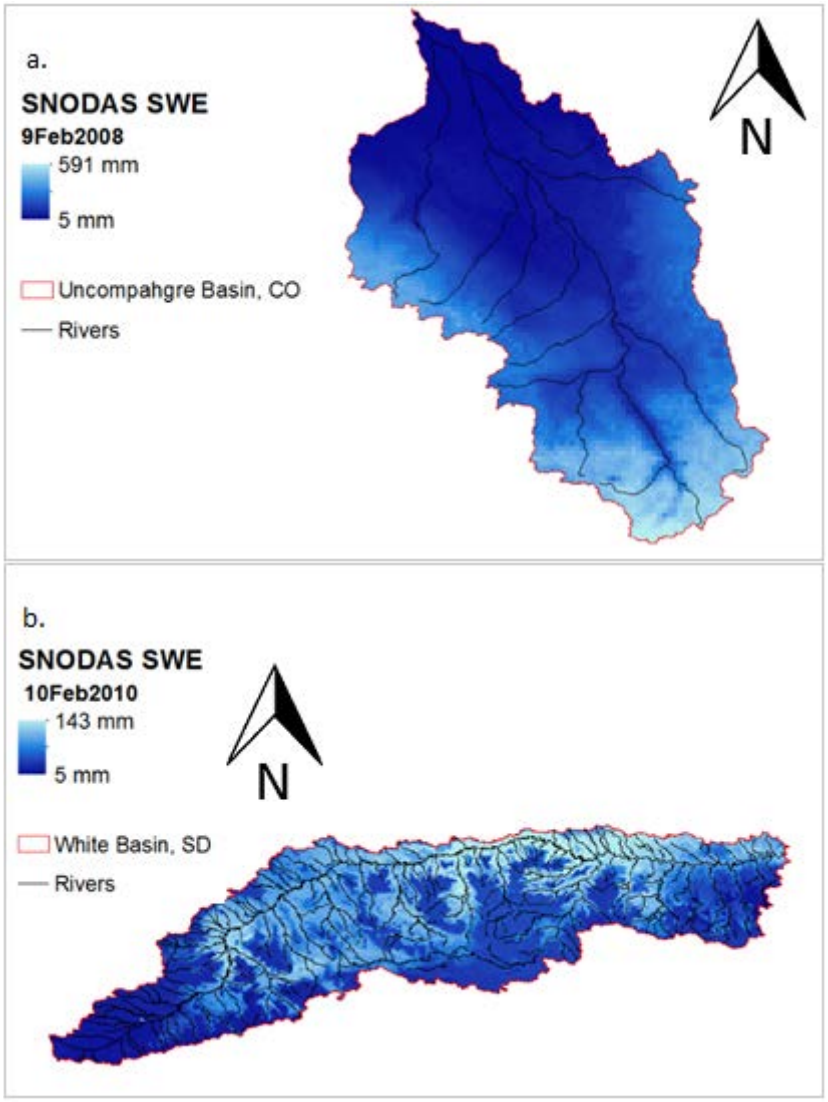

Figure 6. Spatial distribution of snow impacts the sensitivity analysis results in a) the Uncompahgre Basin and b) the White Basin (SD)

4.4.3 Basin Average T_{B37} Difference Index

The aerial extent of wet snow represented by T_BDI computed for SNODAS-MEMLS and AMSR-E were compared to individual runoff events over the nine winter seasons (Table 4). Of the six basins, the AMSR-E T_BDI had a statistically significant correlation to the peak discharge during runoff events in the Sheyenne and Clearwater Basins. The AMSR-E T_BDI in the Sheyenne Basin was also significantly correlated to the change in runoff during these events. There was typically only one major snowmelt runoff event each year in these basins and not

many mid-winter melt periods, which may explain these results. In the other basins, there was generally a positive relationship between increases in AMSR-E T_{B37} and increases in discharge, but the magnitude of the changes were not well correlated. Based on the error matrix analysis, the AMSR-E T_BDI had a computed accuracy between 49 – 69% for all the basins, meaning both the both the change in T_{B37} and the change in discharge were of similar magnitude during approximately half or over half of the events. However, there are several instances of large changes in AMSR-E T_{B37} that do not correspond to large changes in discharge, as shown by the high number of false alarms. These events typically occur early to mid-winter when even wide-spread melting does not lead to significant runoff.

The T_BDI calculated using the results of the SNODAS/MEMLS simulations were typically poorly correlated to the discharge metrics during the individual runoff events. There was often a negative correlation between T_BDI and the change in discharge during individual runoff events. This seems to be related to the estimated snow temperature and melt from SNODAS, though further research is necessary to confirm. Many large T_BDI signals occur early in the season when SNODAS estimates low snow temperatures. Later in the season, the snow temperature from SNODAS was typically close to 273 K and melt was frequently estimated which results in small T_BDI at the time when the largest changes in discharge are occurring. Figure 7 illustrates the results for two basins during the 2011 melt period. The error matrix shows that SNODAS/MEMLS has a very high accuracy for the White River (VT). This is likely the combination of numerous midwinter melt events that are well captured by changes in snow temperature during these brief warming events. In contrast, the Sheyenne basin has warming events, but they are not adequate in timing or magnitude as needed to generate runoff.

Table 4. AMSR-E and SNODAS/MEMLS T_BDI performance during individual runoff events

		AMSR-E					SNODAS/MEMLS				
Basin	T_R (K)	**Peak Q R^2**	**ΔQ R^2**	**Accuracy**	**False Alarms**	**Miss**	**Peak Q R^2**	**ΔQ R^2**	**Accuracy**	**False Alarms**	**Miss**
Clearwater	266	0.42[a]	0.32	49%	28%	23%	0.30*	0.18*	28%	7%	65%
Tuolumne	250	0.16	0.26	59%	24%	17%	0.15*	0.06*	28%	10%	62%
Uncompahgre	259	0.01*	0.03*	61%	12%	27%	0.02*	0.00	33%	24%	43%
White SD	260	0.05	0.03	53%	40%	7%	0.00	0.00	50%	40%	10%
Sheyenne	257	0.77[a]	0.80[a]	69%	25%	6%	0.38	0.34	50%	38%	12%
White VT	263	0.00	0.00	62%	21%	17%	0.01*	0.05*	75%	13%	12%

[a] Significant at the 95% confidence level; *Negative slope

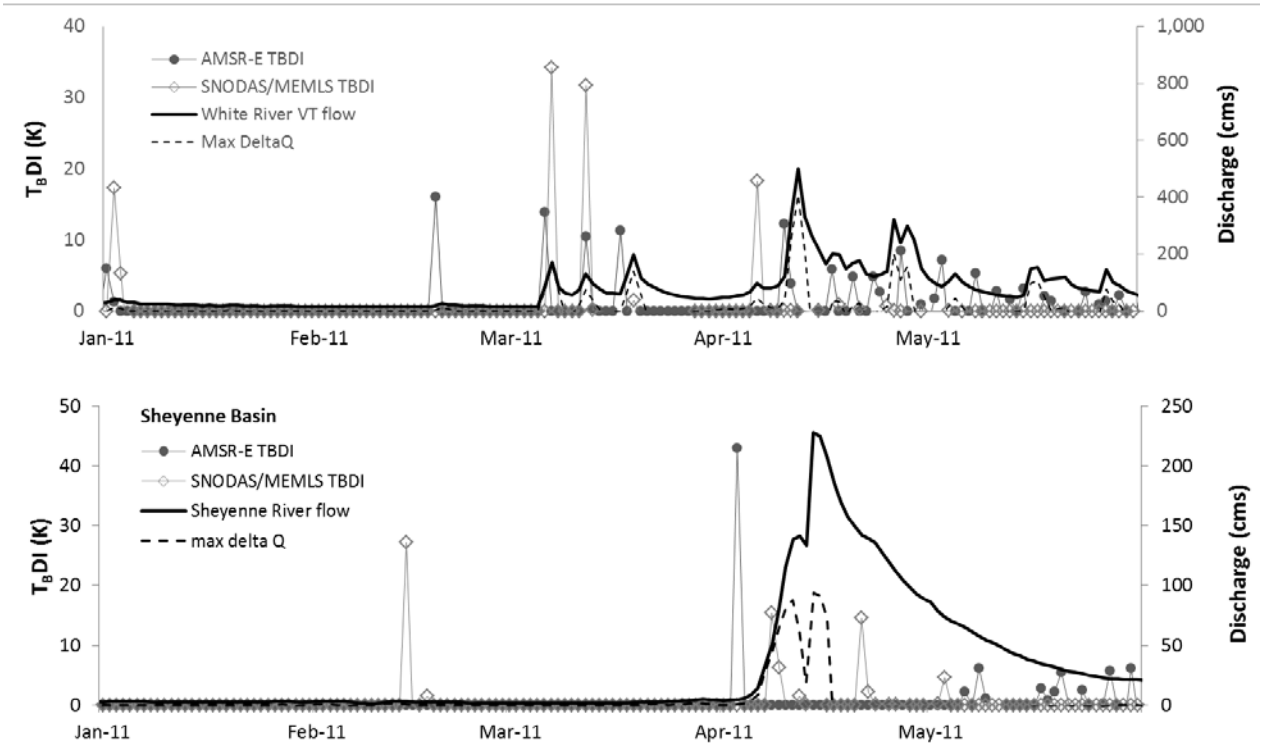

Figure 7. T_BDI results in two basins: White (VT) and Sheyenne in 2011.

The maximum T_BDI that occurred each winter season was compared to the peak runoff and the seasonal volume runoff during the spring melt period (Table 5). The maximum T_BDI generally occurs mid-winter, when the SWE is near the maximum, and a widespread wetting event results in a large impact on T_BDI. This metric was evaluated to assess the magnitude of the T_BDI when the snowpack was ripening, just prior to melt onset. There was a statistically significant relationship between both the AMSR-E and SNODAS/MEMLS T_BDI in the Sheyenne basin.

The AMSR-E T_BDI also had good relationships in the Tuolumne, Clearwater and White (SD) basins, while the SNODAS/MEMLS T_BDI was poorly or negatively correlated to the seasonal discharge metrics for all other basins. The White Basin (VT) basin is heavily vegetated with a temperate climate that experiences numerous warming and rain-on-snow events each winter. This likely affected the relationship between the T_BDI and the seasonal discharge signals. The Uncompahgre Basin did poorly for all metrics for both the AMSR-E and SNODAS/MEMLS T_BDI. This is a region that was expected to do well considering the small annual maximum SWE and low vegetation and in the basin. Since this is the only basin that is not considered a reference basin in GAGES II dataset, there may be discharge withdrawals impacting the results.

Table 5. AMSR-E and SNODAS/MEMLS T_BDI performance during seasonal runoff events

	AMSR-E		SNODAS/MEMLS	
Basin	**Peak Spring Q R^2**	**Seasonal Volume Q R^2**	**Peak Spring Q R^2**	**Seasonal Volume Q R^2**
Clearwater	0.19	0.42	0.13*	0.30*
Tuolumne	0.52	0.47	0.33*	0.15*
Uncompahgre	0.04	0.00	0.07	0.03
White SD	0.27	0.24	0.01	0.05
Sheyenne	0.89[a]	0.78[a]	0.94[a]	0.82[a]
White VT	0.01*	0.14	0.07	0.21

The results of the seasonal comparison of discharge to AMSR-E T_BDI in the Sheyenne Basin are not surprising because the passive microwave SWE estimation has performed well there in previous studies (Chang et al. 2005, Josberger et al. 1998). The reasonable comparison of seasonal data in basins with deep snow was unexpected, though the data still appear to suffer in heavily vegetated regions. These results suggest that passive microwave data may provide better information in regions with deep snow than previously thought since the maximum annual T_BDI is potentially representative of the peak basin SWE prior to melt.

Signal saturation in regions with deep snow generally limits the accuracy of empirical SWE algorithms which use the 18.7 and 36.5 GHz difference to estimate SWE. To test the performance of the 36.5 GHz signal only, a daily T_B difference, $T_{B,D}$ was calculated between the melting temperature, T_f (273.15 K), and the 36.5 GHz AMSR-E T_B.

$$T_{B,D} = T_f - T_{B,36.5\,GHz} \tag{6}$$

The maximum winter difference was then compared to the seasonal volume discharge and the maximum annual SWE from SNODAS (Table 6). The SWE results show that some basins that performed poorly in an earlier comparison study between SNODAS and AMSR-E SWE products have a better relationship when using 36.5 GHz alone. Particularly encouraging are the results in the Tuolumne Basin where deep snow was thought to saturate out the microwave signal after 1 m depth. The Tuolumne, Sheyenne and White (SD) Basins are all significantly correlated to seasonal volume discharge and peak flows (Figure 8).

Table 6. Comparison of maximum annual 36.5 GHz difference to seasonal discharge metrics and SWE from SNODAS, 2004 – 2011

Basin	Peak Spring Flow/AMSR-E Max Ann $T_{B,D}$ R^2	Seasonal Volume Flow vs. AMSR-E Max Ann $T_{B,D}$ R^2	SNODAS Max Ann. SWE/AMSR-E Max. Ann. $T_{B,D}$ R^2	SNODAS Max Ann. SWE/AMSR-E SWE Product[b] R^2
Clearwater	0.08	0.28	0.18	0.34
Tuolumne	0.50[a]	0.56[a]	0.47	0.20
Uncompahgre	0.02*	0.07*	0.11	0.04
White SD	0.73[a]	0.56[a]	0.34	0.17
Sheyenne	0.88[a]	0.67[a]	0.44	0.73
White VT	0.12*	0.06*	0.03	0.19

[a] Significant at the 95% confidence level; [b] results from Vuyovich et al. 2014; *Negative slope

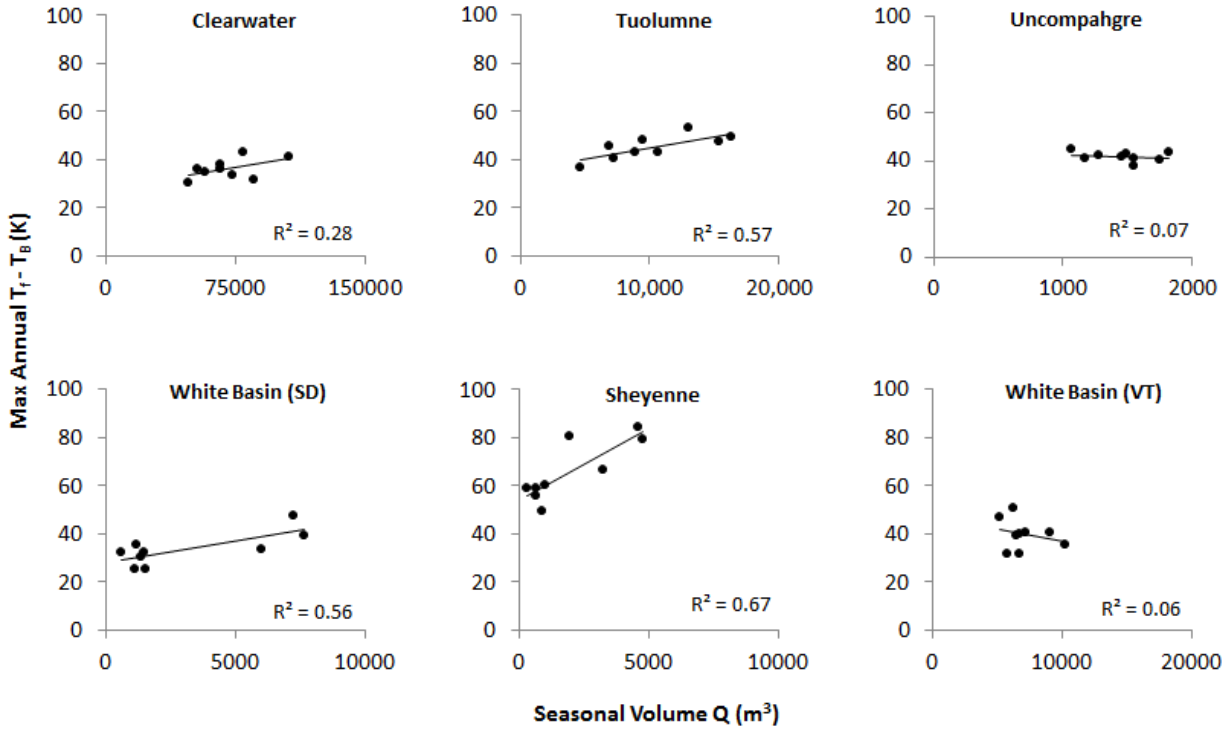

Figure 8. Seasonal volume discharge and the maximum $T_f - T_{B37}$ difference in each basin

4.5 DISCUSSION

In recent years, satellite-based SWE estimation has moved away from empirical approaches in favor of radiance-based assimilation of satellite T_{B37} to inform snow model estimates (Pulliainen 2006; Kelly et al. 2003). To be successful, the snow model must accurately simulate the snow characteristics required by the emission model. A comparison between T_{B37} observed by AMSR-E and estimated by SNODAS/MEMLS showed that in all cases the 36.5 GHz signal decreased during the winter when snow is expected to affect the signal. The seasonal average magnitude of the decrease was similar between the data in many cases, but there were some large differences in the daily results. The AMSR-E observations were not corrected for vegetation impacts in this study, which almost certainly influenced results. Snow grain growth may also be affecting the satellite signal. While the SNODAS SWE data is updated with observations throughout the season, the other snow model variables are not adjusted, which could be

impacting the emission model results. Additional model output, including multiple layer characteristics and grain size information may improve emission estimates. A thorough evaluation of the factors impacting these estimates is left for future research. Based on these results, the SNODAS output appears limited in its ability to inform a microwave emission model or assimilate satellite T_{B37}.

Relationships between the snow extent and volume of water remaining in the snowpack are routinely used to make hydrologic predictions under the assumption that seasonal snow accumulation and ablation patterns are persistent year after year (USACE, 1956; Anderson, 1973; Martinec et al., 2008), and as a function of topography and vegetation (Melloh et al, 2008). The SNODAS/MEMLS model provided an opportunity to conduct sensitivity tests on how the spatial extent of wet snow impacts the average T_{B37} in each of the basins. This was done using realistically distributed snow characteristics from SNODAS as input to MEMLS on days when no LWC was present, and adjusting the distribution of LWC. At the basin scale, the increasing near-linear relationship between the change in T_{B37} and the change in percent area affected by wet snow agrees with earlier work (Vuyovich et al, in press). This suggests that passive microwave data has potential for informing on the spatial extent of snow state at a sub-microwave pixel resolution if the factors that influence melt patterns in the basin are known.

As seen in previous studies, a change in T_{B37} indicated a wetting event and almost always resulted in a subsequent increase in discharge (Ramage and Isaacs, 2002; Grenfell and Putkonen, 2008; Semmens et al., 2013). In basins where there is typically only one annual snowmelt runoff event, such as the Sheyenne, the T_BDI may provide some predictive skill for estimating the discharge response. In basins with a more temperate climate or multiple winter runoff events, too many factors affect the T_BDI signal for it to provide information on discharge magnitude.

For example, a large change in T_{B37} early in the season when the snow is deep, may only cause a small increase in discharge because most of the melt water refroze or drained into the soil. A smaller T_BDI may be observed later in the season when the snow is shallower or when portions of the basins have already started melting (therefore no change in T_{B37}), yet the change in discharge is large because saturated soil conditions result in more surface flow.

The promising results of the AMSR-E T_BDI to seasonal volume discharge comparison suggest the 36.5 GHz channel may provide a better estimate of SWE in deep snow conditions than indicated by previous evaluations of empirical algorithms. Originally, the 18 GHz frequency was used to eliminate the effects of underlying soil conditions from the 36 GHz signal (Kunzi et al 1982). A relationship between the microwave frequency difference and SWE was developed using observations from the Canadian and Russian plains regions. It was noted that similar relationships would need to be developed regionally for the data to be useful (Chang et al 1987). The global SWE products developed from that original algorithm have been found, not surprisingly, to work best in the plains regions and have limited accuracy elsewhere. Future research should investigate regional differences in the satellite algorithms to provide more information for water resources.

4.6 CONCLUSION

This study investigated the potential use of the microwave signal response to wet snow to improve hydrological forecasts of snowmelt timing and magnitude. Several basins were selected in diverse regions of the U.S. to test the ability of the T_{B37} response to detect melt under different vegetation, topographic and seasonal snow conditions. The NOAA SNODAS spatially distributed snow model was loosely coupled with MEMLS to estimate microwave emissions in the selected basins given distributed snow characteristics. A positive relationship between the

subpixel distribution of wet snow and the change in microwave T_{B37} was found in each basin using a sensitivity analysis.

The basin-average changes in T_{B37} were compared to changes in discharge during individual events. While positive increases in T_{B37} correspond to positive increases in discharge, the magnitude of those changes is poorly correlated in most basins. The exception is in the Sheyenne basin in the northern plains of the U.S. where snowmelt runoff typically occurs in one event each spring and where the microwave T_{B37} response may provide information on the magnitude of spring runoff. A seasonal comparison between the 36.5 GHz T_B and discharge showed promising results even in basins with deep annual snowpacks. This suggests further investigation of the SWE algorithms in these regions may lead to better results.

CHAPTER 5

5.1 SUMMARY

The objective of this research was to investigate the potential for passive microwave remotely sensed data to characterize snow and snow melt to improve runoff estimates on a watershed scale. Spatially distributed SWE and snow melt information are critical to land surface characterization and hydrologic applications. Given the temporal and spatial coverage of satellite-based sensors, it is expected that research to expand and improve earth observing techniques will continue to grow (Lettenmaier et al. 2015). The future of snow estimation will likely combine multiple observation sources with physically based numerical models to arrive at the best estimate perhaps using a Land Information System (LIS) (Kumar et al. 2008). Passive microwave, with its long historical record and recognized sensitivity to snow, will almost certainly be an important component in such as system. While numerous factors can affect the microwave signal, there is still potential value for water resources, particularly in regions with little or no snow data available. This research aimed to increase our understanding of the utility and limitations associated with these observations.

The first step was to evaluate the current, empirically-based passive microwave SWE products across multiple regions and snow seasons. This analysis was done by comparison of the satellite-based SWE products to NOAA's SNODAS operational SWE estimates across 2100 watersheds over eight years to determine when and where the products provided a high degree of confidence for water resource applications. Regional influences, including topography, vegetation and snow regime were evaluated in the analysis for impacts on the SWE estimates.

The next step was to investigate microwave observations of snow melt. Microwave emissions are highly sensitive to liquid water in the snow. Numerous studies have investigated this signal response for its ability to detect the timing of snowmelt onset. The presence of liquid water in snow has important hydrologic implications as an indicator of positive net energy going to melt snow and produce water output. In this research, the signal response was analyzed over a spatially distributed area approximately the size of a microwave pixel to assess whether a relationship exists between the aerial extent of wet snow and the magnitude of the T_B response. A sensitivity analysis was performed using a high-resolution, physically based snow-emission model to simulate microwave emissions. The signal response to wet snow was evaluated given a range of spatially distributed snowpack conditions.

Finally, the potential use of the microwave data to improve hydrological forecasts of snowmelt timing and magnitude was investigated on a watershed scale. The hydrologic response of a basin to snow melt is a function of melt volume and the spatially distributed area over which melt is occurring. Several basins were selected in diverse regions of the U.S. to test the ability of the 36.5 GHz T_B response to detect melt under different vegetation, topographic and seasonal snow conditions. The goal was to determine if passive microwave data can provide snowmelt timing and magnitude information even in regions where the satellite-based SWE products performed poorly. The NOAA SNODAS data was used as input to the microwave emission model to test if the results of the sensitivity analysis were valid on a watershed scale.

5.2 Main Findings

Results of the SWE comparison study show large areas where the passive microwave empirically-based SWE products perform well compared to the SNODAS data, particularly in the northern Great Plains and southern Rocky Mountain regions. The best correlations are

associated with basins in which maximum annual SWE is less than 200 mm, and forest fraction is less than 20%. In watersheds with maximum annual SWE values greater than 200 mm, this study found that the relative magnitude of maximum SWE from year-to-year was not captured by the microwave data. This limits the usefulness of the satellite SWE products in regions where seasonal runoff estimates are based on the maximum annual SWE magnitude. Additionally, this study found that where the passive microwave signal is impacted by deep snow and vegetation, the spatial variation also suffers in the SWE products. This is most likely due to saturation effects in areas with SWE greater than 200 mm limiting the algorithm estimates in portions of the basin with deep snow. Finally, regional differences seen between the AMSR-E and SSM/I products in watersheds with shallow snow and vegetation point to differences in the products algorithms' that warrant further exploration.

Earlier research has shown that liquid water in the snow dominates the microwave emission signal over the effects of other snow characteristics. This work confirmed those results and found a near-linear relationship between the T_B signal response over a spatially heterogeneous snowpack and the percent area with LWC present. The results were confirmed by evaluating actual wet snow events over a 9-year period. These findings suggest that the microwave response provides the potential basis for disaggregating melting snow within a microwave pixel. Downscaled estimates of LWC and snow state from passive microwave data could provide valuable snow information required to initialize snow hydrology models beginning in mid-winter.

The results of the sensitivity analysis were confirmed in several basins with diverse vegetation, topographic and seasonal snow conditions. The spatial distribution of snowmelt was found to have an impact on the relationship, which points to the importance of understanding the

topographic drivers of melt, including elevation, aspect and latitude. A comparison of a basin-average T_B difference index and discharge found that while positive increases in 36.5 GHz T_B correspond to positive increases in discharge, the magnitude of those changes is poorly correlated in most basins. The exception is in basins where snowmelt runoff typically occurs in one event each spring and where the T_B response may provide information on the magnitude of spring runoff events. An additional finding of this study was that the passive microwave T_B may be able to detect deeper snow than previously thought without signal saturation. A statistically significant correlation was found between the maximum annual 36.5 GHz T_B difference from AMSR-E and both maximum annual SNODAS SWE and seasonal volume runoff in a basin with an average annual peak SWE of more than 450 mm.

5.3 FUTURE DIRECTION

There is room for improvement in empirically-based SWE algorithms based on the results of this research. Differences between SWE estimates based on a simple linear regression (SSM/I) and an algorithm that uses forest fraction estimates to account for vegetation effects (AMSR-E) demonstrate that it is possible to improve results. Accounting for various vegetation types, instead of just forest fraction may improve results further. Another region where algorithm differences seem to be impacting results is in the Central Plains region of the U.S. where AMSR-E overestimates SWE, using the 89 GHz channel to detect shallow snow. The potential for passive microwave data to detect deeper snow than previously thought is a major finding with significant implications for regions that rely heavily on the seasonal snowpack for water supply.

In the development of the original relationship, a multivariate analysis was used to determine which channels provided the best SWE estimate compared to ground observations (Kunzi et al. 1982). In the Canadian and Russian Plains the 18 GHz T_B showed the best results in removing

the effects of ground state from the signature, however, the 10 GHz channel has also been suggested (Chang et al. 1982), as well as 6.8 GHz (Cagnati et al. 2004). Regional differences in the global SWE product performance may be reduced by evaluating various signal combinations across multiple regions and conditions, as suggested by Chang et al. (1987). Since that early work, significant progress has been made by the soil moisture remote sensing community, including methods for freeze/thaw detection. Investigations that leverage those findings and promote cross-community collaboration could lead to breakthroughs in both soil and snow characterization.

The sub-pixel distributions of snow and vegetation have an impact on the coarse microwave signal which is essentially an average value over those conditions. This study found that the relationship between the aerial extent of wet snow and the average microwave response holds across multiple scales. Additionally, this work suggests that it may be possible to disaggregate wet snow within a satellite footprint if the driving controls or persistent patterns of snowmelt are further understood. Methods to improve the SWE estimates will likely require a deeper understanding of how spatial variability within a microwave pixel impacts the signal, as well as ancillary data to describe the underlying conditions. Fortunately, high resolution datasets, such as vegetation, snow cover and topography already exists and are continuously improving which can help inform on spatial distribution. Field campaigns and methods to integrate multiple data sources efficiently, accounting for uncertainty, will advance the science further.

Passive microwave data have demonstrated potential in informing snow hydrology models. In this research, the magnitude of the T_B change at a basin scale was not able to empirically predict the discharge response magnitude. Basin discharge is a function of numerous factors, including slope and soil characteristics, in addition to the aerial extent of snowmelt. Combining additional

information about the physical hydrology with insight gained from the subpixel distribution of wet snow from microwave data may provide better runoff estimates. Future work should evaluate the utility of microwave data to initialize operational forecast models on snowpack ripeness and LWC to improve estimates of melt timing and magnitude.

In recent years, coupled snow-emission models have been investigated to estimate SWE using radiance-based assimilation of satellite T_B (Pulliainen 2006; Kelly et al. 2003). Promising results have been demonstrated by the GlobSnow product in non-mountainous regions (http://www.globsnow.info/). SNODAS, or other operational snow hydrology models, may benefit from similar use of the microwave emission signal into their already robust assimilation system. Simulated snow physics in these models could be evaluated to improve performance with snow emission models. Such enhancements to operational snow and snow melt estimation are expected to demonstrate improvements to water resource management and flood forecasting.

REFERENCES

Albert, M. and G. Krajeski (1998) A fast, physically based point snowmelt model for use in distributed applications, Hydrological Processes, Vol. 12, pp. 1809-1824.

Anderson, E. (1973) National Weather Service River Forecast System – Snow Accumulation and Ablation Model, NOAA Technical Memorandum, NWS HYDRO-17, November 1973.

Andreadis, K. M., & Lettenmaier, D. P, (2006). Assimilating remotely sensed snow observations into a macroscale hydrology model, *Advances in Water Resources, 29*, 872–886, doi: 10.1016/j.advwatres.2005.08.004.

Apgar, J., J. Ramage, R. McKenney, and P. Maltais (2007) AMSR-E algorithm for snowmelt onset detection in sub-arctic heterogeneous terrain, Hydrological Processes, Vol. 21, pp. 1587 – 1596.

Armstrong, R. and M.J. Brodzik, Arnault, S (Ed.) (1995), An earth-gridded SSM/I data set for cryospheric studies and global change monitoring, *Advances in Space Research*, *16*(10) 155-163, doi: 10.1016/0273-1177(95)00397-W.

Armstrong, R. and M. Brodzik (2002), Hemispheric-scale comparison and evaluation of passive-microwave snow algorithms, Annals of Glaciology, 34, 38 – 44. doi: 10.3189/172756402781817428.

Arslan, A., M. Hallikainen and J. Pulliainen (2005) Investigating of snow wetness parameter using a two-phase backscattering model, IEEE Transaction on Geoscience and Remote Sensing, Vol. 43(8), pp. 1827 – 1833.

Azar, E. A., H. Ghedira, P Romanov, S. Mahani, M. Tedesco and R. Khanbilvardi (2008), Application of satellite microwave images in estimating snow water equivalent, *Journal of the American Water Resources Association*, *44*(6), 1347 – 1362, doi: 10.1111/j.1752-1688.2008.00227.x.

Bailey, A.S., Hornbeck, J.W., Campbell, J.L., & Eagar, C. (2003). Hydrometeorological database for Hubbard Brook Experimental Forest: 1955-2000. In, *Gen. Tech. Rep. NE-305* (p. 36). Newtown Square, PA., : USDA Forest Service Northeastern Research Station

Bales, R.C., Molotch, N.P., Painter, T.H., Dettinger, M.D., Rice, R., & Dozier, J. (2006). Mountain hydrology of the western United States. *Water Resources Research, 42*, 13

Bloschl, G. (1999) Scaling issues in snow hydrology, Hydrological Processes, Vol 13, pp. 2149 – 2175.

Brun, E. (1976) Investigation on swe-snow metamorphism in respect of liquid-water content, Annals of Glaciology, Vol. 13, pp. 22 – 26.

Brun, E., P. David, M. Sudul and G. Brunot (1992) A numerical model to simulate snow-cover stratigraphy for operational avalanche forecasting, Journal of Glaciology, Vol 38(128), pp. 13 – 22.

Byun, K. and M. Choi (2013) Uncertainty of snow water equivalent retrieved from AMSR-E brightness temperature in northeast Asia, Hydrological Processes, DOI: 10.1002/hyp.9846

Cagnati, A., Crepaz, A., Macelloni, G., Pampaloni, P., Ranzi, R., Tedesco, M., Tomirotti, M., & Valt, M. (2004). Study of the snow melt-freeze cycle using multi-sensor data and snow modelling. *Journal of Glaciology, 50,* 419-426

Campbell, J.L., Driscoll, C.T., Eagar, C., Likens, G.E., Siccama, T.G., Johnson, C.E., Fahey, T.J., Hamburg, S.P., Holmes, R.T., Bailey, A.S., & Buso, D.C. (2007). Long-term trends from ecosystem research at the Hubbard Brook Experimental Forest. In U.S.D.o. Agriculture (Ed.). Newton Square, PA: USDA Forest Service

Campbell, J.L., Driscoll, C.T., Pourmokhtarian, A., & Hayhoe, K. (2011). Streamflow responses to past and projected future changes in climate at the Hubbard Brook Experimental Forest, New Hampshire, United States. *Water Resources Research, 47,* 15

Carroll, T., D. Cline, C. Olheiser, A. Rost, A. Nilsson, G. Fall, C. Bovitz and L. Li (2006), NOAA's National Snow Analyses, *Proceeding of the 74th Annual Meeting of the Western Snow Conference,74,* 13.

Cavalieri, D.J., Markus, T., & Comiso, J.C. (2014). AMSR-E/Aqua Daily L3 25 km Brightness Temperature & Sea Ice Concentration Polar Grids, Version 3. In NASA (Ed.). Boulder, CO USA: National Snow and Ice Data Center Distributed Active Archive Center

Chang, A.T.C., Foster, J.L., Hall, D.K., Rango, A., & Hartline, B.K. (1982). SNOW WATER EQUIVALENT ESTIMATION BY MICROWAVE RADIOMETRY. *Cold Regions Science and Technology, 5,* 259-267

Chang, A. T. C., Foster, A., and Hall, D (1987), Nimbus-7 derived global snow cover parameters, *Annals of Glaciology, 9,* 39 – 44.

Chang, A., J. Foster, and D. Hall (1996), Effects of forest on the snow parameters derived from microwave measurements during the boreas winter field campaign, *Hydrological Processes,10,* 1565 – 1574, doi: 10.1002/(SICI)1099-1085(199612)10:12<1565::AID-HYP501>3.0.CO;2-5.

Chang, A., R. Kelly, E. Josberger, R. Armstrong, J. Foster and N. Mognard, (2005), Analysis of ground-measured and passive microwave-derived snow depth variations in midwinter across the Northern Great Plains, *Journal of Hydrometeorology 6,* 20 – 33, doi: 10.1175/JHM-405.1.

Clark, M., J. Hendrikx, A. Slater, D. Kavetski, B. Anderson, N. Cullen, T. Kerr, E. Hreinsson, and R. Woods (2011) Representing spatial variability of snow water equivalent in hydrologic and land-surface models: A review, Water Resources Research, Vol. 47, doi:10.1029/2011WR010745

Clifford, D, (2010), Global estimates of snow water equivalent from passive microwave: history, challenges and future developments, *International Journal of Remote Sensing, 31*(14), 3707 – 3726, doi: 10.1080/01431161.2010.483482.

Clow, D., L. Nanus, K. Verdin, J. Schmidt, (2012), Evaluation of SNODAS snow depth and snow water equivalent estimates for the Colorado Rocky Mountains, USA, *Hydrological Processes*, doi: 10.1002/hyp.9385.

Colbeck, S. (1976) An analysis of water flow in dry snow, Water Resources Research, Vol. 12 (3), pp. 523 – 527.

Congalton, R. G. (1991). A review of assessing the accuracy of classifications of remotely sensed data. Remote Sensing of Environment, 37, 35–46.

Daly, S. F., R. Davis, E. Ochs, and T. Pangburn, (2001), An approach to spatially distributed snow modeling of the Sacramento and San Joaquin basins, California, *Hydrologic Processes,14*, 3257–3271, doi: 10.1002/1099-1085(20001230)14:18<3257::AID-HYP199>3.0.CO;2-Z.

Daly, S.F., C. Vuyovich, E. Deeb, S. Newman, T. Baldwin, and J. Gagnon, (2012), Assessment of the snow conditions in the major watersheds of Afghanistan using multispectral and passive microwave remote sensing, *Hydrological Processes, 26*, 2634 – 2642, doi: 10.1002/hyp.9367.

Dana, G.L., R.E. Davis, A.G. Fountain, and R. A. Wharton (2002) Satellite-derived indices of stream discharge in Taylor Valley, Antarctica, Hydrological Processes, Vol 16, pp. 1603 – 1616.

Davis, R.E., Dozier, J., & Chang, A.T.C. (1987). SNOW PROPERTY MEASUREMENTS CORRELATIVE TO MICROWAVE EMISSION AT 35 GHZ. *Ieee Transactions on Geoscience and Remote Sensing*, *25*, 751-757

Dechant, C. and H Moradkhani (2011) Radiance data assimilation for operational snow and streamflow forecasting, Advances in Water Resources, Vol 34, pp. 351 – 364

Derksen, C., A. Walker, and B. Goodison, (2003), A comparison of 18 winter seasons of in situ and passive microwave-derived snow water equivalent estimates in Western Canada, *Remote Sensing of Environment, 88*, 271 – 282, doi:10.1016/j.rse.2005.02.014.

Derksen, C., A. Walker, B. Goodison, and J. Strapp, (2005), Integrating in situ and multiscale passive microwave data for estimation of subgrid scale snow water equivalent distribution

and variability, *IEEE Transaction on Geoscience and Remote Sensing, 43*(5), 960 – 972, doi: 10.1109/TGRS.2004.839591.

DiMiceli, C.M., M.L. Carroll, R.A. Sohlberg, C. Huang, M.C. Hansen, and J.R.G. Townshend (2011), Annual Global Automated MODIS Vegetation Continuous Fields (MOD44B) at 250 m Spatial Resolution for Data Years Beginning Day 65, 2000 - 2010, Collection 5 Percent Tree Cover, University of Maryland, College Park, MD, USA.

Doesken, N.J. and A. Judson, (1996), *The Snow Booklet: A Guide to the Science Climatology and Measurements of Snow in the United States*, Colorado Climate Center, Fort Collins, CO, 2nd Edition.

Dong, J., J. Walker, and P. Houser, (2005), Factors affecting remotely sensed snow water equivalent uncertainty, *Remote Sensing of the Environment, 97*, 68 – 82, doi: 10.1016/j.rse.2005.04.010.

Dozier, J. (2011), Mountain hydrology, snow color, and the fourth paradigm, *Eos Trans. Am. Geophys. Union, 92*, 373-375, doi: 10.1029/2011EO430001.

Dozier, J., Bair, E.H., & Davis, R.E. (2016). Estimating the spatial distribution of snow water equivalent in the world's mountains. *Wiley Interdisciplinary Reviews: Water, 3*, 461-474

Drobot, S.D., & Anderson, M.R. (2001). An improved method for determining snowmelt onset dates over Arctic sea ice using scanning multichannel microwave radiometer and Special Sensor Microwave/Imager data. *Journal of Geophysical Research-Atmospheres, 106*, 24033-24049

Durand, M, E. Kim, and S. Margulis (2008) Quantifying uncertainty in modeling snow microwave radiance for a mountain snowpack at the point-scale, including stratigraphic effects, IEEE Transactions on geosciences and remote sensing, Vol. 46 (6), pp. 1753 – 1767.

Durand, M, E. Kim, and S. Margulis (2009) Radiance assimilation shows promise for snowpack characterization, Geophysical Research Letters, Vol. 36, L02503.

Durand, M., E.J. Kim, S.A. Margulis, and N.P. Molotch, (2011), A first-order characterization of errors from neglecting stratigraphy in forward and inverse passive microwave modeling of snow, *IEEE Transactions of Geoscience and Remote Sensing, 8*(4), 730 – 734, doi: 10.1109/LGRS.2011.2105243.

Egli, L., Jonas, T., Grunewald, T., Schirmer, M., & Burlando, P. (2012). Dynamics of snow ablation in a small Alpine catchment observed by repeated terrestrial laser scans. *Hydrological Processes, 26*, 1574-1585

Elder, K., Rosenthal, W., & Davis, R.E. (1998). Estimating the spatial distribution of snow water equivalence in a montane watershed. *Hydrological Processes, 12*, 1793-1808

Falcone, J. (2011) GAGES-II: Geospatial Attributes of Gages for Evaluating Streamflow, USGS, Reston, VA, Oct. 2011.

Farmer, C.J.Q, T.A. Nelson, M.A. Wulder, C. Derksen, (2010), Identification of snow cover regimes through spatial and temporal clustering of satellite microwave brightness temperatures, *Remote Sensing of Environment, 114*, 199 – 210, doi: 10.1016/j.rse.2009.09.002.

Foster, J. L., Hall, D. K., Chang, A. T. C., Rango, A., Wergin, W., & Erbe, E, (1999), Effects of snow crystal shape on the scattering of passive microwave radiation, IEEE Transactions on Geoscience and Remote Sensing, 37, 1165–1168, doi: 10.1109/36.752235.

Foster, J., C. Sun, J. Walker, R. Kelly, A. Chang, J. Dong and H. Powell, (2005), Quantifying the uncertainty in passive microwave snow water equivalent observations, *Remote Sensing of the Environment, 94*, 187 – 203, doi: 10.1016/j.rse.2004.09.012.

Foster, J., G. Skofronick-Jackson, H. Meng, J. Wang, G. Riggs, P. Kocin, B. Johnson, J. Cohen, D. Hall, and S.V. Nghiem, (2011), Passive microwave remote sensing of the historic February 2010 snowstorms in the Middle Atlantic region of the USA, *Hydrological Processes*, *26*(22), 3459 – 3471, doi: 10.1002/hyp.8418.

Frankenstein, S., A. Sawyer, and J. Koeberle, (2008), Comparison of FASST and SNTHERM in three snow accumulation regimes, *Journal of Hydrometeorology, 9*, 1443 – 1463, doi: 10.1175/2008JHM865.1.

Frankenstein, S. and E. Deeb (2012) Using microwave remote sensing to determine patterns of SWE and melt timing in remote environments, proceedings, AGU Chapman conference on Remote Sensing of the Terrestrial Water Cycle, 19 – 22 February 2012, Kona, HI.

Frei, A., Tedesco, M., Lee, S., Foster, J., Hall, D.K., Kelly, R., & Robinson, D.A. (2012). A review of global satellite-derived snow products. *Advances in Space Research, 50*, 1007-1029

Girotto, M., G. Cortes, S. Margulis and M. Durand (2014) Examining spatial and temporal variability in snow water equivalent using a 27 year reanalysis: Kern River watershed, Sierra Nevada, Water Resources Research, Doi: 10.1002/2014WR015346.

Grayson, R., G. Bloschl, A. Western and T. McMahon (2002) Advances in the use of observed spatial patterns of catchment hydrological response, Advances in Water Resources, Vol. 25, pp. 1313 – 1334.

Grenfell, T.C., & Putkonen, J. (2008). A method for the detection of the severe rain-on-snow event on Banks Island, October 2003, using passive microwave remote sensing. *Water Resources Research, 44*, 9

Grody, N.C. (1988) Surface Identification Using Satellite Microwave Radiometers, IEEE Transactions on Geoscience and Remote Sensing, Vol 26 (6), pp. 850-859.

Grunewald, T., M. Schirmer, R. Mott and M. Lehning (2010) Spatial and temporal variability of snow depth and ablation rates in a small mountain catchment, The Cryosphere, Vol. 4, pp. 215 – 225.

Guan, B., N. Molotch, D. Waliser, S. Jepsen, T. Painter, and J. Dozier, (2013), Snow water equivalent in the Sierra Nevada: Blending snow sensor observations with snowmelt model simulations, *Water Resources Research, 49*, 1-18, doi: 10.1002/wrcr.20387.

Hall, D. K., Chang, A. T. C., & Foster, J. L, (1986), Detection of the depth-hoar layer in the snow-pack of the Arctic coastal-plain of Alaska, USA, using satellite data, *Journal of Glaciology, 32*, 87–94.

Hallikainen, M. T., Ulaby, F. T., & Abdelrazik, M, (1986), Dielectric-properties of snow in the 3 to 37 Ghz range, *IEEE Transactions on Antennas and Propagation, 34*, 1329–1340, doi: 10.1109/TAP.1986.1143757.

Hansen, M., R. DeFries, J.R. Townshend, M. Carroll, C. Dimiceli, and R. Sohlberg, (2006), *Vegetation Continuous Fields MOD44B, 2001 Percent Tree Cover, Collection 4*, University of Maryland, College Park, Maryland, 2001.

Helsel, D. R., and Hirsch, R. M, (2002), *Statistical methods in water resources*, US Geological Survey Techniques of Water Resources Investigations, Book 4, Ch. A3, Reston, VA.

Homer, C., Dewitz, J., Yang, L.M., Jin, S., Danielson, P., Xian, G., Coulston, J., Herold, N., Wickham, J., & Megown, K. (2015). Completion of the 2011 National Land Cover Database for the Conterminous United States - Representing a Decade of Land Cover Change Information. *Photogrammetric Engineering and Remote Sensing, 81*, 345-354

Ide, R., & Oguma, H. (2013). A cost-effective monitoring method using digital time-lapse cameras for detecting temporal and spatial variations of snowmelt and vegetation phenology in alpine ecosystems. *Ecological Informatics, 16*, 25-34

Jordan, R, (1990), *User's Guide for USACRREL One-Dimensional Snow Temperature Model (SNTHERM.89)*, U.S. Army Cold Regions Research and Engineering Laboratory, Hanover, New Hampshire.

Jordan, R., M. Albert, and E. Brun (2008) Physical processes within the snow cover and their parameterization, Snow and Climate, edited by R. Armstrong and E. Brun, Cambridge University Press.

Josberger, E., N. Mognard, B. Lind, R. Matthews, and T. Carroll, (1998), Snowpack water-equivalent estimates from satellite and aircraft remote-sensing measurements of the Red River basin, north-central U.S.A, *Annals of Glaciology, 26*, 119 – 124.

Josberger, E. G., and Mognard, N. M, (2002), A passive microwave snow depth algorithm with a proxy for snow metamorphism, *Hydrological Processes, 16*, 1557–1568.

Kang, D. and A. Barros (2012a), Observing system simulation of snow microwave emissions over data sparse regions – Part I: Single Layer Physics, IEEE transactions on geosciences and remote sensing, Vol. 50 (5), pp. 1785 – 1805.

Kang, D. and A. Barros (2012b), Observing system simulation of snow microwave emissions over data sparse regions – Part II: Multi-Layer Physics, IEEE transactions on geosciences and remote sensing, Vol. 50 (5), pp. 1785 – 1805.

Kang, D.H., Barros, A.P., & Dery, S.J. (2014). Evaluating Passive Microwave Radiometry for the Dynamical Transition From Dry to Wet Snowpacks. *Ieee Transactions on Geoscience and Remote Sensing, 52*, 3-15

Kelly, R.E., Chang, A.T., Tsang, L., & Foster, J.L. (2003). A prototype AMSR-E global snow area and snow depth algorithm. *Ieee Transactions on Geoscience and Remote Sensing, 41*, 230-242

Kelly, R, (2009), The AMSR-E snow depth algorithm: Description and initial results, *Journal of the Remote Sensing Society of Japan, 29*, 307–317.

Knowles, K., M. Savoie, R. Armstrong, and M. Brodzik. 2006. *AMSR-E/Aqua Daily EASE-Grid Brightness Temperatures, Version 1*. [NSIDC-0301]. Boulder, Colorado USA. NASA National Snow and Ice Data Center Distributed Active Archive Center. doi: http://dx.doi.org/10.5067/XIMNXRTQVMOX. [May 2016].

Kopczynski, S.E., Ramage, J., Lawson, D., Goetz, S., Evenson, E., Denner, J., & Larson, G. (2008). Passive microwave (SSM/I) satellite predictions of valley glacier hydrology, Matanuska Glacier, Alaska. *Geophysical Research Letters, 35*

Kumar, S., R. Reichle, C. Peters-Lidard, R. Koster, X. Zhan, W. Crow, J. Eylander, and P. Houser, 2008: A land surface data assimilation framework using the Land Information System: Description and applications. Adv. Water Resour., 31, 1419–1432, doi:10.1016/j.advwatres.2008.01.013.

Kunzi, K., S. Patil and H. Rott (1982) Snow-cover parameters retrieved from Nimbus-7 Scanning Multichannel Microwave Radiometer (SMMR) Data, IEEE Transactions on Geoscience and Remote Sensing, Vol GE-20 (4), pp. 452 – 467.

Lea, J. and I. Reid, (2006), An evaluation of the SNODAS for determining snow water equivalent on Mount St. Helens, Washington, *74th Annual Western Snow Conference*, Las Cruces, NM, 2006.

Lettenmaier, D.P., Alsdorf, D., Dozier, J., Huffman, G.J., Pan, M., & Wood, E.F. (2015). Inroads of remote sensing into hydrologic science during the WRR era. *Water Resources Research, 51,* 7309-7342

Liston, G.E., & Elder, K. (2006a). A distributed snow-evolution modeling system (SnowModel). *Journal of Hydrometeorology, 7*, 1259-1276

Liston, G.E., & Elder, K. (2006b). A meteorological distribution system for high-resolution terrestrial modeling (MicroMet). *Journal of Hydrometeorology, 7,* 217-234

Liston, G.E., & Hiemstra, C.A. (2008). A Simple Data Assimilation System for Complex Snow Distributions (SnowAssim). *Journal of Hydrometeorology, 9*, 989-1004

Lundquist, J.D., Cayan, D.R., & Dettinger, M.D. (2004). Spring onset in the Sierra Nevada: When is snowmelt independent of elevation? *Journal of Hydrometeorology, 5,* 327-342

Lundquist, J.D., & Dettinger, M.D. (2005). How snowpack heterogeneity affects diurnal streamflow timing. *Water Resources Research, 41*, 14

Martinec, J., A. Rango and R. Roberts (2008) Snowmelt Runoff Model (SRM) User's Manual. WSRM Version 1.11, New Mexico State University, Las Cruces, NM.

Mätzler, C, (1987), Application of the interaction of microwaves with the natural snow cover, *Remote Sensing Reviews, 2*(2), 259 – 287, doi: 10.1080/02757258709532086.

Matzler, C., & Standley, A. (2000), Relief effects for passive microwave remote sensing, *International Journal of Remote Sensing, 21*, 2403–2412, doi: 10.1080/01431160050030538.

Matzler, C., & Wiesmann, A. (1999). Extension of the microwave emission model of layered snowpacks to coarse-grained snow. *Remote Sensing of Environment, 70*, 317-325

McCabe, G.J., M. P. Clark, and L.E. Hay (2007). Rain-on-snow events in the western United States. Bulletin of the American Meteorological Society, DOI:10.1175/BAMS-88-3-319.

Melloh, R.A., Richmond, P., Shoop, S.A., Affleck, R.T., & Coutermarsh, B.A. (2008). Continuous mapping of distributed snow depth for mobility models using shaped solutions. *Cold Regions Science and Technology, 52*, 155-165

Meromy, L., N.P. Molotch, T.E. Link, S.R. Fassnacht, R. Rice, (2013), Subgrid variability of snow water equivalent at operational snow stations in the western USA, *Hydrological Processes, 27*(17), DOI: 10.1002/hyp.9355.

Mitterer, C., A. Heilig, J. Schweizer and O. Eisen (2011) Upward-looking ground-penetrating radar for measuring wet-snow properties, Cold Regions Science and Technology, Vol. 69, pp. 129 – 138.

Mizukami, N. and S. Perica, (2012), Towards improved snow water equivalent retrieval algorithms for satellite passive microwave data over the mountainous basins of western USA, *Hydrological Processes, 26*(13), 1991-2002, doi: 10.1002/hyp.8333.

Molotch, N.P., and R.C. Bales, (2005), Scaling snow observations from the point to the grid-element: implications for observation network design, *Water Resources Research, 41*, doi: 10.1029/2005WR004229.

Mote, T. L., Grundstein, A. J., Leathers, D. J., & Robinson, D. A, (2003), A comparison of modeled, remotely sensed, and measured snow water equivalent in the northern Great Plains, *Water Resources Research, 39*(8), 1209, doi: 10.1029/2002WR001782.

Nash, J. E., and J. V. Sutcliffe, (1970), River flow forecasting through conceptual models part I -- A discussion of principles, *Journal of Hydrology 10*, 282-290, doi: 10.1016/0022-1694(70)90255-6.

NOAA (2012) The Missouri/Souris River Floods of May-August 2011, U.S. Department of Commerce Service Assessment, National Weather Service, Kansas City MO and Salt Lake City, UT, May 2012.

Pan, J.M., Jiang, L.M., & Zhang, L.X. (2014). Comparison of the multi-layer HUT snow emission model with observations of wet snowpacks. *Hydrological Processes, 28*, 1071-1083

Parrett, Charles, and Hunrichs, R.A., 2006, Storms and flooding in California in December 2005 and January 2006—A preliminary assessment: U.S. Geological Survey Open-File Report 2006–1182, 8 p.

Pope, A. (2014), The Cryosphere in a Changing Climate, EOS, Vol. 95(15), April 2014

Proksch, M., Lowe, H., & Schneebeli, M. (2015). Density, specific surface area, and correlation length of snow measured by high-resolution penetrometry. *Journal of Geophysical Research-Earth Surface, 120*, 346-362

Pulliainen, J. (2006). Mapping of snow water equivalent and snow depth in boreal and sub-arctic zones by assimilating space-borne microwave radiometer data and ground-based observations. *Remote Sensing of Environment, 101*, 257-269

Ramage, J. and B. Isacks (2002) Determination of melt-onset and refreeze timing on southeast Alaskan icefields using SSM/I diurnal amplitude variations, Annals of Glaciology, Vol. 34(1), pp. 391 – 398.

Ramage, J., & Semmens, K.A. (2012). Reconstructing snowmelt runoff in the Yukon River basin using the SWEHydro model and AMSR-E observations. *Hydrological Processes, 26*, 2563-2572

Ramage, J.M., McKenney, R.A., Thorson, B., Maltais, P., & Kopczynski, S.E. (2006). Relationship between passive microwave-derived snowmelt and surface-measured discharge, Wheaton River, Yukon Territory, Canada. *Hydrological Processes, 20*, 689-704

Rittger, K., A. Kahl, and J. Dozier, (2011), Topographic distribution of snow water equivalent in the Sierra Nevada, *Proc. Western Snow Conf., 79*, 37-46.

Rutter, N., D. Cline and L. Li, (2008), Evalutation of the NOHRSC Snow Model (NSM) in a One-Dimensional Mode, *Journal of Hydrometeorology*, *9*(4), 695-711, doi: 10.1175/2008JHM861.1.

Schmid, M., S. Gubler, J. Fiddes and S. Gruber (2012) Inferring snowpack ripening and melt-out from distributed measurements of near-surface ground temperatures, The Cryosphere, Vol. 6, pp. 1127 – 1139.

Schmugge, T.J., Kustas, W.P., Ritchie, J.C., Jackson, T.J., & Rango, A. (2002). Remote sensing in hydrology. *Advances in Water Resources, 25*, 1367-1385

Schneiderman, E., A. Matonse, M. Zion, D. Lounsbury, R. Mukundan, S. Pradhanang, and D. Pierson, (2013), Comparison of approaches for snowpack estimation in New York City watersheds, *Hydrological Processes*, DOI: 10.1002/hyp.9868.

Semmens, K.A., Ramage, J., Bartsch, A., & Liston, G.E. (2013). Early snowmelt events: detection, distribution, and significance in a major sub-arctic watershed. *Environmental Research Letters, 8*, 11

Stiles, W.H., & Ulaby, F.T. (1980). THE ACTIVE AND PASSIVE MICROWAVE RESPONSE TO SNOW PARAMETERS .1. WETNESS. *Journal of Geophysical Research-Oceans and Atmospheres, 85*, 1037-1044

Sturm, M., J. Holmgren, and G.E. Liston, (1995), A seasonal snow cover classification system for local to global applications, *J. Climate, 8*(5), 1261 – 1283, doi: 10.1175/1520-0442.

Tait, A. B, (1998), Estimation of snow water equivalent using passive microwave radiation data, *Remote Sensing of the Environment, 64*, 286 – 291, doi: 10.1016/S0034-4257(98)00005-4.

Tedesco, M., & Kim, E.J. (2006). Intercomparison of electromagnetic models for passive microwave remote sensing of snow. *Ieee Transactions on Geoscience and Remote Sensing, 44*, 2654-2666

Tedesco, M., Kim, E.J., England, A.W., De Roo, R.D., & Hardy, J.P. (2006). Brightness temperatures of snow melting/refreezing cycles: Observations and modeling using a multilayer dense medium theory-based model. *Ieee Transactions on Geoscience and Remote Sensing, 44*, 3563-3573

Tedesco, M., Brodzik, M., Armstrong, R., Savoie, M., & Ramage, J. (2009). Pan arctic terrestrial snowmelt trends (1979-2008) from spaceborne passive microwave data and correlation with the Arctic Oscillation. *Geophysical Research Letters, 36*, 6

Tedesco, M. and P. S. Narvekar, (2010), Assessment of the NASA AMSR-E SWE product, *IEEE Journal of Selected Topics in Applied Earth Observations and Remote Sensing*, *3*(1), 141-159, doi: 10.1109/JSTARS.2010.2040462.

Todhunter, P.E, (2001), A hydroclimatological analysis of the Red River of the North snowmelt flood catastrophe of 1997, *Journal of the American Water Resources Association, 37*(5), 1263 – 1278, doi: 10.1111/j.1752-1688.2001.tb03637.x.

Tong, J., S. Dery, P. Jackson and C. Derkson, (2010), Testing snow water equivalent retrieval algorithms for passive microwave remote sensing in an alpine watershed of western Canada, *Canadian Journal of Remote Sensing, 36*(1), S74 – S86, doi: 10.5589/m10-009.

Ulaby, F., R. Moore, and A. Fung (1986) Microwave Remote Sensing: Active and Passive, Volume 3 – From Theory to Applications, Remote sensing of the snow. MA: Artech House, 1603 – 1624.

USACE (1956) Snow Hydrology; Summary of the Snow Investigations. N. Pacific Division, COE, Portland, OR.

USACE, (2012), *Mississippi River and Tributaries System: 2011 Post-Flood Report*, US Army Corps of Engineers, Mississippi Valley Division, December 2012.

USGS (2001). National Water Information System data available on the World Wide Web (Water Data for the Nation). In U.S.G. Survey (Ed.)

U.S. Geological Survey, 2012, National Water Information System data available on the World Wide Web (USGS Water Data for the Nation), accessed August 10, 2016 at http://waterdata.usgs.gov/nwis/

USGS (2009). National Elevation Dataset (NED). In U.S.G.S. (USGS) (Ed.). Sioux Falls, SD

U.S. Geological Survey and US Dept. of Agriculture, Natural Resources Conservation Service, 2013, Federal Standards and Procedures for the National Watershed Boundary Dataset (WBD), Techniques and Methods 11-A3, Fourth edition.

Vander Jagt, B., M.T. Durand, S.A. Margulis, E.J. Kim, and N.P. Molotch, (2013), The effect of spatial variability on the sensitivity of passive microwave measurements to snow water equivalent, *Remote Sensing of Environment, 136*, 163 – 179, doi: 10.1016/j.rse.2013.05.002.

Vachon, F., K. Goita, D.De Seve, and A. Royer (2010) Inversion of a snow emission model calibrated with in situ data for snow water equivalent monitoring, IEEE Transactions on Geoscience and Remote Sensing, Vol 48(1), pp. 59 – 71.

Vuyovich, C. and J. Jacobs, (2011), Snowpack and runoff generation using AMSR-E passive microwave observations in the Upper Helmand Watershed, Afghanistan, *Remote Sensing of the Environment, 115*, 3313 – 3321, doi: 10.1016/j.rse.2011.07.014.

Vuyovich, C.M., Jacobs, J.M., & Daly, S.F. (2014). Comparison of passive microwave and modeled estimates of total watershed SWE in the continental United States. *Water Resources Research, 50*, 9088-9102

Vuyovich, C. and J. Jacobs (in press) Snowmelt runoff prediction through spatial characterization of melt-based microwave response, submitted to Remote Sensing of the Environment

Walker, A., and Goodison, B, (1993), Discrimination of a wet snow cover using passive microwave satellite data, *Annals of Glaciology, 17*, 307–311.

Wang, H., Arslan, A.N., Pulliainen, J., & Hallikainen, M. (2001). Microwave emission model for wet snow by using radiative transfer and strong fluctuation theory. *Journal of Electromagnetic Waves and Applications, 15*, 57-59

Wiesmann, A., & Matzler, C. (1999). Microwave emission model of layered snowpacks. *Remote Sensing of Environment, 70*, 307-316

Wiesmann, A., Matzler, C., & Weise, T. (1998). Radiometric and structural measurements of snow samples. *Radio Science, 33*, 273-289

Wilmott, C.J. (1982). Some comments on the evaluation of model performance. American Meteorological Society Bulletin, Vol 63 (11), pp. 1309-1313.

Yan, F.L., Ramage, J., & McKenney, R. (2009). Modeling of high-latitude spring freshet from AMSR-E passive microwave observations. *Water Resources Research, 45*, 14